Identification of novel targets for rational chemoradiotherapy strategies in non-small-cell lung cancer

Inaugural-Dissertation

zur

Erlangung des Doktorgrades

Dr. rer. nat.

der Fakultät für Biologie

an der Universität Duisburg-Essen

vorgelegt von

Sophie Kalmbach

aus Schönebeck/Elbe

Juni 2018

Die der vorliegenden Arbeit zugrunde liegenden Experimente wurden im Labor für Molekulare Onkologie der Inneren Klinik (Tumorforschung) am Universitätsklinikum Essen durchgeführt.

1. Gutachter: Prof. Dr. Martin Schuler
2. Gutachter: Prof. Dr. Christian Johannes
3. Gutachter: -

Vorsitzender des Prüfungsausschusses: Prof. Dr. Verena Jendrossek

Tag der mündlichen Prüfung: 18.10.2018

Table of contents

1. Abstract

1.1 English

Worldwide, lung cancer accounts for most cancer-related deaths. The majority of lung cancer patients is diagnosed with metastatic non-small-cell lung cancer (NSCLC). Treatment modalities include surgery, chemotherapy, and radiotherapy. Still, 5-year survival rates for patients diagnosed with advanced NSCLC are poor as those patients frequently suffer from localized or systemic relapse. Nevertheless, efforts in translational and clinical research led to the discovery of “driver mutations” that can greatly differ between NSCLC entities and can strongly influence therapy outcome. Based on this, targeted therapies are now a firmly established modality in the treatment of patients harboring characteristic molecular aberrations. In contrast, radiotherapy still does neglect the observed molecular heterogeneity between tumors.

In this thesis it was hypothesized that altered signaling transduction pathways can influence the impact of radiotherapy on NSCLC and that an improved understanding of cellular responses to ionizing radiation can pave the way for the development of personalized chemoradiotherapeutic strategies.

To this end, an unbiased, functional, genomic shRNA screen was conducted to identify novel modulators of radiation response and to subsequently characterize them. This shRNA screen revealed several targets involved in i) the Wnt-signaling pathway ii) choline metabolism and iii) the vesicular transport machinery.

After initial experiments, the SNARE protein Syntaxin18 (STX18) was chosen for in depth characterization. Knockdown of *STX18* led to increased radiosensitivity in the NSCLC cell line A549 as shown by short-term and long-term *in vitro* assays, thus supporting a global role of the cellular transport machinery in the stress response. Interestingly, overexpression of STX18 by either CRISPR SAM or a conventional cDNA vector did not translate into an increased radioresistance in A549 cells. Furthermore, the knockdown of *STX18* in A549 correlated with a decrease of mRNA levels and enzymatic activity of *MMP9* (matrix metalloproteinase 9). This was further associated with an increased susceptibility to anoikis *in vitro*. A preliminary *in vivo* experiment in an orthotopic mouse model revealed reduced formation of distant metastasis in mice injected with *STX18* knockdown cells.

Altogether, these findings support that the downregulation of *STX18* in A549 cells by shRNAs modulates the response to irradiation *in vitro* and *in vivo*.

In the second part of this thesis, a previously found modulator of the radiation response – GADD45B - was further analyzed. Short-term survival assays confirmed that enhanced expression of GADD45B protects from radiation-induced cell death in lung cancer models.

Collectively, in this thesis a framework for functional studies of radiation response modulators of lung cancers was established. This may lead to an improved understanding of the impact of specific cellular processes on the radiotherapy response in NSCLC and eventually to improved patient outcome.

1.2 German

Lungenkarzinome sind weltweit für die meisten Krebs-assoziierten Todesfälle verantwortlich. Die Mehrheit der Patienten wird mit dem nicht-kleinzelligen Lungenkarzinom (*non-small-cell lung cancer*, NSCLC) diagnostiziert. Therapie-Modalitäten für Patienten mit fortgeschrittenem NSCLC umfassen die operative Entfernung des Tumors, Chemotherapie und Strahlentherapie. Dennoch ist die 5-Jahres-Überlebensrate für Patienten mit fortgeschrittenem NSCLC sehr schlecht, da diese Patienten häufig von lokal-begrenztem oder systemischem Rezidiv betroffen sind. Bestrebungen in der translationalen und klinischen Forschung haben zur Entdeckung von sogenannten „*driver*-Mutationen“ geführt. Diese können sich zwischen verschiedenen NSCLC Subtypen stark unterscheiden und den Erfolg der Therapie beeinflussen. Darauf basierend sind zielgerichtete Therapien ein fester Bestandteil bei der Behandlung von Patienten mit charakteristischen molekularen Veränderungen. Im Gegensatz dazu bezieht die Strahlentherapie die molekulare Heterogenität des Tumors nicht ein.

Hypothese dieser Doktorarbeit ist, dass veränderte Signaltransduktionswege einen Einfluss auf die Strahlentherapie in NSCLC haben und dass ein verbessertes Verständnis der zellulären Antworten auf ionisierende Strahlung zur Entwicklung von personalisierten kombinierten Chemo- Strahlentherapie Protokollen beitragen kann.

Dazu wurde ein ergebnisoffener, funktioneller, genomischer shRNA Screen durchgeführt um neue Modulatoren der Strahlenantwort zu identifizieren und abschließend zu charakterisieren. Der shRNA Screen hat verschiedene potentielle Kandidaten aufgedeckt die im i) Wnt-Signalweg, ii) Cholin Metabolismus und iii) dem vesikulären Transport von Zellen eine Rolle spielen.

Nach initialen Versuchen wurde das SNARE Protein Syntaxin18 (STX18) für eine detaillierte Charakterisierung ausgewählt. Knockdown von *STX18* führte zu einer

erhöhten Strahlensensitivität in der NSCLC Zelllinie A549 sowohl in Kurzzeit- als auch Langzeit *in vitro* Versuchen. Diese Ergebnisse unterstützen eine globale Rolle der zellulären Transportmaschinerie in der Antwort auf Stress. Interessanterweise führte eine erhöhte Expression von STX18 durch CRISPR SAM oder einen konventionellen cDNA Vektor nicht zu einer erhöhten Strahlenresistenz in A549 Zellen. Außerdem korrelierte ein Knockdown von *STX18* in A549 Zellen in unserem System mit einer Verringerung des mRNA Levels und der enzymatischen Aktivität von *MMP9* (Matrix-Metalloproteinase 9). Dies wurde weiterhin mit einer erhöhten Anfälligkeit für Anoikis *in vitro* in Verbindung gebracht. Ein *in vivo* Versuch im orthotopen Mausmodell zeigte, dass *STX18*-knockdown Zellen eine verringerte Fähigkeit besitzen systemische Metastasen zu formen. Zusammenfassend unterstützen diese Ergebnisse die Hypothese, dass ein Knockdown von *STX18* in A549 durch shRNAs die Strahlenantwort *in vitro* und *in vivo* moduliert.

Im zweiten Teil dieser Arbeit wurde ein im Vorfeld identifizierter Modulator der Strahlenantwort – GADD45B – detaillierter charakterisiert. Kurzzeit-Überlebensversuche bestätigten, dass eine erhöhte Expression von GADD45B vor strahleninduziertem Zelltod in Lungenkrebsmodellen schützt.

Insgesamt wurde in dieser Arbeit ein Grundgerüst für funktionelle Studien von Modulatoren der Strahlenantwort in Lungenkrebsmodellen etabliert. Dies kann zu einem verbesserten Verständnis des Einflusses von spezifischen zellulären Prozessen auf die Strahlenantwort in NSCLC und letztlich zu verbesserten Therapieoptionen für Patienten führen.

2. Introduction

2.1 Lung Cancer

Worldwide, cancer is one of the leading causes of death, accounting for approximately eight million deaths in 2012. This number is expected to grow in the upcoming years, due to the aging of the population and the growing popularity of an unhealthy lifestyle. This behavior includes habits that increase cancer risks, e.g. smoking or obesity (Torre et al. 2015).

Specifically, lung cancer is the leading cause of cancer-related death worldwide. In 2012, nearly two million new lung cancers were diagnosed. This equates to about 13% of all new cancer cases per year. Many risk factors for lung cancer have been discovered, e.g. smoking, radon, and asbestos – implying that avoiding exposition to these agents will contribute to the prevention of lung cancer development (Torre et al. 2015; McGuire 2016).

2.1.1 Types and Stages of Lung Cancer

Lung cancers are grouped into small cell lung cancers (SCLC) and non-small-cell lung cancers (NSCLC), based on histopathology and clinical presentation. NSCLC accounts for more than 80% of cases and can be further subtyped into three main types: adenocarcinomas, squamous cell carcinomas and large cell carcinomas. Adenocarcinomas are the most common type of NSCLC and arise from the lungs' periphery, whereas squamous cell carcinomas usually arise from the bronchi, and large cell carcinomas can arise in various parts of the lung (Zappa and Mousa 2016).

Lung cancer prognosis is strongly determined by tumor stage at diagnosis, which is based on tumor size, local and regional lymph node status, and presence of distant metastases. The UICC staging system differentiates in 4 stages: Stage I comprises single primary tumors without nodal or systemic metastases, while stage IV tumors have disseminated within the contralateral lung or pleura (stage IV A) or into distant organs (stage IV B). Lung cancer patients generally have poor survival rates, due to indolent tumor growth and consecutively advanced stages at primary diagnosis, the high risk of relapse, and the severe comorbidities which are frequently present. Up to 80% of NSCLC patients are diagnosed with Stage IV disease. Once at stage IV, the median 5-year overall survival reaches only 2%, as opposed to more than 50% in stage IA NSCLC (Hammerschmidt and Wirtz 2009; Carson and Finley 2011; McGuire 2016).

2.1.2 Lung Cancer Therapy

Treatment of medically fit patients with early stage NSCLC includes surgical resection in stage I with addition of adjuvant chemotherapy in stages II and III. In stage III (N2), adjuvant radiotherapy is further added. Medically unfit patients with localized tumors (stage I and II) can be treated by stereotactic radiotherapy with curative intent. This form of radiotherapy uses advanced imaging techniques and immobilization aids to ensure precise dose delivery (Hammerschmidt and Wirtz 2009; Abreu et al. 2015). Furthermore, medically fit patients with stage III NSCLC have curative options with multimodality treatment protocols including concurrent chemoradiotherapy followed by resection in some cases. Stage III NSCLC patients with severe comorbidities and patients with stage IV NSCLC are offered palliative systemic therapies as well as radiation therapy for local palliation (Hammerschmidt and Wirtz 2009; Goeckenjan et al. 2011). Several studies have shown that radiotherapy of stage III NSCLC is more efficient when administered with concurrent chemotherapy (Pignon et al. 2008). A variety of platinum-based derivates are used because of their radiosensitizing effects (Kvols 2005), which outweigh their generally higher toxicity (D'Addario et al. 2005). Platinum compounds are also a mainstay of palliative chemotherapy for NSCLC and SCLC (Hammerschmidt and Wirtz 2009).

Over the past decade, efforts in translational and clinical research resulted in more specific therapies which are based on molecular characteristics. Several so-called "driver mutations" have been discovered in lung cancer and a variety of targeted therapies has led to improved tumor control in patients harboring the respective genomic alterations (Vijayalakshmi and Krishnamurthy 2011; Luo and Lam 2013; Chan and Hughes 2015; Wang et al. 2015).

A prime example are "activating" *EGFR* (epidermal growth factor receptor) mutations, that may lead to a deregulated activation of the RAS-RAF-MAPK, PI3K/AKT (Phosphatidylinositol-4,5-Bisphosphate 3-Kinase Catalytic Subunit Alpha/ Protein Kinase B), and the JAK/STAT (Janus Kinase/ Signal Transducer And Activator Of Transcription) pathways resulting in enhanced cell proliferation, cell survival, enhanced angiogenesis, and an increased capability to metastasize (Normanno et al. 2006) (Figure 1A).

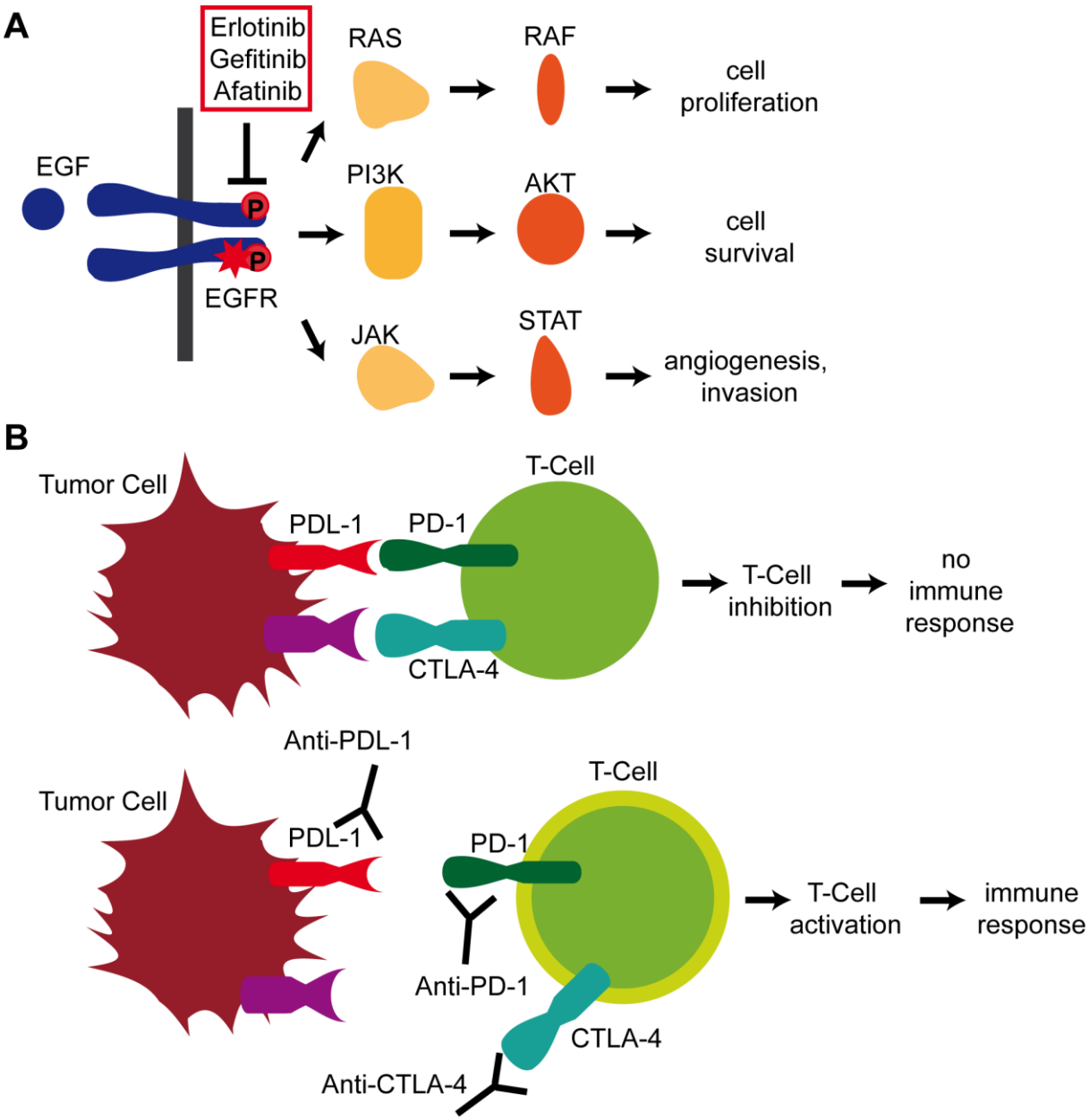

Figure 1: Targeted therapy as well as immunotherapy elicits positive response in cancer patients.
A: Schematic overview of the EGFR signaling pathway. EGFR is activated by EGF which in turn activates downstream signaling pathways leading to increased cell proliferation, survival as well as enhanced angiogenesis and invasive capability. However, activating EGFR mutations (red star) turn on downstream signaling constitutively, negating the need for EGF ligands. EGFR Inhibitors (red box) can suppress this activated signaling. **B:** Schematic overview of the mechanism of action elicited by checkpoint inhibitors. Tumor cells can inhibit T-Cell activation by binding to PD1 or to CTLA-4, thus evading an immune response (upper panel). Inhibition of PD-1, CTLA-4 or PDL-1 demolishes the tumor cells escape mechanism, activates T-Cells and initiates an immune response (lower panel).

TKI (tyrosine kinase inhibitor) treatment of patients with stage IV NSCLC harboring activating *EGFR* mutations greatly improves progression-free survival as well as general quality of life (Paez et al. 2004; Mok et al. 2009; Maemondo et al. 2010; Rosell et al. 2012). On the other hand, patients with *EGFR* mutation-negative NSCLC show better survival when treated with conventional chemotherapy, underlining the

importance of molecular typing of NSCLC (Mok et al. 2009; Maemondo et al. 2010; Rosell et al. 2012). The first generation of EGFR TKIs comprises Erlotinib and Gefitinib, two reversible EGFR inhibitors that are approved for treatment of patients with metastatic NSCLC harboring activating *EGFR* mutations (Bayraktar and Rocha-Lima 2013; Lin et al. 2014). Unfortunately, patients develop resistance against these competitive small molecule inhibitors by several distinct mechanisms within a median of 10 months. When resistant tumors are reanalyzed, more than 50% of cases exhibit a specific gatekeeper mutation, EGFR T790M, which interferes with drug-target interaction. Additional resistance mechanisms include activation of bypass signaling pathways and transdifferentiation into an “EMT phenotype” or SCLC (Lin et al. 2014; Morgillo et al. 2016). Second generation EGFR TKIs, such as Afatinib or Dacomitinib, covalently bind EGFR, HER2 (Erb-B2 Receptor Tyrosine Kinase 2) and HER4 (Erb-B2 Receptor Tyrosine Kinase 4). These TKIs exhibit enhanced target inhibition and are clinically more effective in terms of median progression-free survival and depth of response (Park et al. 2016; Wu et al. 2017). Interestingly, Afatinib also increased radiation sensitivity in NSCLC tumor models (Zhang et al. 2015).

Although the development of acquired resistance limits the therapeutic benefit of TKI, identification of driver mutations and development of targeted drugs greatly improved quality of life in patients (Vijayalakshmi and Krishnamurthy 2011; Luo and Lam 2013; Chan and Hughes 2015; Wang et al. 2015).

A parallel line of research aims to develop therapies that activate the patient’s own immune system for durable control of advanced cancers. During the past decades multiple strategies have been devised, including cytokines and cellular and acellular vaccines (Kelly et al. 2010; Massarelli et al. 2014; Cho 2017). Recently, the introduction of antibodies which modulate positive and negative regulatory signals in the communication between cancer, stroma and immune system has shown clinical activity. Today, three monoclonal antibodies targeting either PD-1 (programmed cell death 1) or PD-L1 (programmed cell death 1 ligand 1) are globally approved for treatment of recurrent metastatic lung cancer and multiple additional agents are under clinical investigation (Massarelli et al. 2014; Helissey et al. 2015; Antonia et al. 2017; Chen 2017; Hellmann et al. 2017). Their activity is based on the inhibition of immune checkpoints that regulate the attack of immune cells. In short, T-cell activation can be inhibited by tumor cells by interacting with PD-1 expressed by immune cells. Inhibition of this negative communication abrogates this escape mechanism and may reinvigorate preexisting immune responses (Figure 1B) (Maher

and Davies 2004). Early studies combining a PD-1 antibody with an anti-CTLA-4 (Cytotoxic T-Lymphocyte Associated Protein 4) antibody, which is thought to foster priming of antigen specific T cells, have suggested increased response rates as compared to monotherapy with a PD-1 antibody in NSCLC (Hellmann et al. 2017). Most recently, the anti-PD-L1 antibody Durvalumab has shown efficacy when administered as consolidation therapy following simultaneous radiochemotherapy in stage III NSCLC (Antonia et al. 2017).

Still, the majority of patients with metastatic NSCLC do not benefit from these novel treatment options. Interestingly, radiotherapy of lung cancer so far neglects molecular heterogeneity of lung cancer, although studies have already shown the influence of genetics on susceptibility to radiation (McKenna et al. 2003; Gong et al. 2008; Advani et al. 2015; Wieczorek et al. 2017).

2.2 Radiotherapy

Approximately 50% of cancer patients receive radiotherapy, thus qualifying radiation as an important treatment modality (Baskar et al. 2012). In NSCLC, patients receive radiotherapy either as curative or palliative treatment. Depending on disease stage and general condition of the patient, radiotherapy is applied with conventional fractionation or as continuous, hyperfractionated, accelerated radiotherapy (CHART). Patients treated with conventional radiotherapy receive cumulative doses of up to >60 Gy in daily fractions for six weeks. While CHART patients receive 54 Gy on twelve consecutive days in fractions of 1.5 Gy thrice daily (Saunders et al. 1999; Goeckenjan et al. 2011).

Generally, radiotherapy aims to deliver the highest possible dose to the tumor without harming normal tissue. Recent technological innovations, e.g. intensity modulated radiation therapy (IMRT) or cone-beam computed tomography (CBCT), have greatly improved the precision of treatment delivery (Baskar et al. 2012; Maciejczyk et al. 2014). Nonetheless, toxicity on adjacent tissues still restricts the radiation doses that can be homogenously applied to a given tumor or tumor region. Also, radiation toxicities cannot be entirely avoided in therapeutically active protocols. While acute effects such as radiation dermatitis or mucositis occur during or shortly after treatment, pneumonitis or fibrosis of the lung can appear months after (Prasanna et al. 2012; Yazbeck et al. 2013). As a result, improving radiotherapy regimens means to either reduce normal tissue toxicity or to sensitize the tumor towards radiation. For

both endeavors, understanding the molecular consequences of radiotherapy as well as in depth analysis of the radiation response of cells and tissues are essential.

Radiation is defined as the energy that is emitted from a source and absorbed from another object. Depending on the amount of energy that is emitted, radiation can either raise an electron to a higher energy level (excitation) or it can lead to the ejection and thus complete removal of the electron (ionization). The latter releases energy, that is about seven times higher than the amount needed to break strong chemical bonds. Ionizing radiation (IR) can be classified as being particulate or electromagnetic (Hall et al. 2012). The work of this thesis focusses on electromagnetic radiation.

X-rays and γ-rays are the forms of electromagnetic radiation with the shortest wavelengths and therefore the highest energy. They possess equal properties and only differ in their origin, with X-rays being produced extranuclearly in an accelerator and γ-rays being formed intranuclearly by radioactive isotopes (Hall et al. 2012).

In general, ionizing radiation can either directly damage molecules or lead to the production of free radicals that afflict cells indirectly. The latter process induces DNA damage and subsequent cell death. Free radicals produced by ionizing radiation have a much more severe impact on a cell's DNA than free radicals produced by e.g. chemical agents. This is because IR produces radicals that are tightly localized along the tracks of IR while chemically produced radicals appear to be evenly distributed within a cell. Tightly localized radicals are much more likely to cause DNA breaks that are close to each another. The extent of clustered DNA breaks positively correlates with the increase in LET (linear energy transfer), which is defined as the energy (keV) transferred per length (µm) of the track. X-rays and γ-rays are considered to possess a low-LET, while particulate forms of IR (e.g. α-particles) have high LET, signifying that they generate more ionizing events along their tracks (Hall et al. 2012; Schipler and Iliakis 2013) (Figure 2A). Those ionizing events can result in single- and double-strand breaks with the latter being the most lethal type of lesion (Hall et al. 2012).

Apoptosis and mitotic catastrophe are the two main mechanisms that are responsible for cell death following radiation. Multiple additional processes, e.g. necrosis, autophagy, and senescence, also play a role (Figure 2B) (Bolus 2001; Golden et al. 2012). Apoptosis usually occurs during interphase and is executed by activation of pro-apoptotic factors that lead to caspase activation and cell death. In short, ionizing radiation triggers the activation of pro-apoptotic BCL-2 family proteins that lead to

mitochondrial outer membrane permeabilization (MOMP) followed by release of cytochrome C into the cytosol. Cytochrome C initiates formation of the apoptosome complex formed by APAF-1 (apoptotic protease activating factor 1) which recruits and activates caspases. Caspase cleavage results in degradation of chromosomal DNA, cytoskeletal reorganization, and disintegration of cells (Cohen 1997; Zhou et al. 2003; Elmore 2007). Mitotic catastrophe occurs when cells fail to correctly undergo mitosis due to severe DNA damage and defects in proteins involved in repair and mitotic regulation. This usually happens at the first cell division after irradiation and is characterized by the emergence of cells with multiple (micro-)nuclei (Golden et al. 2012).

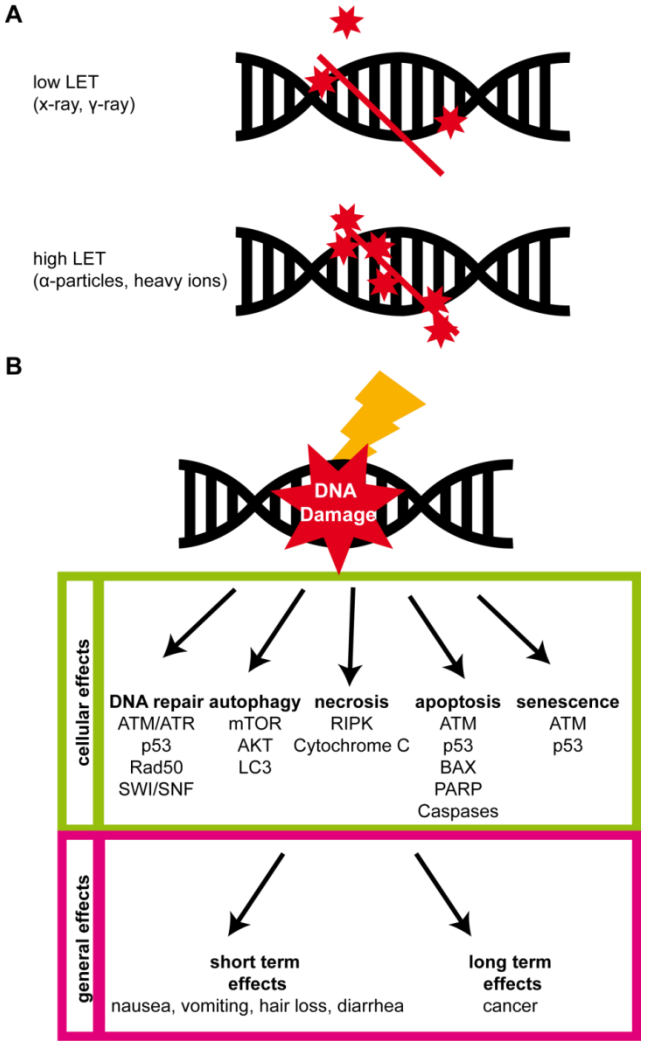

Figure 2: IR induced DNA Damage.
A: Schematic overview about low and high LET. While low LET irradiation causes sparsely distributed ionizing events, high LET causes densely packed ionizing events. **B:** Cells can respond to DNA damage in a variety of ways. A subset of involved key proteins is given to each pathway.

2.2.1 Radiosensitizers

Improving the effect of radiotherapy is possible by sensitizing the tumor to ionizing radiation and thus enhancing cytotoxicity, preferentially without affecting normal tissue. Radiosensitizers differ in the mechanism they use to increase the effect of radiation.

Cisplatin is used in combination with radiotherapy in several cancer entities because of its radiosensitizing effect that increases patient survival and delays cancer progression (Schaake-Koning et al. 1992; Rose et al. 1999). Its effect is due to interference with DNA replication in proliferating cells (Donaldson et al. 1994; Wagner and Karnitz 2009).

Furthermore, Fluorouracil is used in combination with radiotherapy in e.g. rectal cancer (Klinkenbijl et al. 1999; Wang and Kumar 2011). Its sensitizing effect relies in part on alterations in cell cycle distribution that makes cells more prone to the damaging effects of ionizing radiation (Lawrence et al. 1997, 2003; Klinkenbijl et al. 1999; McGinn and Lawrence 2001).

Additionally, many endeavors are undertaken to use oxygen because of its ability to form DNA-damaging free radicals. However, tumors often contain hypoxic regions that possess a greatly increased radioresistance. Thus, oxygen tanks or hypoxic cell radiosensitizers have been developed to reoxygenate the tumor, making it more sensitive to IR (Roizin-Towle et al. 1986; Wardman 2007).

For several years, targeting proteins that are involved in cellular signaling has been in the focus of scientists. Knockdown of the oncogene *RAS* has been shown to lead to increased tumor cell cytotoxicity following irradiation *in vitro* (Pirollo et al. 1997; Kim et al. 2004; Cengel and McKenna 2005). In lung squamous cancers, activation of NRF2 (Nuclear Factor Erythroid 2- Related Factor 2) was shown to confer radioresistance that could be overcome by PI3K inhibitors (Abazeed et al. 2013; Wang et al. 2017).

2.2.2 DNA Repair

While radiation can potentially be catastrophic for cells, a great variety of cellular mechanisms may counteract and repair DNA damage. Because DSBs represent the most severe types of IR induced lesions, this introduction will solely focus on DSB repair mechanisms. DSBs are mainly repaired by either homologous recombination repair (HRR) or non-homologous end-joining (NHEJ). The main steps of those key repair pathways are depicted in Figure 3.

HRR is a high-fidelity repair mechanism that is based on homologous recombination and thus requires homologous DNA as a template. HRR is limited to the S- and G2-phases of the cell cycle, in which a sister chromatid is available. To execute its function, HRR requires single-stranded 3' DNA overhangs that are generated by the initial process of end resection orchestrated by the MRN complex (Mre11-Rad50-Nbs1) together with CtIP (C-terminal binding interacting protein), BLM (Bloom`s syndrome protein), EXO1 (exonuclease 1) and BRCA1 (breast cancer 1). Stabilization of ssDNA is achieved by recruitment of RPA (replication protein A), which is subsequently replaced by RAD51 with help of the mediator protein BRCA2 (breast cancer type 2 susceptibility protein). Rad51, in liaison with BRCA1-BARD1 (BRCA1 associated RING domain protein 1) then recognizes homologous sequences which are unwound to form a displacement loop with the damaged strand (Zhao et al. 2017). Following DNA synthesis with undamaged DNA as a template, the newly synthesized strand is ligated to the original strand (Mladenov and Iliakis 2011a; b; Schipler and Iliakis 2013).

Classical NHEJ (c-NHEJ) is a DNA-PK (DNA dependent protein kinase) dependent mechanism. It displays a unique flexibility with regard to its substrates comprising variable DNA ends, the working order of involved proteins, and the cell cycle phase. It involves multifunctional enzyme complexes that quickly repair DNA lesions throughout the cell cycle. Besides repairing pathologic DSB, c-NHEJ is also responsible for the repair of physiologic DSB that occur during V(D)J- and class switch-recombination during the maturation of antibodies and assists in TCR (T-cell receptor) rearrangement (Pierce and Jasin 2001; Deriano et al. 2009; Lieber 2010). c-NHEJ is initiated by binding of KU70/80 proteins to free DNA ends effectively impeding with processes that require end resection. In a next step, DNA-PKcs (DNA-PK catalytic subunits) are recruited that subsequently attract additional proteins needed for end-processing, such as Artemis and Polymerase μ/λ. Here, blunt ends are generated by filling in nucleotides before both strands are ligated by LigIV (Ligase IV), XLF (XRCC4-linke factor), and XRCC4 (X-ray repair cross-complementing protein 4). In contrast to HRR, the absence of a DNA template may cause insertions/deletions (indels) in the junction; hence, c-NHEJ mainly restores overall DNA integrity (Mladenov et al. 2013).

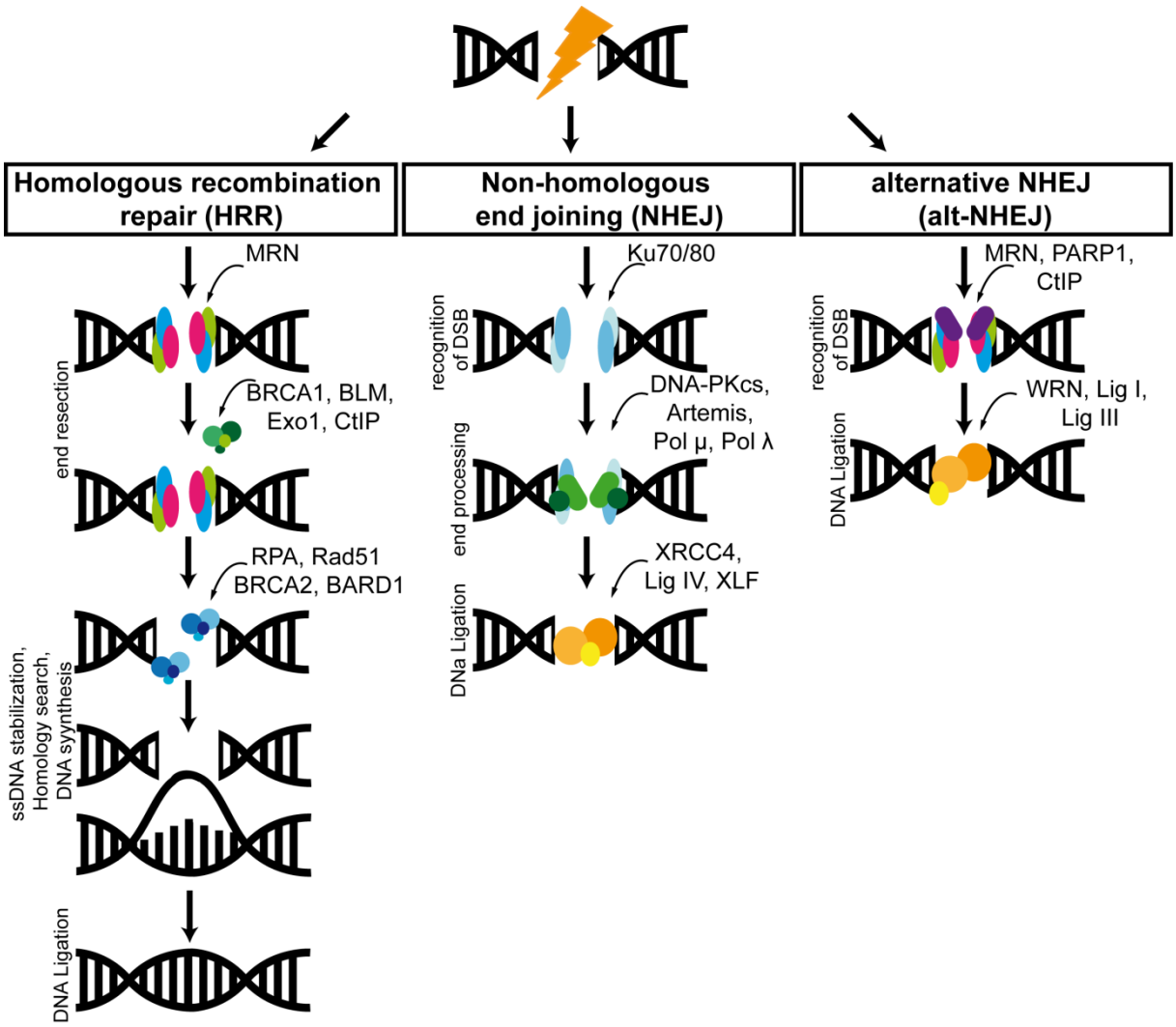

Figure 3: Schematic overview of the main DSB repair mechanisms and the key proteins involved.
Homologous recombination repair (HRR), Non-homologous end joining (NHEJ) and alternative NHEJ (alt-NHEJ) differ in their availability throughout the cell cycle as well as the involved proteins. In general, HRR acts in S-phase and NHEJ is available in all phases of the cell cycle.

In recent years, an alternative NHEJ pathway (alt-NHEJ/backup NHEJ) has been identified that acts as a backup when c-NHEJ or HRR are impaired. While it can theoretically act throughout the cell cycle, studies have shown that it is preferentially active during G2 phase (Wu et al. 2008). The process is highly error-prone and increases the risk of genomic rearrangements. The detailed pathway mechanism remains to be completely characterized, though repair is facilitated by PARP-1 (Poly(ADP-ribose)-Polymerase 1) and ligation by XRCC1 (X-ray repair cross-complementing protein 1) and Ligase III (Mladenov et al. 2013).

Altogether, radiation-induced DSB can be removed by a variety of cellular mechanisms that differ in their fidelity and are determined by cell cycle phase and availability of involved proteins. In general, while the whole process of HRR takes

significantly longer it is much more precise than NHEJ and alt-NHEJ (Mao et al. 2008) and is the only pathway that maintains genomic stability.

2.2.3 DNA Repair and Cancer

DNA repair is of utmost importance for maintenance of genomic integrity, rendering any defects in associated genes potentially catastrophic. Mutations causing defects in DNA repair proteins have been first identified for breast cancer susceptibility genes, BRCA1 and BRCA2 (Miki et al. 1994; Wooster et al. 1995). These mutations cause hereditary breast cancer (Walsh 2015). This is because the failure of HRR forces the use of the more error-prone alternative NHEJ pathways, leading to genomic instability. For cancer treatment, this is an intriguing concept that has led to development of PARP (poly(ADP-ribose)polymerase) inhibitors that have greatly improved patient survival in BRCA deficient tumors (Fong et al. 2009). Briefly, PARP is one of the main enzymes needed for repair of single-strand DNA breaks. Its inhibition leads to the accumulation of those breaks, ultimately resulting in DSB. Because of the tumor's BRCA deficiency, HRR cannot fix those breaks, forcing the cells to employ NHEJ which subsequently leads to cell death (Kelley et al. 2014; Walsh 2015).

2.3 Phenotypic and Functional Screens

High throughput functional screens represent an essential tool for scientific research that enable the identification of candidate genes/proteins involved in a specific biological process in an unbiased manner. Different screening approaches exist, e.g. using shRNA (small hairpin RNA) libraries, CRISPR/CAS dropout screens, or viability screens after drug treatment (Sims et al. 2011; Diehl et al. 2014).

The main aim of this thesis was to establish and conduct an shRNA screen to identify functional regulators of the radiation response in lung cancer models. In short, shRNAs are molecules able to silence gene expression by RNAi (RNA interference). Viral vectors efficiently deliver the shRNA into the target cells, where it is integrated into the host genome. After transcription, the shRNA is bound by RISC (RNA-induced silencing complex) which directs the complex to mRNA with a complementary sequence. This mRNA is then cleaved and translation is repressed (Elbashir et al. 2001; Abbas-Terki et al. 2002).

Nowadays, shRNA screens are well-developed, and a variety of pooled, barcoded libraries have become available, eliminating the need to generate them single-handedly. Those libraries usually provide an adequate coverage of the

respective targets by containing a set of different shRNAs that target the same gene. Next Generation Sequencing (NGS) subsequently allows precise analysis of the representation of each shRNA clone in the DNA isolated from a given cell population. shRNA screens are a widely used method and have e.g. been used to identify genes required for proliferation and survival (Schlabach et al. 2008) or to investigate the therapeutic effect of the BRAF(V600E) inhibitor Vemurafenib on colon tumors (Prahallad et al. 2012).

The basis of the experimental work of the first part of this thesis was the establishment of a functional shRNA screen to identify novel modulators of the radiation response of NSCLC. To this end, a complex, barcoded shRNA library was introduced into an NSCLC cell line. Several putative candidates have been identified and were selected for further functional characterization.

3. Aim of the Study

This work was based on the hypothesis that specific molecular alterations occurring in lung cancers impact on the outcome of radiotherapy. A better understanding of the underlying mechanisms conferring radioresistance and radiosensitivity is needed to identify patient subgroups that either respond exceptionally well or rather poorly to radiotherapy.

The main part of this thesis aimed to identify novel modulators of radiation response by conducting an unbiased, functional genomic shRNA screen, and to subsequently characterize the selected targets.

In the second part of this thesis a modulator of the radiation response identified by a previous cDNA library-based screen, GADD45B, was further characterized.

Altogether this thesis aimed to identify molecular alterations that modulate the radiation response. This could allow the definition of new drug targets which could be developed into molecularly defined, novel radiosensitization strategies for cancer therapy.

4. Methods

If not indicated otherwise, all steps were carried out at room temperature (RT) and samples were centrifuged for 5 minutes at ~300g.
Compositions of buffers/solutions can be found in section 8.2.7.
Collaborating groups are located at the University Hospital Essen.

4.1 Execution of the shRNA Screen

4.1.1 Generation of a lentiviral shRNA library

The DECIPHER shNRA Library Human Module 1 (27500 pooled shRNAs targeting 5043 Signaling Pathway Genes) for Academic Institutions supplied by Cellecta Inc. was used for generation of a lentiviral shRNA library. In this library, each shRNA can be identified by a unique barcode and transfection/transduction efficiencies can be determined by flow cytometry for RFP signal. The procedure was done according to the manufacture's protocol. In short, 22x 15cm dishes were coated with fibronectin. $5.5 \cdot 10^6$ HEK293FT cells were seeded onto each dish. The next day, medium was changed to RPMI w/o antibiotics and cells were transfected with the shRNA library 2 hours later. Please refer to section 4.7.1 for a detailed description of the transfection process. Briefly, 3µg of library DNA was used for transfection of one 15cm dish, with 20 dishes being transfected in total. A master mix was prepared to ensure equal transfection efficiency. Furthermore, one dish was transfected with a control RFP-vector and one dish was used as an untransfected control. The next day, medium was withdrawn, cells washed twice with PBS and normal culture medium supplemented with antibiotics was added to the cells (20ml/dish). 48 hours later, viral supernatant was pooled and filtrated through 0.45µm filters. Transfection efficiency was determined for the mock transfected cells, the RFP-vector control cells, as well as cells from five dishes transfected with the shRNA library by flow cytometry.

4.1.2 Procedure of the shRNA screen

To ensure uptake of single shRNA vectors transduction of A549 cells was done with an efficiency of ≤ 30%. The appropriate amount of viral supernatant to reach this efficiency was determined by flow cytometry. Therefore A549 cells were seeded and

on the next day transduced (section 4.7.2) with different amounts of diluted viral supernatant. Transduction efficiency was determined 48 hours later by flow cytometry.

For the screen, 28 15cm dishes were seeded with $2 \cdot 10^6$ A549 cells each. The next day, 27 dishes were transduced with the shRNA library in a volume of 13.5ml/dish and supplemented with polybrene (5µg/ml). One dish was used as a negative control. 24 hours later viral supernatant was withdrawn, cells were washed twice with PBS and detached using trypsin. Cells from 5 15cm dishes were pooled and transferred to 5 square dishes (~22x22cm) in 70ml medium each. The next day, cells from one shRNA library transduced dish were harvested and used for flow cytometry to determine transduction efficiency. Untransduced A549 were used as a negative control. Flow cytometry revealed transduction efficiency of about 30%. Afterwards medium on the other square dishes was changed to medium supplemented with puromycin. Five days later, no living cells could be detected in the untransduced control dish. Cells from one shRNA library transduced dish were harvested and used for flow cytometry to determine selection efficiency. Untransduced A549 cells were used as a control. Flow cytometry revealed >95% of RFP positive cells, confirming the successful selection of transduced cells.

For irradiation, all shRNA library transduced cells (24 dishes) were harvested, pooled, counted, and divided into three samples: i) T0 cells were frozen at -80°C ii) 0 Gy cells were transferred to a suspension cell culture flask iii) 10 Gy cells were transferred to a suspension cell culture flask. Irradiation was done while cells were in suspension (refer to section 4.3). Immediately afterwards, cells were replated on a total of 32 square dishes. 72 hours after irradiation many detached cells could be observed in the irradiated sample set, while the control cells looked fine. Cells were harvested, pooled, counted, and frozen at -80°C. Subsequently, DNA was isolated using QIAGEN Genomic-tip 500/G (QIAGEN) according to the manufacturer's protocol.

The procedure was done in two independent experiments. A schematic overview of the screening experiment is given in Figure 4.

DNA was sent to BioCat GmbH where shRNA specific barcodes were amplified, sequenced on the Illumina HiSeq and data deconvoluted. BioCat GmbH provided a sequencing report with the relative abundance of shRNAs in each population.

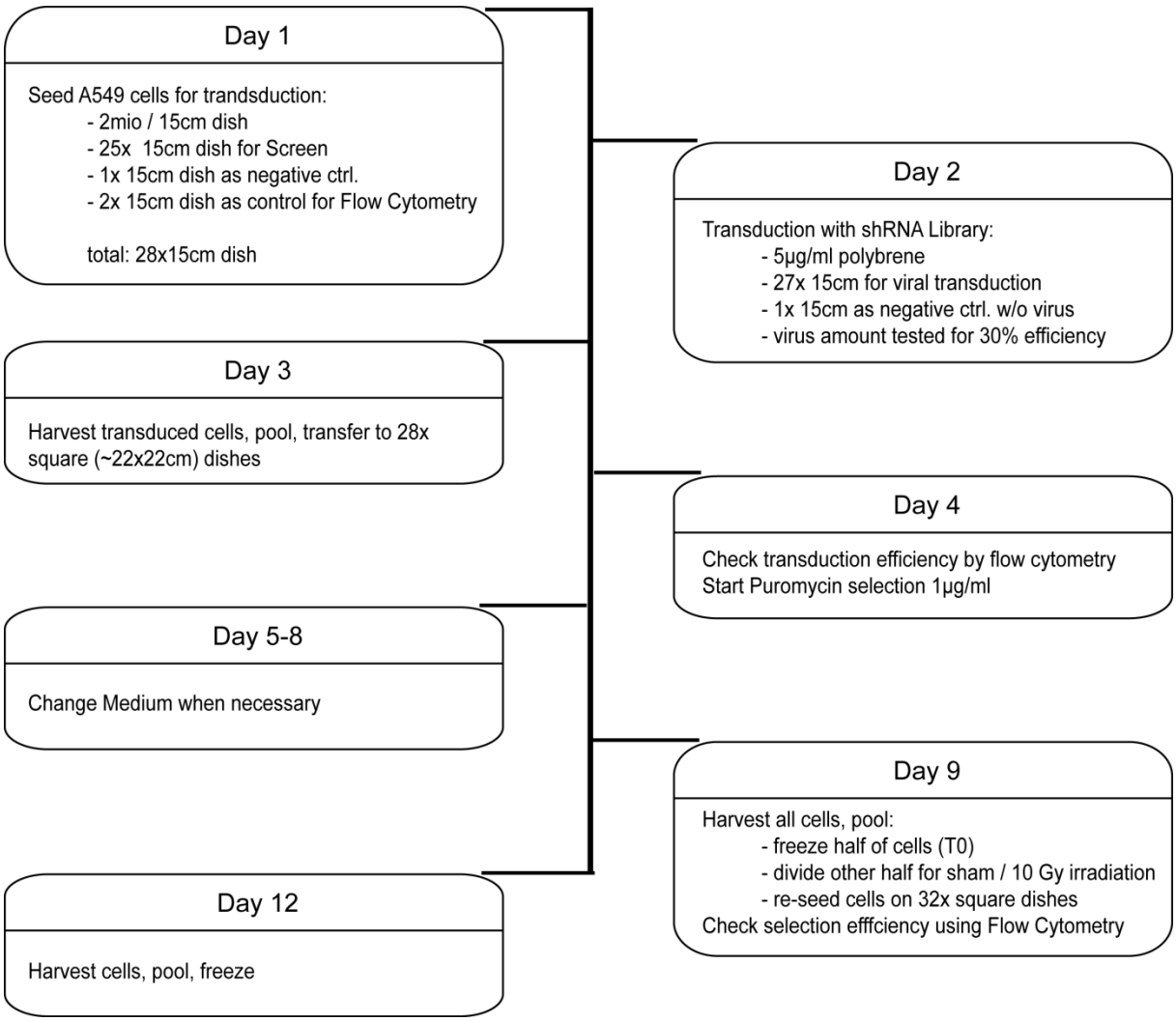

Figure 4: Schematic overview of the screening procedure.

4.1.3 Analysis of the shRNA screen

After sequencing, BioCat GmbH provided a sequencing report with the relative abundance of shRNAs in each population. Taking into account the T0 sample as a representative of the starting distribution of shRNAs, shRNAs either enriched or reduced by at least 40% in the irradiated sample of both screening experiments were considered hits. shRNAs enriched after irradiation are considered to target genes that confer radiosensitivity. Consequently shRNAs reduced after irradiation were considered to target genes conferring a more radioresistant phenotype. Further data analysis using gene ontology (section 4.9) as well as extensive literature research revealed several targets clustering in certain cellular pathways.

4.2 Cell Biology Methods

4.2.1 Cell culture

In general, cells were cultured in DMEM or RPMI (Gibco) supplemented with 10% FBS (Biochrom), 1% L-Glutamine (Gibco), and 1% penicillin-streptomycin (Gibco) at 37°C and 5% CO_2.

Cells stably transfected/ transduced with transgenes carrying antibiotic resistances were cultured in medium containing the appropriate antibiotic.

For maintenance, cells were passaged twice weekly at a confluency of ~70%. Briefly, medium was discarded, cells were washed once with PBS (Gibco), incubated with Trypsin-EDTA (Gibco) for about 5 minutes, and seeded into a fresh cell culture flask at an appropriate density. Only cells with passages <30 were used for experiments.

4.2.2 Freezing and thawing

Cells were frozen in early passages (<8) in FBS supplemented with 10% DMSO and stored short-term at -80°C and long-term in liquid nitrogen. Cells were thawed at 37°C and added to a flask containing warm medium. Medium was changed 6-24 hours later and cells were passaged at least once before using them in experiments.

4.2.3 Counting and cell viability

Cells were counted and the amount of viable cells was determined using a Countess™ Automated Cell Counter (Invitrogen) and Cell Counting Chamber Slides (Invitrogen).

4.2.4 Colony formation assay

The Colony Assay was used to determine clonogenic survival following irradiation with doses ranging from 0 Gy-10 Gy. Cells were seeded in appropriate numbers, aiming for about 100 colonies at the end of the experiment, in triplicates in 6-well plates and irradiated 4 – 6 hours later. After 8 – 12 days, colonies were fixed for 1 hour at RT or O/N at 4°C with 70% ethanol and stained with colony staining solution. Subsequently, colonies consisting of 50 or more cells were counted. Plating efficiency of sham irradiated cells was used as a control for each cell line.

4.2.5 Transgene induction

Induction of GADD45B in the inducible H1975/ HCC rtTA GADD45B cells was done by adding doxycycline (1µg/ml) to the cell culture medium 24 hours prior to the start of experiments.

4.3 Irradiation

Irradiation was done using an RS320 X-ray irradiator (X-Strahl) provided by the group of Prof. Stuschke/Sak. Cells were irradiated at 300 kV and 10 mA.

4.4 Flow Cytometry

If not indicated otherwise, flow cytometry was done using a FACSCelesta™ (BD) equipped with a HTS module that allowed analysis of samples in a 96-well plate. Some initial experiments were done using a FC 500 (Beckman Coulter, Inc.).

4.4.1 Determination of Cell Viability

Propidiumiodid (PI) staining was used for cell cycle analysis and determination of Sub-G1 (apoptotic) fraction. Cells were harvested, thereby also collecting the supernatant and the PBS used for washing. After centrifugation, the supernatant was discarded; cells were washed once with PBS, pellets were resuspended in HFS, and incubated for at least 30 minutes in the dark at 4°C after which flow cytometry was carried out. Experiment were read out on a BD FACSCelesta™ instrument, or on a Gallios Flow Cytometer (Beckman Coulter, Inc.) provided by the group of Prof. Dr. Iliakis.

4.4.2 Combined EdU-DAPI staining

Combined EdU-DAPI staining was used to visualize cellular proliferation. The protocol was adapted from the group of Prof. Iliakis. Cells were seeded in 6-well plates in appropriate cell numbers, so that cells reached about 80% confluency at the last day of the experiment. Cells were labeled with 10 µM EdU followed by incubation for 30 minutes. After that, cells were harvested using trypsin, thereby also collecting the supernatant and the PBS used for washing. Following centrifugation, the supernatant was discarded and cells were permeabilized in the dark for 5 minutes on ice with 500 µl ice-cold Triton X-100 (0.2% in PBS). Cells were centrifuged, supernatant was discarded, and cells were fixed with 500 µl 2% PFA for 15 minutes. Subsequently, cells were centrifuged again, supernatant was discarded and cells were stored in PBG at 4°C for 45 minutes or up to 5 days. Prior to flow cytometry cells were transferred to a 96-well plate, centrifuged, and supernatant was discarded.

Cells were stained using 50 µl “Staining-Master-Mix” in the dark for 30 minutes during which the plate was shaken gently. For washing 200 µl PBS was added, the plate was centrifuged, the supernatant discarded, and the pellets resuspended in 150 µl DAPI (5µg/ml in PBS) followed immediately by flow cytometry.

4.4.3 GFP/RFP detection

To determine the amount of GFP/RFP positive cells, cells were harvested, washed once with PBS, and resuspended in PBS. Samples were kept on ice and flow cytometry was carried out immediately.

Measurement of RFP to determine transduction efficiency in the shRNA screen was done using a LSR Fortessa™ (BD) kindly provided by the group of Prof. Dr. Lang.

4.4.4 Assessment of anoikis

Anoikis describes cell death of adherent cells caused by detachment from the ECM. Escape from anoikis can be a sign for increased metastatic ability of cells.

To assess anoikis, 6-well plates were coated with PolyHema (20g/ml; Sigma), which was allowed to evaporate O/N. Plates were washed with PBS prior to use. Cells were seeded at an appropriate density, so that controls seeded on non-polyHema coated dishes will reach about 80-90% confluency at the end of the experiment. Cells were incubated for 72 hours and the amount of apoptotic cell death was measured using PI-staining (section 4.4.1).

4.5 Biochemical Methods

4.5.1 Protein extracts

For cellular protein extractions, cells were harvested using trypsin or, were scraped from the plates while on ice using a cell scraper for phosphoprotein detection. To prevent protein degradation all further steps were carried out on ice or at 4°C. Cells were resuspended in an appropriate volume of NP-40 buffer (gentle lysis, suitable for cytosolic proteins) or RIPA buffer (intense lysis, for nuclear proteins) supplemented with Complete Protease Inhibitor Cocktail (Roche Molecular Systems, Inc.) and Phosphatase Inhibitor Cocktails 2/3 (Sigma). Cells were vortexed, incubated for >20 minutes on ice, and snap frozen in liquid nitrogen. After thawing on ice, tubes were centrifuged for 10 minutes at maximum speed and the supernatant transferred to a new tube. Samples were stored at -80°C.

To isolate secreted proteins from supernatant, cells were grown on 10 cm dishes in medium containing 0.5% FBS. The supernatant was transferred to a 50 ml conical tube, centrifuged to remove any debris, and transferred to a new 50 ml conical tube. An equal volume of acetone was added and the tube frozen at -80°C for >24 hours. Supernatant was thawed on ice and centrifuged at 4°C for 30 minutes at maximum speed. Supernatant was discarded, pellet resuspended in 200 µl 1% NP-40 buffer supplemented with Complete Protease Inhibitor Cocktail (Roche Molecular Systems, Inc.) and Phosphatase Inhibitor Cocktail 2/3 (Sigma) and stored at -80°C. Equal volumes were used for SDS-PAGE.

4.5.2 Measurement of protein concentration

Protein concentration was determined using Bio-Rad Protein Assay Dye Reagent Concentrate (Bio-Rad). Proteins were thawed on ice. Per sample 800 µl H_2O, 200 ml Bio-Rad Concentrate, and 2 µl protein extract were mixed and absorbance against a reference was measured at 595 nm using a Gene Quant™ pro spectrophotometer (GE Healthcare).

4.5.3 SDS-PAGE

SDS-PAGE was done using the Mini-PROTEAN electrophoresis system (Bio-Rad). Equal amounts (20-50 µg) of proteins were supplemented with 6x SDS-Sample-buffer, adjusted to equal volumes with H2O, and denatured for 5 minutes at 95°C. PageRuler Prestained Protein Ladder (Thermo Scientific) was used as marker. Separation was done at 95-105 V until proteins were sufficiently separated.

4.5.4 Western blotting

Western blotting was conducted using the Trans-Blot® Turbo™ (Bio Rad) and the Mini Nitrocellulose Transfer Kit (Bio Rad). Transfer efficiency was analyzed by Ponceau S staining.

Subsequently membranes were blocked in NET-G for ≥1 hour and incubated with primary antibodies O/N at 4°C while shaking after which membranes were washed thrice with Net-G for 10 minutes. Incubation with secondary antibodies was done at RT for ~2 hours. After washing the membranes, signals were detected with the Super Signal West Pico/Femto system (Thermo Scientific) on the ChemiSmart Imaging System (VILBER LOURMAT Deutschland GmbH).

4.5.5 Stripping of Western blot membranes

Antibodies were removed from the nitrocellulose membranes by shaking in 50 ml stripping-solution supplemented with 350 µl β-Mercaptoethanol (Sigma-Aldrich, Inc.) in a tightly closed container at 50°C for 30 minutes while shaking. Afterwards the membrane was washed thrice with H_2O, blocked in Net-G for at least 1 hour, and incubated with primary antibody O/N at 4°C.

4.5.6 Zymography

Gel zymography was used to assess the activity of gelatinases MMP2 and MMP9. A protocol provided by the group of Prof. E. Gulbins was adapted. Cells were seeded at high density, shifted to medium containing 0.5% FBS after they became adherent and cultivated O/N. Supernatant was centrifuged and transferred to a new tube. Samples were supplemented with 5x zymography-sample buffer and incubated at RT >15 minutes. Cells were harvested using a cell scraper, pellet was resuspended in NP40-zymography-lysis buffer and incubated for 15 minutes on ice. Samples were centrifuged at maximum speed for 10 minutes at 4°C and supernatant was transferred to a new tube. Samples were supplemented with 5x zymography-sample buffer and incubated at RT >15minutes. Equal volumes of supernatant and cell samples were loaded on a zymography-gel and run at 95 V. Afterwards the gel was incubated for 1 hour in 2.5% Triton, 1 hour in enzyme buffer while shaking at RT and then transferred to 37°C O/N. Staining was done by incubating the gel in staining-solution for 1 hour at RT while shaking before it was destained in Destaining solution for 30 minutes – 2 hours. Finally, white bands were visible where MMPs have degraded the gelatin gel against the blue background of the rest of the gel. For presentation, the images were converted to black/white. Here a black band represents the gelatin metabolized by the MMPs while the background is white/gray.

4.5.7 Luciferase assay to measure *XBP1* splicing

XBP1 splicing activity was measured using the Dual-Luciferase® Reporter Assay (Promega Corporation) according to the manufacturer's protocol. In short, the pFLAG-XBP1-Luc vector (Addgene # 31239, provided by the group of Eric Metzen) was transfected into cells seeded into a 24-well plate using FuGene® (Promega Corporation). Two days after transfection, control cells were treated with DTT to induce ER stress and Dual-Luciferase® Reporter Assay (Promega) was conducted 24 hours later in a white 96 well plate using a Spark® (Tecan Trading AG)

luminescence reader. Firefly luciferase activity was normalized to Renilla luciferase activity. Per biological experiment, samples were done in duplicates.

4.5.8 Fluorometric assessment of beta-galactosidase activity

Cells were seeded in 10cm dishes and irradiated the following day. After 72 hours, dishes were placed on ice, medium was removed and cells were washed 5 times with PBS. 100µl of lysis-buffer supplemented with protease inhibitors was added to each dish, cells scraped using cell-scraper, and dishes placed on ice in an inclined position for 5 minutes. Subsequently, lysates were transferred to a reaction tube and centrifuged for 10 minutes at maximum speed at 4°C. Supernatant was either stored at -80°C or directly processed by adding 50 µl of lysate to 50 µl 2x reaction buffer. Samples were incubated for 1.5 hours at 37°C. In the meantime, protein concentration of the lysates was measured. Reaction was stopped by mixing 50 µl of lysate with 500 µl stop solution. Samples were added in triplicates of 150 µl each to a black 96-well plate and fluorescence measured at 360 nm excitation and 465 nm emission in a Spark® (Tecan Trading AG) fluorescence reader. Mean values of triplicates were calculated, normalized to respective protein concentration and to respective control.

4.5.9 Immunofluorescence staining

For staining of intracellular Syntaxin 18, cells were seeded at equal densities in 96 well plates. The next day, medium was removed, cells were washed twice with PBS and fixed with ice cold methanol for 10 minutes at RT. Cells were washed three times with PBS and blocked with PBG for 1 hour. Primary antibody was diluted in PBG, incubated for 1 hour after which cells were washed three times with PBS. Incubation with secondary antibody (AlexaFluor488, 1:400 in PBG) was again done for 1 hour. Subsequently cells were washed thrice with PBS and analyzed with a fluorescence microscope.

4.6 Molecular Biology Methods

4.6.1 DNA isolation

DNA isolation from A549 cells in the *in vitro* screen was done using QIAGEN Genomic-tip 500/G (QIAGEN) according to manufacturer’s protocol.

4.6.2 RNA isolation and cDNA synthesis

RNA was isolated according to manufacturer's protocol from cell lines using the HighPure RNA Isolation Kit (Roche Molecular Systems, Inc. Molecular Systems, Inc.) while isolation from tissues was done using the RNeasy Mini Kit (QIAGEN).

RNA isolation was followed by synthesis of cDNA with the Transcriptor High Fidelity cDNA Synthesis Kit (Roche Molecular Systems, Inc.) according to manufacturer's protocol.

4.6.3 Quantitative reverse transcription and polymerase chain reaction (qRT-PCR)

qRT-PCR was carried out with the LightCycler® 480 SYBR Green I Master Kit (Roche Molecular Systems, Inc.). Reactions were performed in duplicates or triplicates in 96-well plates using the LightCycler® 480 System (Roche Molecular Systems, Inc.). A master mix (15 µl per reaction) consisting of SYBR Green I Master and 20 pM of each primer was prepared and 5 µl diluted cDNA was used for each reaction. A negative control without cDNA was used for each primer set. Cycling was executed according to the following protocol:

program	Temperature [°C]	Time [minutes]	Number of cycles
initialization	95	5:00	1
Amplification	95	0:10	45
	57	0:10	
	72	0:10	
Melting-curve	95	0:05	1
	65	1	
	97	continuous	
Cooling	40	0:10	1

Results were analyzed using the ΔΔCt model. Statistical analysis was only done for experiments done in at least three independent biological replicates. Primers were designed using Primer3 (www.primer3plus.com) and ordered at Thermo Fisher Scientific or Integrated DNA Technologies.

4.6.4 Agarose gel electrophoresis and gel extraction

Agarose gel electrophoresis was done using 0.8-2% agarose in TBE supplemented with ~0.4 µg/ml ethidium bromide at ~200 V depending on fragment length. When

DNA was to be extracted from the gel, TAE was used and the gel allowed to run for >2 hours at ~100 V.

DNA was isolated from TAE agarose gels with the QIAquick Gel Extraction Kit (QIAGEN) according to manufacturer's protocol.

4.6.5 PCR and purification of PCR products

Conventional PCR was done using the MyTaq HS Red Mix (Bioline) in a sample volume of 20µl. Cycling conditions were chosen regarding the appropriate annealing temperature of the primers and the manufacturers protocol of the polymerase.

For generation of cDNA vectors, the Q5^{TM} High-Fidelity DNA Polymerase (NEB) was used to ensure error-free amplification. A reaction volume of 40µl was used.

When necessary, PCR reactions were purified using the QIAquick PCR Purification Kit according to manufacturer's protocol.

Primers were designed using Primer3 (www.primer3plus.com) and ordered at Thermo Fisher Scientific or Integrated DNA Technologies.

4.6.6 cDNA vector generation

The overexpression of STX18 was achieved with a retroviral MSCV vector (provided by the group of Dr. Grüner). The CDS was amplified from A549 cDNA using a forward primer that contained an *EcoRI* site and the Kozak sequence and a reverse primer that contained a *BglII* site. The PCR product was purified digested with *EcoRI* and *BglII*, and run on a TAE gel with the equally digested vector. Following gel purification, PCR product and vector were ligated and transformed into Stbl3 cells (Invitrogen). Two bacterial clones were selected for DNA isolation and sequencing. Both showed an error-free sequence. Resulting vectors were named STX18-1 and STX18-2. The vector without STX18 CDS was used as a control vector.

4.6.7 CRISPR SAM

The CRISPR/Cas9 SAM System was additionally used to overexpress STX18 (Konermann et al. 2015). The system is comprised of three individual vectors: Lenti dCas-VP64-Blast, Lenti-MS2-P65-Hygro and Lenti-sgRNA(MS2)Puro that were purchased from Addgene (see section 8.2.2). Briefly this system makes uses of three activation domains (VP64, P65 and HSF1) that mediate a stable transcriptional activation. Two pairs of gRNAs were designed using the Cas9 Activator Tool provided by the Zhang lab and ligated into the vector as described by Ran *et al.*

(Ran et al. 2013) using *Esp3I* cutting sites. Cloning experiments with the CRISPR SAM system were done by Marc Schulte.

4.6.8 Plasmid isolation

Plasmid isolation from bacterial cells was done using either the QIAprep Spin Miniprep Kit (QIAGEN) or the Plasmid Plus Maxi Kit (QIAGEN) for small scale and large scale isolation, respectively. Isolations were carried out according to manufacturer's protocol.

4.6.9 Restriction digest

Conventional restriction digest of either plasmid DNA or purified PCR product was done for 1-2 hours at 37°C. For double digests, the buffer recommended by the manufacturer or FastDigest Green Buffer (Thermo Fisher Scientific) was used. Samples, including negative controls in form of undigested DNA, were run on an agarose gel to evaluate fragment patterns.

4.6.10 Transformation of competent bacteria

Plasmid DNA was transformed into One Shot® Stbl3™ chemically competent E. *coli* (Invitrogen) according to the manufacture`s protocol.

4.6.11 Sequencing

Sanger sequencing of Plasmid DNA was done by Microsynth Seqlab.

4.7 Generation of stable Transgenic Cell Lines

Note that viral particles are handled at BSL-2.

4.7.1 Transfection

Lentiviral particles were produced by HEK293 FT cells using cotransfection of the packaging plasmid pSPAX (gag and Pol) and the envelope plasmid pMD2.G (VSV-G).

Retroviral particles were produced in Phoenix cells (FNX), with the packaging plasmid HIT60 (gag and pol) and the envelope plasmid pCMV-VSV-G.

Cells were seeded on fibronectin-coated 10 cm dishes 24 hours before transfection, to reach approximately 70% confluency. 1 to 4 hours prior to transfection medium was replaced by 6 ml fresh medium without antibiotics.

In general, FuGENE HD Transfection Reagent was used in polypropylene tubes only and was pipetted directly into the medium. A positive (GFP/RFP) and a negative control was used in every experiment and master mixes were used when suitable.

For each sample 15 µl FuGENE HD Transfection Reagent was added to 485 µl Opti-MEM and incubated for 5 minutes. In the meantime, 7.5 µg DNA (3 µg packaging plasmid, 1.5 µg envelope plasmid, 3 µg POI) were diluted in 500 µl Opti-MEM. Subsequently, the FuGENE-Mix was added to the DNA-Mix in a dropwise manner, vortexed shortly, and incubated for 15 minutes after which the transfection mix was added dropwise to the cells. After 24 hours the supernatant was removed, cells were washed twice with PBS and 6 ml fresh medium was added. Another 48 hours later, the transfection efficiency was determined using flow cytometry or fluorescence microscopy when applicable. The viral supernatant was filtered using 0.45µm filters and either used immediately for transduction or stored at -80°C.

4.7.2 Transduction

Cells were seeded in 6-well plates the day before transduction, when they were ~60% confluent. For the transduction 1 ml medium per well supplied with 5 µg/ml polybrene and 300 – 500 µl viral supernatant were used. After 24 hours the supernatant was discarded, cells were washed twice with PBS, and 2 ml fresh medium were added. Another 24 hours later, transduction efficiency was determined using flow cytometry or fluorescence microscopy when applicable. Furthermore, antibiotic selection was started or cells were expanded for subsequent cell sorting.

4.7.3 Antibiotic selection

Transduced/Transfected cells were selected by addition of appropriate concentrations of antibiotics to the culture medium for 7 days. Concentrations of selecting agents were used that lead to complete cell death after 7 days in mock-transduced/transfected control cells. The respective concentrations are given in Table 1.

Table 1: Concentration of Antibiotics used for selection process.

Cell line	Antibiotic	Concentration
A549	Puromycin	1mg/ml
	G418	800µg/ml
	Blasticidin	100µg/ml
	Hygromycin	200µg/ml
H1975	Puromycin	0.5mg/ml

4.7.4 Cell sorting

Sorting of GFP-positive cells was done by K. Lennartz using a BD FACSVantage SE with BD FACSDiVA Option (BD Biosciences) that was modified by addition of a S2 bench as described in Lennartz *et al.* (Lennartz et al. 2005).

4.7.5 Generation of single cell clones

Single-cell clones were generated using serial limiting dilution. Cells were harvested, counted, and diluted to a concentration of 2.5 cells/ml. A 96-well plate was filled with 200 µl of the dilution per well and cultivated for several days at 37°C and 5% CO_2, after which wells containing single-cell colonies were marked and cultivated further until the wells reached a confluency of ~60%. Monoclonal lines were expanded to larger dishes until cells could be used for experiments or long-term storage in liquid nitrogen.

4.8 *In vivo* Experiments

For orthotopic transplantation of lung cancer cells, $1*10^6$ cells in 10µl PBS/Matrigel® (Corning Incorporated) were prepared per mouse. Mice were narcotized using isoflurane and placed on a heating plate to prevent hypothermia. A small incision was made on the left lateral thorax, and 10µl cell/Matrigel suspension was injected into the left lung, carefully avoiding injecting any air bubbles. The incision was sutured and mice were injected with Carprofen as analgesic.

Subsequently, tumor growth and development of metastases was followed *in vivo* using a IVIS Lumina II (Caliper Life Science) at the IMCES of the University Hospital Essen. To this end, Luciferin (Caliper Life Science) was diluted in PBS, filtrated using a 0.2µm filter and placed in the dark on ice. Immediately prior to imaging, mice were narcotized using isoflurane, injected i.p. with 150µl Luciferin, placed in the imaging device and imaged.

Irradiation of mice was conducted using the RS320 X-ray irradiator (X-Strahl) available at the group of Prof. Stuschke/Sak and with help from M. Groneberg. Mice were narcotized using isoflurane and the left lung was irradiated at a dose of 10 Gy while shielding the rest of the body.

The *in vivo* experiments were conducted with the help of Prof. Dr. A. Schramm., Dr. F. Breitenbücher, S. Nothdurft, K. Batzke and S. Vogt.. Dr. F. Breitenbücher performed the procedure of injecting the cells into the lung.

All *in vivo* experiments were approved by the Landesamt für Natur, Umwelt und Verbraucherschutz Nordrhein-Westfalen (Az. G1399/13).

4.9 Gene Ontology Analysis

Gene ontology analysis was done using the online tool provided at geneontology.org (Ashburner et al. 2000; Thomas et al. 2003, 2006; Carbon et al. 2009, 2017; Mi et al. 2009).

Figures in this work are based on data provided by the GO Ontology database (released 2017-12-27) using the PANTHER overrepresentation test (released 2017-12-05). Data was analyzed using a Fisher test.

4.10 Statistics

Statistical analysis was done for experiments carried out in at least 3 biological replicates. If not stated otherwise, graphs show mean +/- SEM. For statistical analysis GraphPad Prism 6 was used, applying t-test or ANOVA where applicable.

The following representations for P-values/ the level of significance were used:

ns (not significant)	$P > 0.05$
*	$P \leq 0.05$
**	$P \leq 0.01$
***	$P \leq 0.001$

5. Results

5.1 Functional Genomics Screen for Modulators of the Radiation Response of Non-small Cell Lung Cancer

To identify novel targets for personalizing chemo-radiotherapy strategies in NSCLC, a functional genomic screen was conducted in a human NSCLC cell line *in vitro* (Figure 5).

To determine the most appropriate cell model for this screen, the NSCLC cell lines A549 and H1299 were irradiated with doses from 0 Gy to 10 Gy. Apoptotic cell death (fraction of cells with subgenomic DNA, “Sub-G1 cells”) was determined 72 hours later using flow cytometry (Figure 6A). A549 cells exhibit high resistance against irradiation with only minor increases in cell death after applying 10 Gy. In contrast, H1299 cells exhibited approximately 25% of apoptotic cells after irradiation with 10 Gy. Accordingly, A549 cells were chosen for the screen as it was intended to identify targets mediating intrinsic radioresistance. Next the irradiation setup was tested. Screening a very high number of cells was necessary to ensure a sufficient representation of all shRNA constructs of the library that was selected. It is recommended to transduce a number of cells that exceeds the complexity of the library by 1,000-fold, i.e. 90 x 10^6 cells, because transduction should be done with an efficiency of about 30% as measured by flow cytometry (Figure 6C) to ensure only uptake of a single shRNA vector per cell. Irradiation of large cell number cultured in dishes is very time consuming and increases contamination risk because of the transport to the irradiation device. Consequently, the irradiation setup was tested while cells were in suspension. A549 cells as well as A549 cells stably expressing an shRNA suppressing endogenous *BCL-xL* (A549 shBCL-xL, positive control) and the respective control cell line (A549 shCtrl, negative control) were used. Cells were irradiated while either adherently growing on a dish, or in suspension after harvesting. Immediately after irradiation suspension cells were reseeded on cell culture dishes. No difference in the amount of apoptotic cells could be observed 72 hours after between cells irradiated when adherent or in suspension (Figure 6B). For this reason, the selection process of this screen was performed by irradiating pooled cell suspensions. This method also prevents unequal distribution of shRNA transduced cells between different dishes.

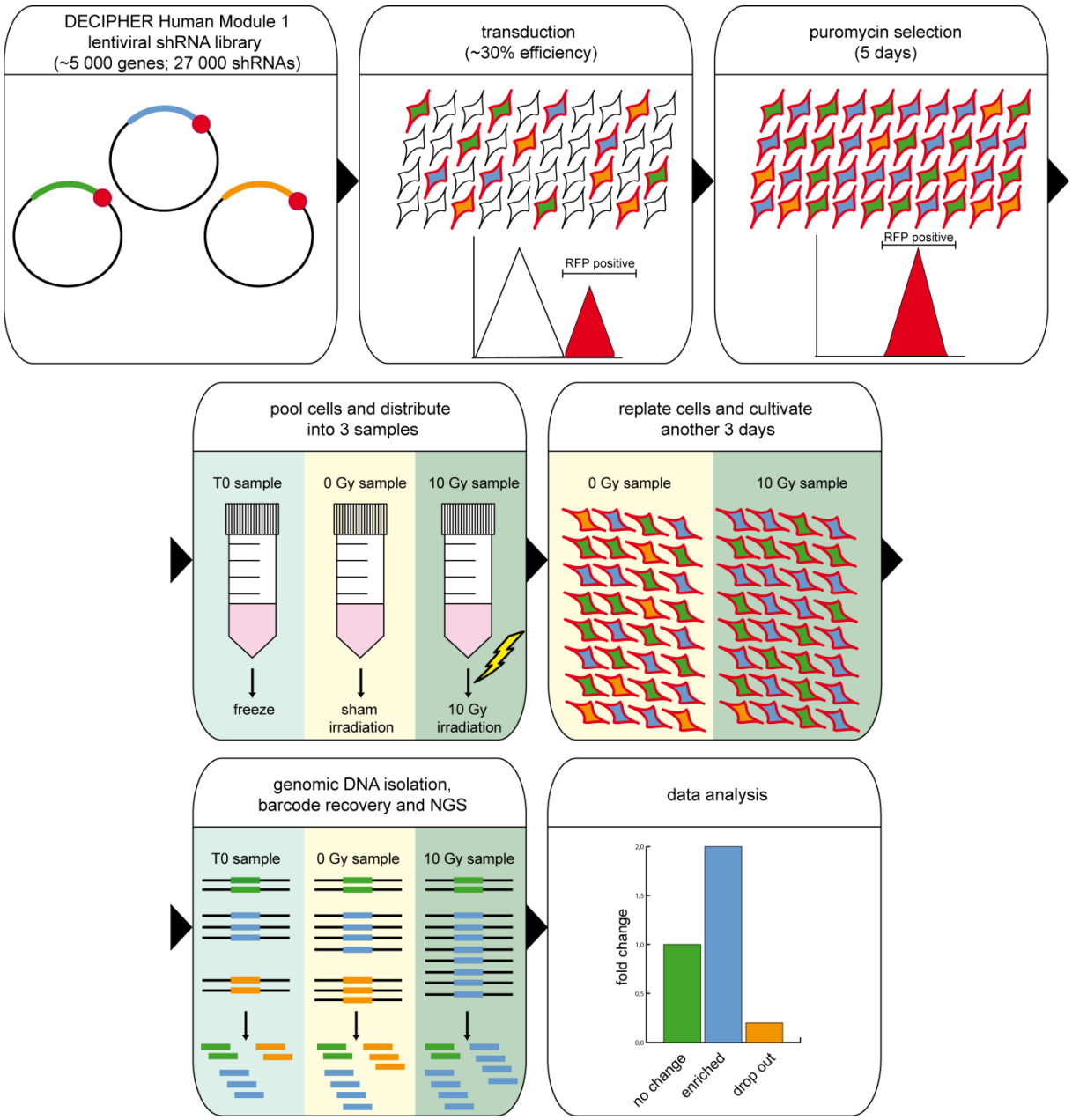

Figure 5: Schematic overview of the functional genomic screen conducted to identify novel modulators of the radiation response.
In short, lentiviral particles were generated using the DECIPHER Human Module 1 shRNA Library, A549 cells were transduced, selected with puromycin, and cells either frozen to show the initial shRNA distribution or irradiated (0 Gy vs. 10 Gy). Subsequently, DNA was isolated and sequenced for further analysis.

For the screen cells were seeded and transduced with an appropriate amount of viral supernatant containing shRNA library-encoding lentiviral particles on the next day. Transduction efficiency was determined using flow cytometry 48 hours later and cells were selected with puromycin for 5 days (Figure 6C). After harvesting and pooling them, cells were divided into three samples: “T0 cells” were frozen to preserve the initial representation of shRNAs, the “10 Gy sample” was irradiated with 10 Gy and the “0 Gy sample” was sham irradiated. Irradiation was done while cells were in

suspension, cells were replated immediately afterwards and cultured for another 3 days. Then all adherent cells were harvested and genomic DNA was isolated.
Subsequently, shRNA-specific barcodes were amplified and sequenced on the Illumina® HiSeq platform by BioCat GmbH. Two independent transduction experiments were performed; no cells were discarded during the process.
shRNA sequences whose abundance decreased or increased by at least 40% in both experiments were considered as “hits” (see section 8.1). shRNAs enriched after irradiation were considered to target genes that confer radiosensitivity. Consequently shRNAs reduced after irradiation were considered to target genes conferring radioresistance. These hits were further analyzed using the Gene Ontology and Panther database (http://geneontology.org/) (Ashburner et al. 2000; Thomas et al. 2003, 2006; Carbon et al. 2009; Mi et al. 2009) that allows enrichment analysis of given datasets. First, enriched biological processes were analyzed. Interestingly, several of hits were involved in the Wnt singaling pathway, intracellular transport, or in the response to organic stimuli (Figure 7, Table 2). Focusing on enriched cellular components showed that several hits belong to the SNARE complex (STX16, 18, 19) (Figure 8). Extensive literature research that is summarized in the discussion part of this thesis revealed the following signaling pathways / proteins to be selected for further characterization:

Choline metabolism: PLA2G4B (Phospholipase A2 Group IVB), shRNA negatively selected

Wnt signaling: FZD5 (Frizzled Class Receptor 5), shRNA negatively selected

Vesicular transport: STX18 (Syntaxin 18), shRNA negatively selected

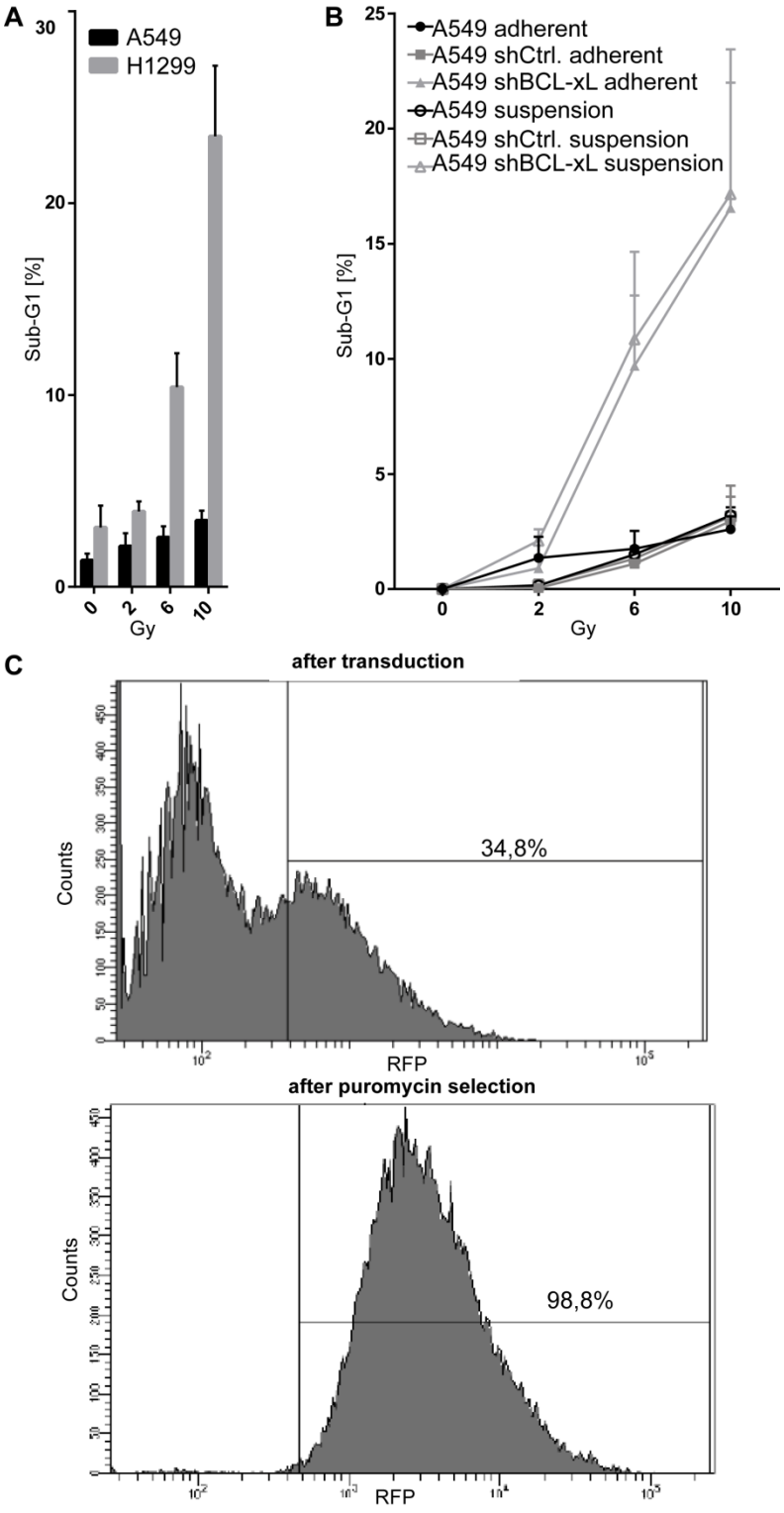

Figure 6: Optimization steps for the shRNA screen.
A: Cell cycle analysis of irradiated NSCLC cell lines. Cells were irradiated and the amount of apoptotic cell death (Sub-G1) was measured using PI-Staining 72 hours later. **B:** Cell Cycle analysis of A549 cells irradiated while adherent vs. cells irradiated while in suspension. Cells were irradiated and the amount of apoptotic cell death (Sub-G1) was measured using PI-Staining 72 hours later. Previous studies have shown that shRNA mediated knockdown of *BCL-xL* leads to increased cell death after irradiation. No difference could be observed between both growth conditions. **C:** Flow cytometric analysis of RFP+ cells in one of two screening approaches. Transduction efficiency was tested after 48 hours and determined to be 34.8%. After puromycin selection only RFP positive cells remained. RFP gates were adjusted using RFP negative control cells. Data shown for one of two independent experiments.

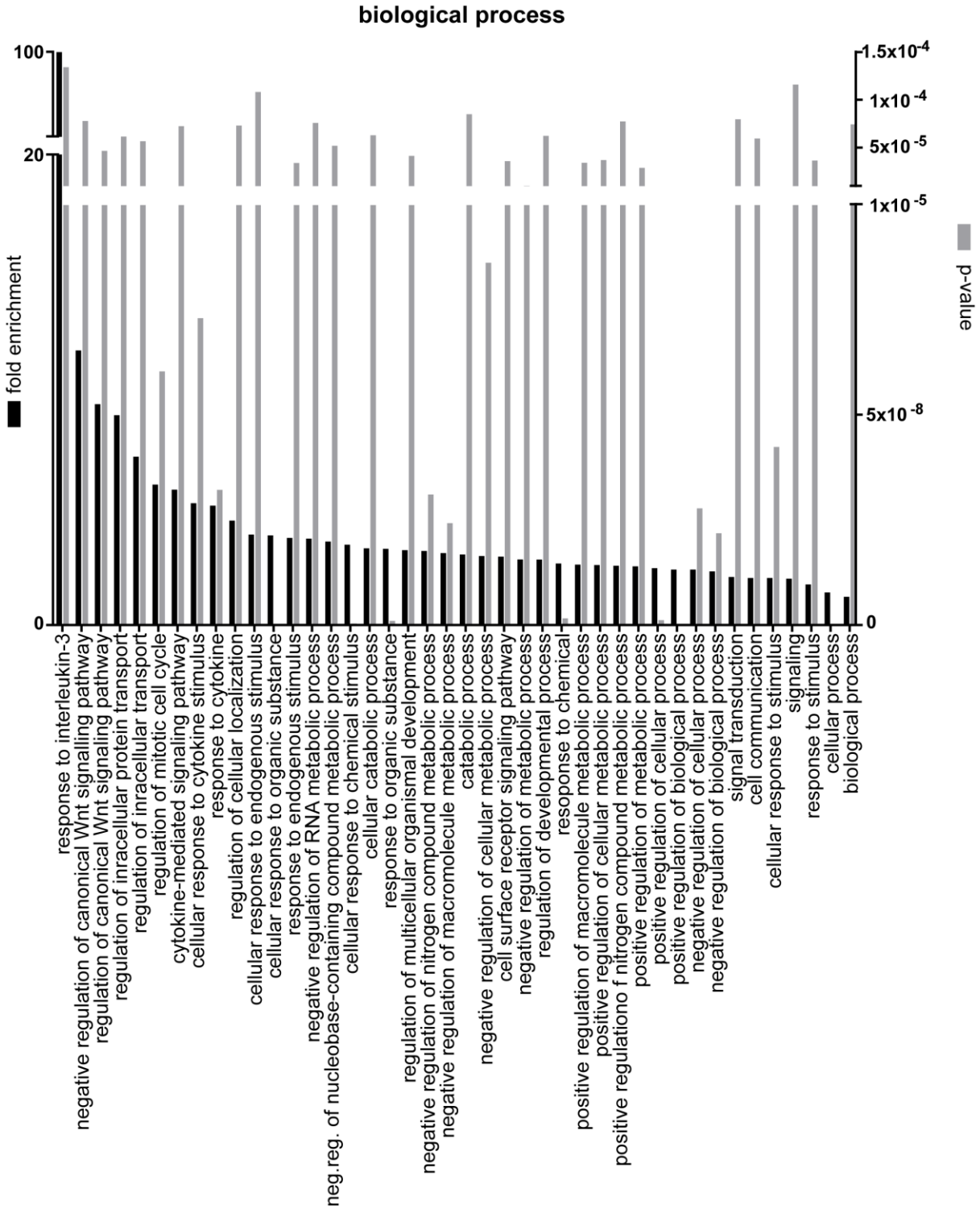

Figure 7: Enrichment Analysis (biological processes) of the identified targets using the Gene Ontology/Panther database.

Table 2: Overview of the identified targets that are enriched in distinct biological processes.
Proteins choosen for further characterization are marked in green.

Biological Process	
regulation of canonical Wnt Signaling Pathway	
Gene ID	**Gene Name**
PSMA1	Proteasome subunit alpha type-1
FZD5	Frizzled-5
GSK3A	Glycogen synthase kinase-3 alpha
PSMA5	Proteasome subunit alpha type-5
WNT5B	Protein Wnt-5b
CYLD	Ubiquitin carboxyl-terminal hydrolase
cellular response to organic substance	
Gene ID	**Gene Name**
SH2B2	SH2B adapter protein 2
PSMA1	Proteasome subunit alpha type-1
IRF2	Interferon regulatory factor 2
XCL1	Lymphotactin
MSX1	Homeobox protein MSX-1
APEX1	DNA-(apurinic or apyrimidinic site) lyase
DDX18	ATP-dependent RNA helicase
WIPI1	WD repeat domain phosphoinositide-interacting protein 1
HCLS1	Hematopoietic lineage cell-specific protein
GSK3A	Glycogen synthase kinase-3 alpha
CXCL13	C-X-C motif chemokine 13
DUOX1	Dual oxidase 1
MBTPS2	Membrane-bound transcription factor site-2 protease
RXRB	Retinoic acid receptor RXR-beta
PSMA5	Proteasome subunit alpha type-5
PDE2A	cGMP-dependent 3',5'-cyclic phosphodiesterase
BPTF	Nucleosome-remodeling factor subunit BPTF
WNT5B	Protein Wnt-5b
CES1	Metallothionein-2
PLA2G4B	Cytosolic phospholipase A2 beta
FOXC2	Forkhead box protein C2
regulation of intracellular transport	
Gene ID	**Gene Name**
STX18	Syntaxin-18
FZD5	Frizzled-5
SREBF2	Sterol regulatory element-binding protein 2
GSK3A	Glycogen synthase kinase-3 alpha
PDE2A	cGMP-dependent 3',5'-cyclic phosphodiesterase
CYLD	Ubiquitin carboxyl-terminal hydrolase
B3GAT3	Galactosylgalactosylxylosylprotein 3-beta-glucuronosyltransferase 3

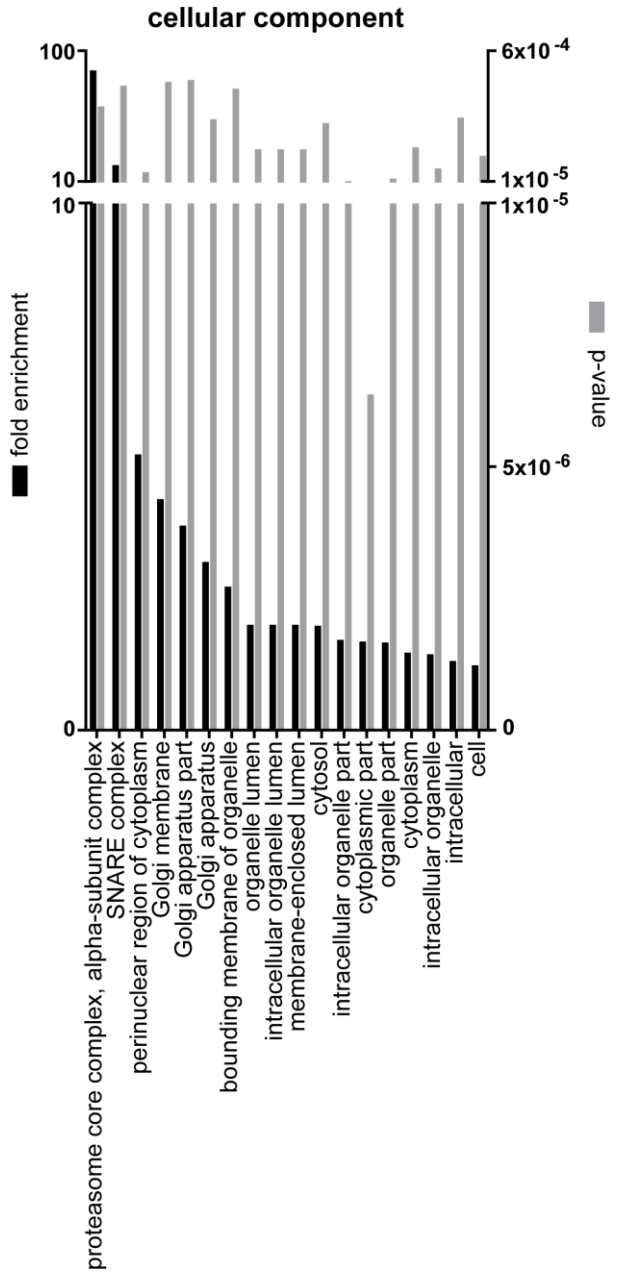

Figure 8: Enrichment analysis for cellular components of the identified targets by using the Gene Ontology/Panther database.

5.2. Functional Validation of Selected Hits

5.2.1 Knockdown of *FZD5* does not influence radiation response in NSCLC

The shRNA screen nominated several targets involved in the Wnt signaling pathways as putative modulators of the radiation response, including GSK3A, WNT5B, and FZD5. The Wnt pathway is an evolutionarily conserved pathway mediating crucial functions in embryonic development where it controls cell fate specification and axis patterning (Komiya and Habas 2008; MacDonald et al. 2009). Aberrant Wnt signaling was demonstrated to be involved in carcinogenesis (MacDonald et al. 2009; Zang et al. 2014; Zhan et al. 2017).

The hit FZD5 was chosen for further validation. FZD5 (Frizzled class receptor 5) is the receptor for the Wnt5A ligand. A xenograft study with human tumors revealed that inhibition of frizzled receptors using the monoclonal antibody OMP-18R5 could inhibit tumor growth (Gurney et al. 2012).

To analyze the effect of FZD5 downregulation on the irradiation response, clonal cell lines stably expressing an shRNA targeting *FZD5* (shFZD5) vector were generated using the NSCLC lines A549 and H1975. A non-mammalian shRNA target vector (shCtrl) was used as a control.

Western blot using an anti-FZD5 antibody was performed to evaluate knockdown efficiency. In A549 cells, all of the generated clonal cell lines showed varying degrees of FZD5 suppression when compared to the control cell line (shCtrl) or with the original cell pool (shFZD5) (Figure 9A). In H1975 cells, the clones K1, K5 and K11 showed effective suppression of FZD5 when compared to controls (Figure 9A).

In a subset of cell lines (A549 shFZD5 K1 / K15 / K16; H1975 shFZD K1 / K4 / K5 / K11) this FZD5 suppression was also validated at the mRNA level using qRT-PCR (Figure 9B).

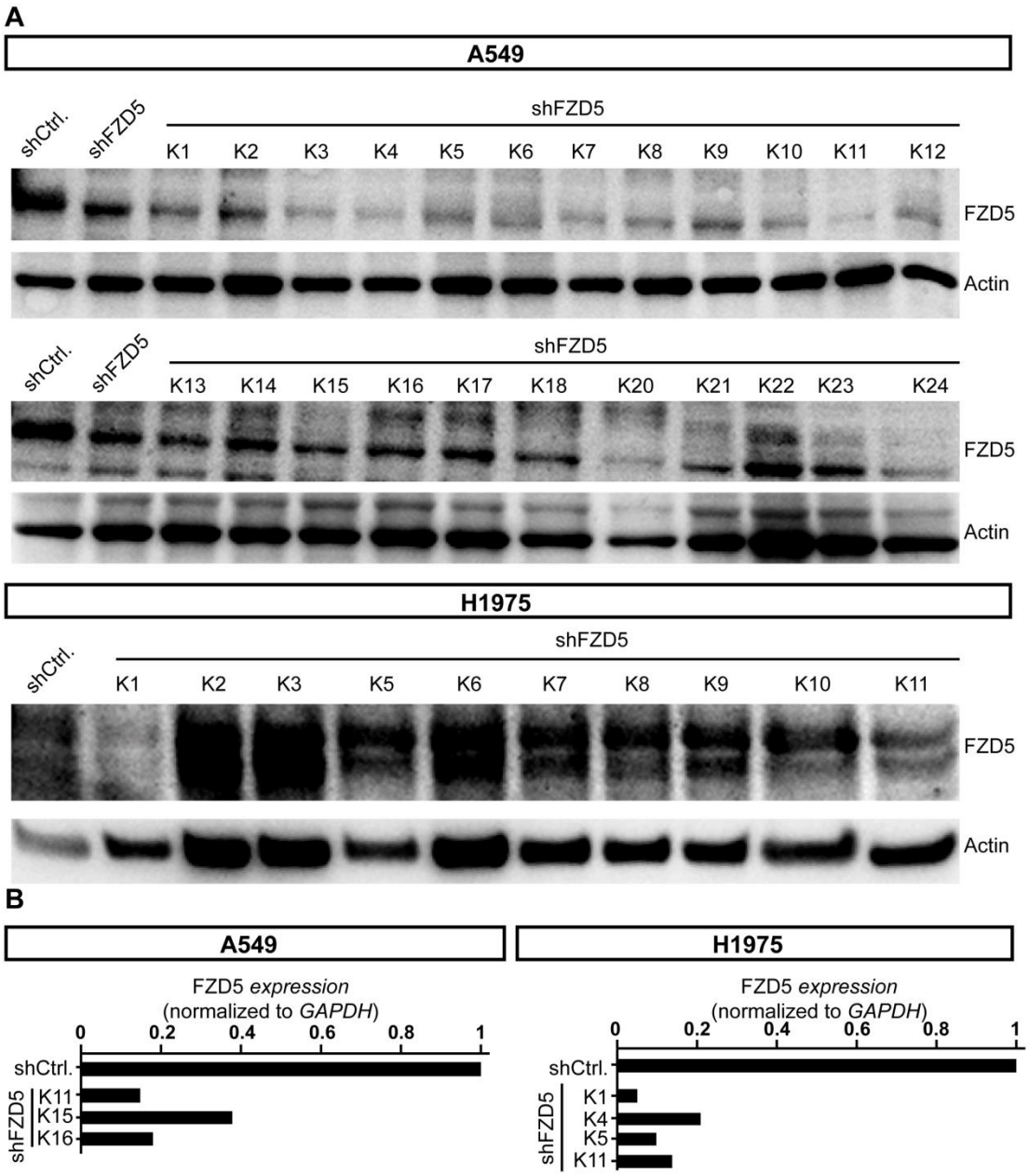

Figure 9: Stable expression of shFZD5 leads to successful knockdown of *FZD5* in several clonal cell lines. **A:** The FZD5 protein levels were assessed using western blot. Actin was used as a reference. **B:** Expression of *FZD5* RNA level was assessed using qRT-PCR. *GAPDH* was used as a reference and expression of shCtrl cell line was set to 1 (n=1).

In a first experiment, short-term survival of cell populations and clones was analyzed using cell cycle analysis (Figure 10A). Cells were irradiated at doses ranging from 0 Gy to10 Gy and apoptosis (Sub-G1 fraction) was measured 24 hours, 48 hours or 72 hours later using flow cytometry. For A549 cells, the shFZD5 knockdown pool cells, as well as 7 clones (A549-shFZD5 K3, K4, K7, K11, K15, K16, K24) were tested. For H1975, 4 clones (H1975-shFZD5 K1, K4, K5, K11) were tested. In A549-shFZD5 cells, only slight differences in apoptotic cell death between control cells and FZD5-deficient (clonal) cells were detected. Only A549 shFZD5 K16

showed a marked increase in apoptotic cell death following irradiation with 10 Gy. On the other hand, A549–shFZD5 K15 seemed to be more resistant when compared to the respective control cells. In H1975 cells, all four clonal cell lines showed decreased apoptotic cell death following irradiation when compared to the control cell line (Figure 10B). In H1975-shFZD5 K1, K4, and K5 this effect reached statistical significance.

To evaluate long-term survival following irradiation with 2 Gy, 6 Gy, and 10 Gy colony formation assay was used in A549-FZD5 K15 and K16 (Figure 10C, left panel). The surviving fractions following irradiation were calculated by normalizing the arising colonies to the plating efficiency determined by unirradiated controls. No differences in the surviving fraction between the *FZD5* knockdown cell lines and the control cell line could be observed. Colony formation assay in H1975-shFZD5 K1, K4, K5, and K11 revealed no significant differences in the surviving fraction when compared to control cells (Figure 10, right panel).

Overall, the knockdown of *FZD5* did not seem to impact on the radiation response of A549 and H1975 cells under the experimental conditions used in our study. Therefore, FZD5 was not pursued for further analyses.

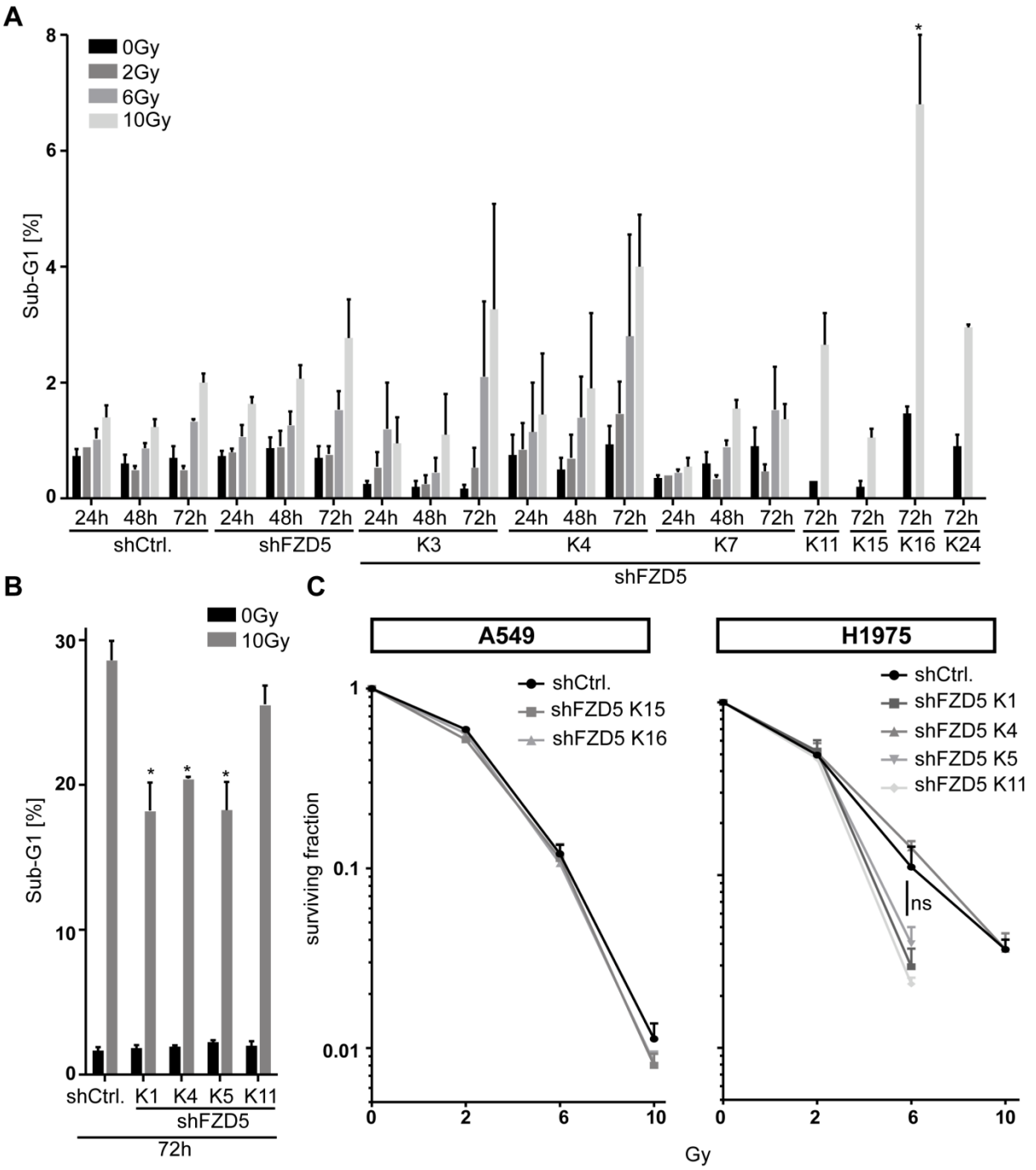

Figure 10: Analysis of the influence of *FZD5* knockdown on radiosensitivity.
A: Short-term survival assay in A549 cells. Cells were irradiated (0 Gy-10 Gy) and the amount of apoptotic cell death (Sub-G1 fraction) was determined at the indicated time points. (mean ± SEM) **B:** Short-term survival assay with H1975 cells was conducted as in A (mean ± SEM). **C:** Colony formation assay was used to determine long-term survival following irradiation (mean ± SEM).

5.2.2 Knockdown of *PLA2G4B* increases radiosensitivity in NSCLC cell lines

PLA2G4B was another hit of the shRNA screen and encodes a protein involved in choline metabolism. Choline is an essential nutrient that is a constituent of the cell membranes' phospholipids and hence is needed to maintain the cells' structural integrity (Michel et al. 2006; Sanders and Zeisel 2007). Recently, alterations in choline metabolism have been associated with carcinogenesis and tumor progression. Several key enzymes are elevated in cancers thus potentially being of prognostic use (Finney et al. 2000; Glunde et al. 2011; Awwad et al. 2012).

The shRNA vector targeting *PLA2G4B* were negatively selected in our screen. Thus, the hypothesis was that a knockdown of *PLA2G4B* leads to increased radiosensitivity. To study the role of PLA2G4B in the response to ionizing radiation, A549 cells were lentivirally transduced to express an shRNA targeting *PLA2G4B* (shPLA2G4B) or a control shRNA (shCtrl). Subsequently clonal cell lines were generated by serial dilution. Three of the clonal cell lines (A549 shPLA2G4B K3, K11 and K14) were chosen for Western blot analysis, which revealed suppression of *PLA2G4B* in A549 shPLA2G4B K3 cells (Figure 11A). Short-term survival analysis using flow cytometry revealed increased radiosensitivity in shPLA2G4B K3 cells when compared to A549 shCtrl and the other two clonal A549 shPLA2G4B cell lines (Figure 11B). This result was confirmed by colony formation assay, where A549 shPLA2G4B K3 also showed a reduction in clonogenic survival when compared with A549 shCtrl cell lines (Figure 11C). Colony formation assays also revealed an increased radiosensitivity of A549 shPLA2G4B K14, although suppression of PLA2G4B protein was not confirmed by Western blotting. Because of this inconsistency PLA2G4B was not selected for further characterization.

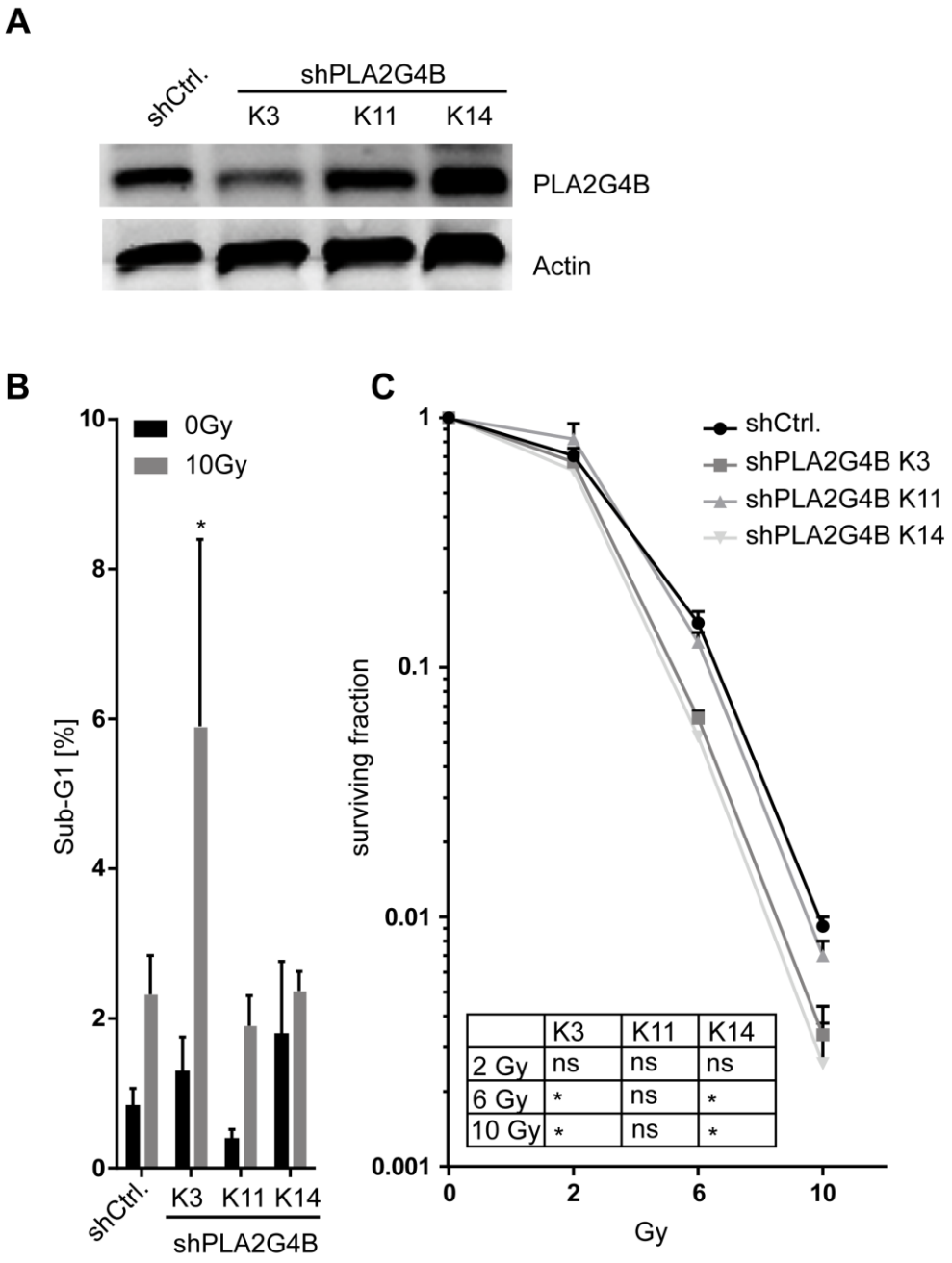

Figure 11: Characterization of clonal A549 *PLA2G4B* knockdown cell lines.
A: The PLA2G4B protein levels were determined using Western blot. Actin was used as a reference. **B:** Short-term survival assay to assess the apoptotic cell death following irradiation. Cells were seeded, irradiated with 0 Gy or 10 Gy on the following day and the amount of apoptotic cell death (Sub-G1 fraction) was determined 72 hours later using flow cytometry. (mean ± SEM; n=3) **C:** Colony formation assay was used to evaluate long-term survival following irradiation (mean ± SEM).

5.2.3 Regulators of vesicular trafficking impact on the radiation response of specific lung cancer models

Several targets identified by the functional genomic screen belong to the SNARE protein family of the cells transport machinery. Vesicular transport is a key mechanism involved in a wide range of cellular processes responsible for delivery of biomolecules within the cell, as well as the uptake and secretion of molecules. In this context, vesicle fusion is a fundamental process regulated by SNARE proteins, which have been implicated in cancer signaling and progression (Teng et al. 2001; Duman and Forte 2003; Hsu and Yang 2009; Meng and Wang 2015).

Against this background it was decided to further study the influence of an inhibited vesicular transport on the radiotherapy response in NSCLC cells. In a first set of experiments, vesicular transport was chemically inhibited by the lactone Brefeldin A and the impact on the radiation response of NSCLC cells was studied (see section 5.2.3.1). In the second part, expression of the SNARE protein Syntaxin 18 (STX18) was suppressed by shRNA in NSCLC cells, and the functional consequences on the radiation response were studied (see section 5.2.3.2).

5.2.3.1 Inhibition of vesicular trafficking by Brefeldin A increases radiosensitivity in radioresistant A549 lung cancer cells

Brefeldin A (BFA) is a bacterial lactone that efficiently inhibits protein transport between ER and Golgi. It is used as standard reagent for the study of protein transport (Fujiwara et al. 1988; Alvarez and Sztul 1999).

Optimal inhibitory concentrations of BFA were determined in NSCLC cells. The secreted protein TGFBI (Transforming Growth Factor Beta Induced) was used as a marker protein. Under regular culture conditions, TGFBI is secreted into the cell culture medium. If BFA inhibits protein transport, and thus protein secretion, BFA treatment should decrease the amount of TGFBI secreted into the medium while increasing intracellular TGFBI levels. A549 and H1975 NSCLC cells were treated with BFA (50ng/ml) for 24 hours and the levels of TGFBI present within the cells as well as in the medium were assessed using Western blotting (Figure 12A). An H1975 cell line stably expressing a shTGFBI vector was used as negative control. As expected, BFA inhibited secretion of TGFBI in the A549 and H1975 cells, leading to increased intracellular protein levels while protein levels in the supernatant decreased.

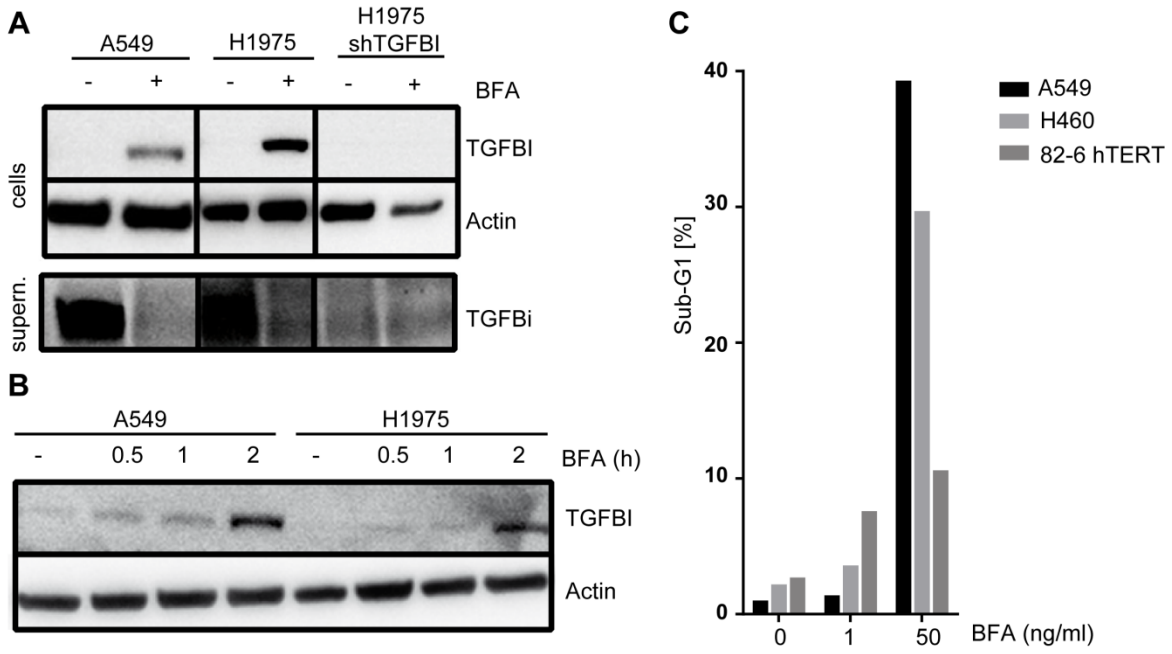

Figure 12: Initial characterization of the impact of BFA treatment on NSCLC cells.
A: Western blot was used to determine the TGFBI protein level following BFA treatment. Cells were treated with BFA (50ng/ml) for 24 hours in medium containing 0.5% FCS before proteins were extracted from cells and from supernatant (supern.). **B:** Western blot was used to determine the TGFBI protein levels following short-term BFA treatment. Cells were treated with BFA for the indicated time before proteins were extracted. **C:** Cell cycle analyzes was used to measure the amount of apoptotic cell death (Sub-G1 fraction) following BFA treatment. Cells were treated with the indicated amount of BFA for 48 hours (n=1).

To assess the kinetics of inhibition of TGFBI secretion by BFA (50ng/ml), cells were treated for 30 minutes to 2 hours and the amount of cellular TGFBI was visualized by Western blotting (Figure 12B). In both cell lines, intracellular TGFBI levels increased 30 minutes after treatment, with further increase after 2 hours. These results confirmed that BFA treatment is a useful tool to study protein transport and secretion, with its effect starting almost immediately.

Next, the NSCLC cell lines A549 and H460 as well as the fibroblast cell line 82-6 hTERT were treated with BFA for 48 hours and the amount of apoptotic cell death was determined using flow cytometry (Figure 12C). BFA at a concentration of 1ng/ml only marginally induced apoptosis, while 50ng/ml BFA effectively induced apoptotic cell death in the NSCLC cell lines. The fibroblast cell line was profoundly resistant against BFA-induced apoptosis, indicating tissue and possibly tumor selectivity.

Next, H1975 and A549 cells were treated with BFA (50ng/ml) for 4 hours and subsequently irradiated with doses from 0 Gy to 10 Gy. Apoptotic cell death was

determined by flow cytometry (PI-staining) at 24 hours, 48 hours and 72 hours after irradiation. BFA sensitized both cells lines to radiation-induced cell death. In A549 cells, treatment with BFA (50ng/ml) without irradiation led to about 8% of apoptotic cells after 24 hours. This increased to approximately 25% after 48 hours and to more than 50% after 72 hours (Figure 13A, left). Irradiation detectably increased apoptosis after 24 hours and 48 hours. After 72 hours an additive effect of irradiation was not consistently detectable on the already high background death induced by BFA alone (Figure 13A, left).

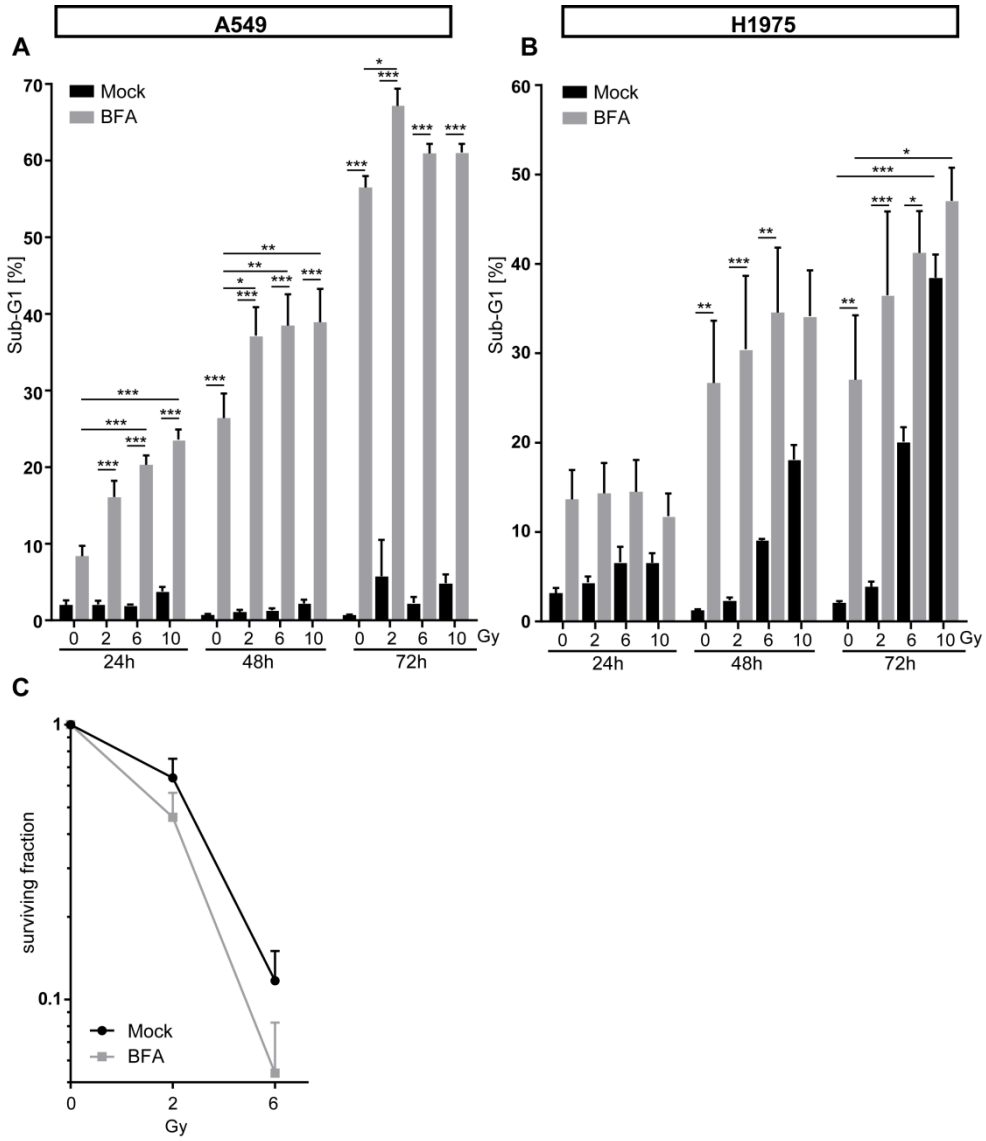

Figure 13: Assessment of the impact of BFA treatment on the irradiation response.
A: The influence of BFA treatment on radiosensitivity of A549 cells was assessed using cell cycle analysis (PI-staining). Cells were treated with BFA starting 4 hours before irradiation and the amount of apoptotic cell death was measured at the indicated time points. (mean ± SEM) **B:** The influence of BFA treatment on radiosensitivity of H1975 cells was assessed using cell cycle analysis (PI-staining). Cells were treated with BFA starting 4 hours before irradiation and the amount of apoptotic cell death was measured at the indicated time points. (mean ± SEM) **C:** Long-term clonogenic survival following irradiation (mean ± SEM).

H1975 cells were more sensitive to BFA and irradiation. Irradiation without BFA treatment with 6 Gy and 10 Gy increased apoptosis from <10% of cells at 24 hours

after irradiation to approximately 20% after 48 hours, and almost 40% after 72 hours (Figure 13A, right). Radiation-induced cell death was not further increased by BFA in H1975 cells (Figure 13A right).

To examine the impact of BFA treatment combined with irradiation on long-term survival of A549 cells, a colony assay was performed. BFA treatment further sensitized A549 cells to irradiation, leading to a decrease in clonogenic survival (Figure 13C).

5.2.3.2 Knockdown of *STX18* increased radiosensitivity of radioresistant A549 lung cancer cells

SNARE proteins are essential for a variety of cellular mechanisms, including vesicular transport and vesicle fusion. STX18 (Syntaxin18) is a SNARE protein bound to the ER-membrane and is involved in transport between ER and Golgi (Iinuma et al. 2009).

To study the contribution of STX18 to the irradiation response in NSCLC models, A549 and H1975 cells were transduced to stably express shRNA targeting *STX18* (shSTX18). The respective cell line expressing a non-mammalian shRNA target (shCtrl) was used as a control.

In A549 cells, qRT-PCR verified successful suppression of *STX18* mRNA to approximately 20% of control transcripts (Figure 14A). Suppressed STX18 protein expression confirmed by Western blotting using an anti-STX18 primary antibody (Figure 14B).

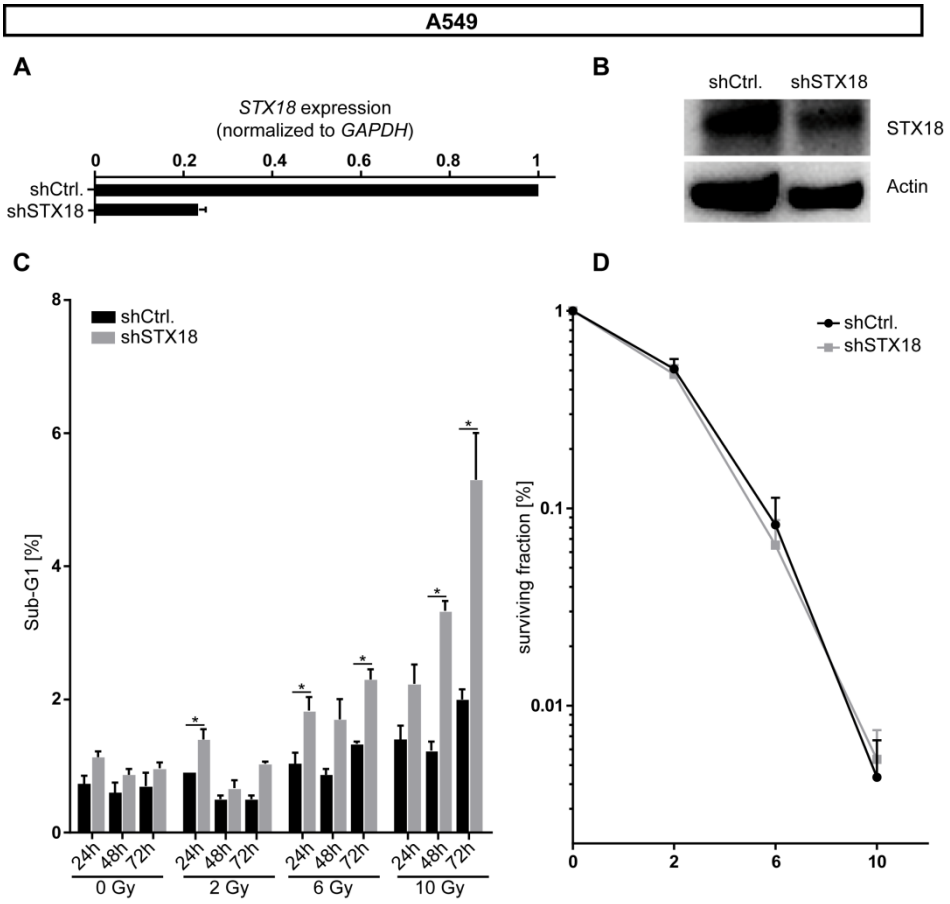

Figure 14: Initial characterization of A549 cells with stable *STX18* knockdown.
A: RNA was extracted and the expression of *STX18* mRNA was assessed using qRT-PCR. Expression is normalized to *GAPDH* and relative to expression of control. (mean ± SEM; n=3). **B:** Expression of STX18 protein was analyzed using western blot. Actin was used as a reference. **C:** Short-term survival assay using cell-cycle analysis (PI-Staining) by flow cytometry at the indicated doses and time points after irradiation. (mean ± SEM; n=3) **D:** Colony formation assay was done to assess the impact of *STX18* knockdown on long-term survival following irradiation. Colonies were counted and normalized to non-irradiated control cells. (mean ± SEM; n=3).

To study the impact of *STX18* knockdown on radiosensitivity cells seeded for 24 hours followed by irradiation at up to 10 Gy. The fraction of apoptotic cells (Sub-G1 fraction) was determined 24 hours, 48 hours, and 72 hours following radiation. There was no difference in viability between A549-shSTX18 and control cells (Figure 14C). Interestingly, A549-shSTX18 cells exhibited enhanced radiosensitivity at all doses and time points studied. This effect reached statistical significance (Figure 14C).

Next, colony formation assay was used to analyze the effect of *STX18* knockdown on the long-term survival following irradiation. Briefly, cells were seeded, irradiated 4-6 hours later and colonies were stained subsequently. No differences in the surviving fraction between A549 shCtrl and A549 shSTX18 cells could be detected (Figure 14D). Hence, at a population level STX18 appears to be primarily involved in the short term radiation response to apoptotic cell death. In contrast, the long-term response which usually is dominated by cell cycle arrest, senescence and non-apoptotic cell death seems less modulated by STX18.

To exclude the impact of heterogeneity in the studied cell population, single cell clones of the A549 shSTX18 cell line were generated by serial dilution. The resulting clonal population were named A549 shSTX18 K1 – K3, and suppression of *STX18* RNA by approximately 80% was confirmed by qRT-PCR (Figure 15A). Decreased STX18 protein levels were confirmed by Western blotting in A549 shSTX18 K3 (Figure 15B). Efficient knockdown was also verified using immunocytochemistry and microscopy (Figure 15D).

Despite exhibiting slightly increased base line apoptosis, A549 shSTX18 K3 clearly were more sensitive to radiation-induced apoptosis than control cells (Figure 14C). A549 shSTX18 K1 and K2 also showed increased apoptotic cell death following irradiation. In K1, these changes reached statistical significance at 72 hours after irradiation with 6 Gy and 10 Gy (Figure 15E).

Studying long-term clonogenic survival following radiation, all three clonal *STX18* knockdown cell lines showed significantly increased radiation sensitivity at 2 Gy and 6 Gy. A marked decrease in colony number in *STX18* knockdown cell lines could also be observed after irradiation with 10 Gy, although statistical significance was not reached (Figure 15C).

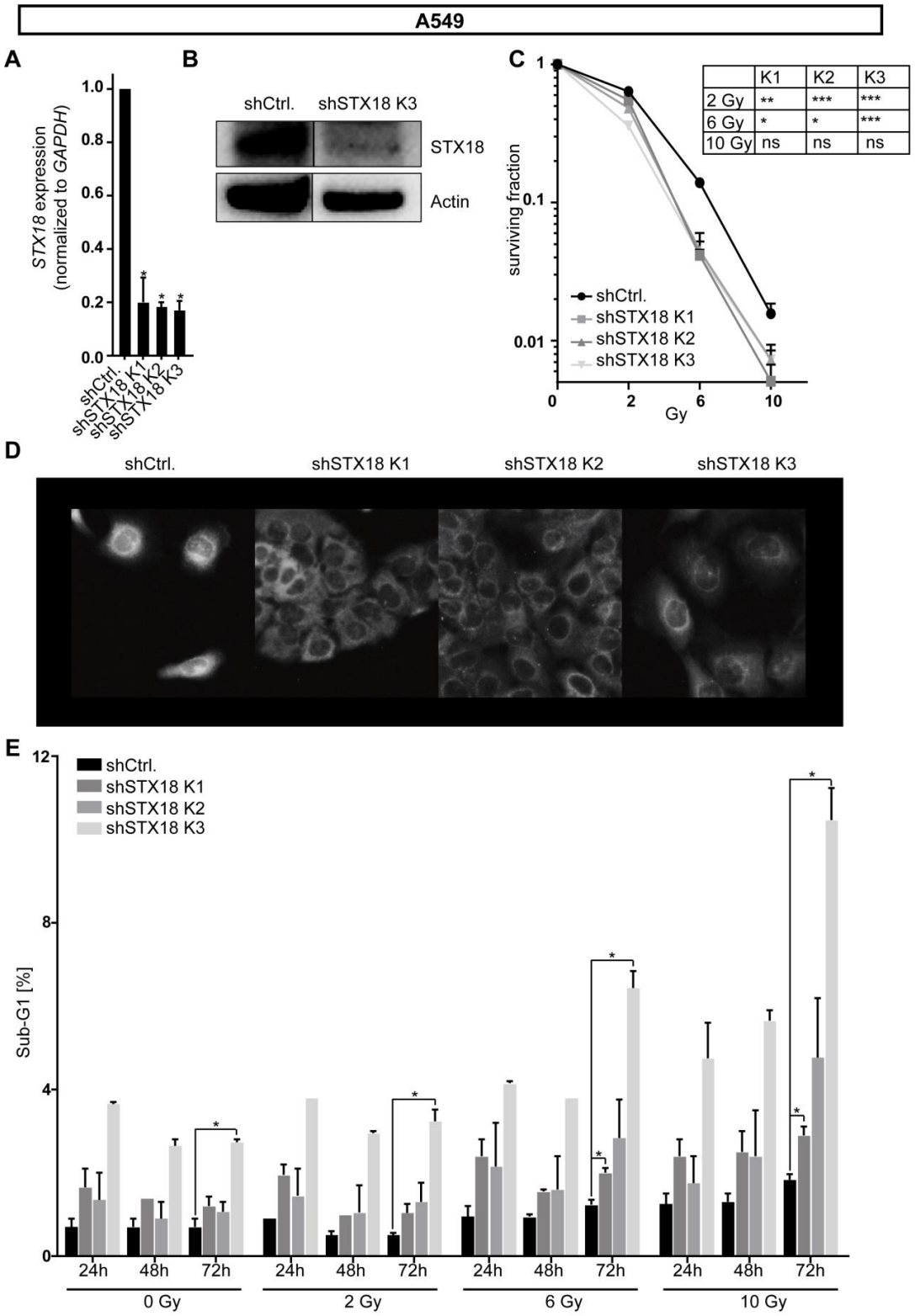

Figure 15: Characterization of clonal A549 *STX18* knockdown cell lines.
A: RNA was isolated from stable *STX18* knockdown cell lines as well as the control cell line. Expression of *STX18* mRNA was assessed using qRT-PCR. Expression is normalized to *GAPDH* and relative to expression of control. (mean ± SEM; n=3) **B:** Western blot was done to assess the STX18 protein level in A549 shCtrl as well as A549 shSTX18 K3 cells. **C:** Colony assay was used to analyze the effect of STX18 knockdown on long-term survival following irradiation. Number of surviving colonies was normalized to non-irradiated control. (mean ± SEM; n=3) **D:** Immunofluorescence staining of STX18 protein in three clonal STX18 knockdown cell lines as well as control cell line. **E:** Short-term survival assay to assess the influence of *STX18* knockdown cell viability following irradiation. Amount of apoptotic cell death (sub-G1) following irradiation (0 Gy-10 Gy) was determined using flow cytometry (PI-staining) at the indicated time points following irradiation. (mean ± SEM; n=2-3).

In a selected H1975 shSTX18 population, Western blot analysis revealed only slight differences in the STX18 protein expression as compared to controls (Figure 16A). Also there was no further sensitization of the radiation-sensitive H1975 cells by *STX18* knockdown. To the contrary there was increased radioresistance at higher doses and late time points (Figure 16B). Because the knockdown was not very efficient at a population level, clonal cell lines were generated with the aim to identify clones with stronger *STX18* suppression.

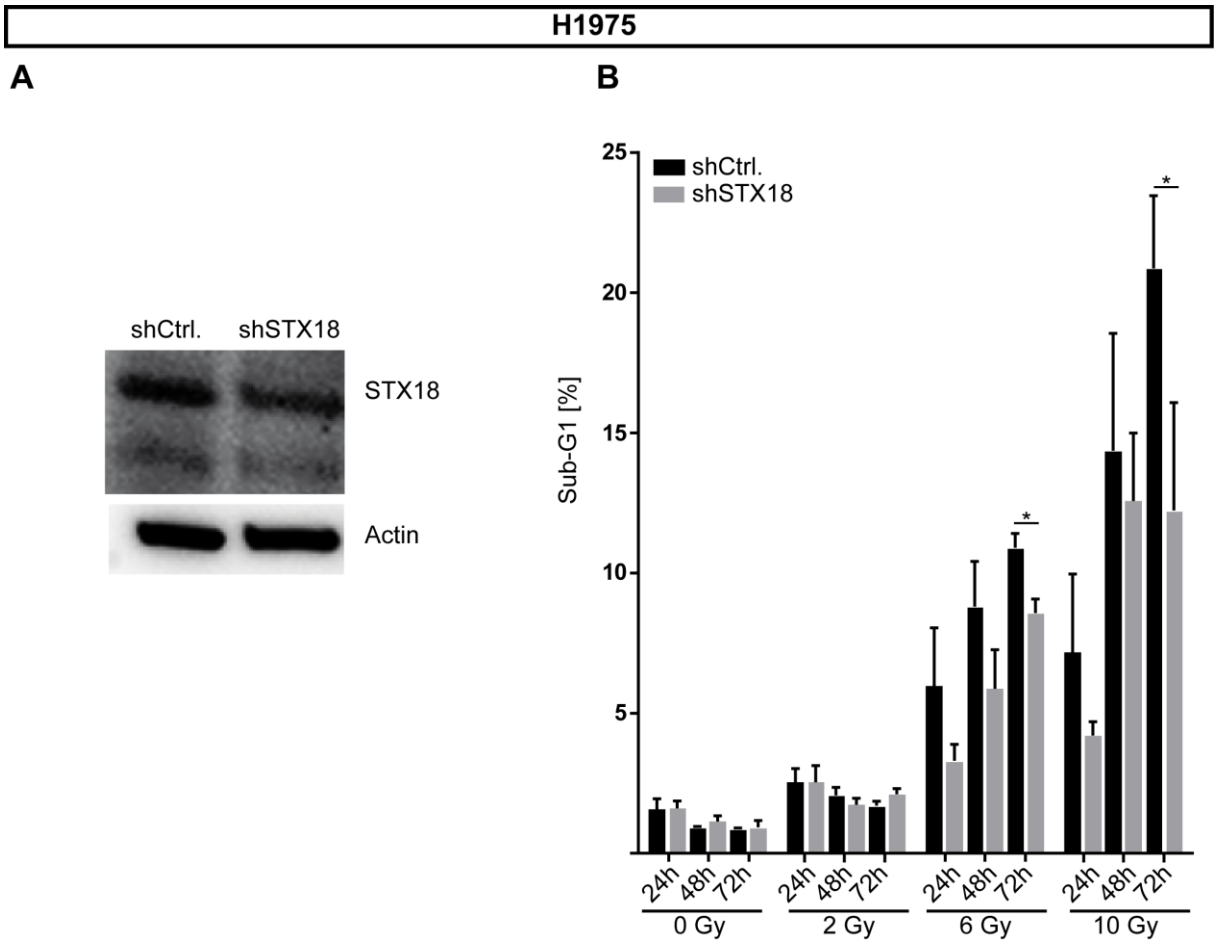

Figure 16: Characterization of H1975 stably expressing an shRNA against *STX18*.
A: The amount of STX18 protein was determined in A549 shSTX18 and A549 shCtrl cell lines using Western Blot. **B:** Cell cycle analysis was used to determine the effect of *STX18* knockdown following irradiation with doses ranging from 0 Gy to 10 Gy. The amount of apoptotic cell death (Sub-G1 fraction) was assessed using flow cytometry at the indicated time points following irradiation. (mean ± SEM; n=3)

Several of the tested clonal H1975 shSTX18 cell lines showed a suppression in *STX18* protein and mRNA level by approximately 50% (Figure 17A and B). Again, no enhanced radiation sensitivity was detected in H1975 shSTX18 clones (Figure 17C). This might be due to the poor knockdown efficiency. Evaluation of the surviving fraction in a colony formation assay also did not reveal any significant differences between cells with *STX18* knockdown and H1975 shCtrl cells (Figure 17D). This

could suggest an intrinsic toxicity of effective suppression of endogenous STX18 in H1975 cells. Alternatively, these relatively radiosensitive NSCLC cells are not further sensitized by abrogating the STX18-dependent resistance pathway.

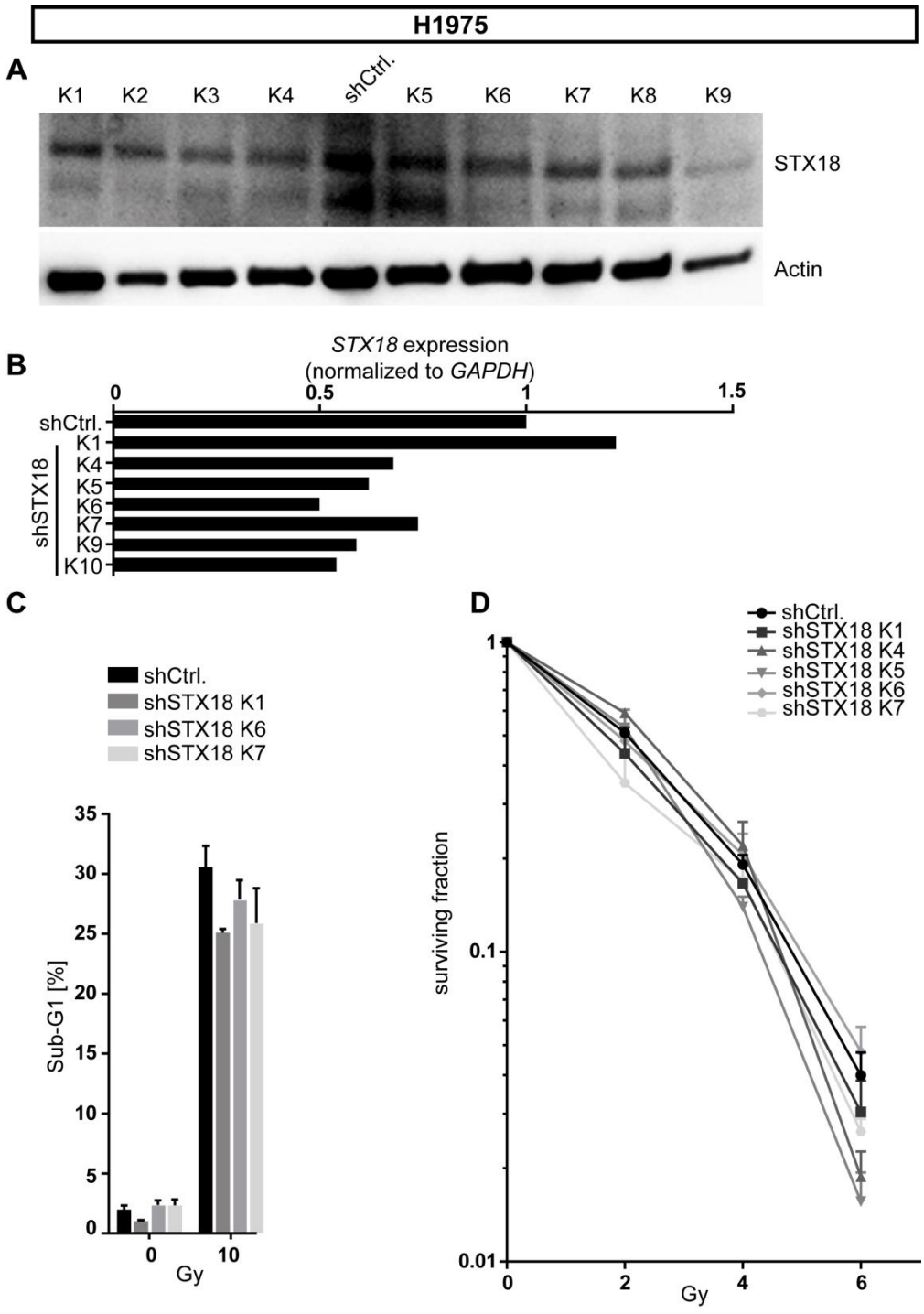

Figure 17: Characterization of H1975 shSTX18 clonal cell lines.
A: Western blot was done to assess the amount of STX18 protein in several clonal cell lines *STX18* knockdown cell lines (K1-K9) as well as the control cell line (shCtrl). Actin was used as a control. **B:** RNA was isolated from several clonal H1975 *STX18* knockdown cell lines as well as the control cell line. Expression of *STX18* mRNA was assessed using qRT-PCR. Expression is normalized to *GAPDH* and relative to expression of control. (n=1) **C:** The effect of *STX18* knockdown on the short-term survival following irradiation was determiend using cell-cycle analysis. Cells were irradiated and the amount of apoptotic cell death was measured by flow cytometry 72 hours later. (mean ± SEM; n=2-4) **D:** Colony formation assay was done to assess the influence of *STX18* knockdown on long-term survival after irradiation (mean ± SEM; n=2-3).

5.2.3.3 Enforced expression of STX18 does not influence radiosensitivity *in vitro*

To explore the effect of overexpression of STX18 on radiosensitivity of A549 cells, endogenous gene expression was upregulated using CRISPRa (CRISPR SAM) and two different guide RNAs (g1 and g2). This method allows transcriptional upregulation by positioning activation domains in close proximity to promotor region of a target gene. This is achieved using a nucleolytically inactive Cas9 protein and a guide RNA. The two guide RNAs (g1 and g2) used here differ in their distance from the *STX18* TSS (transcriptional starting site). The efficiency of *STX18* upregulation by this technology was determined using qRT-PCR (Figure 18A). While guide 1 had no effect on the RNA expression level of *STX18*, guide 2 increased the amount of *STX18* RNA copies approximately 1.5-fold. As A549 cells are intrinsically radioresistant in short-term cell death assays we expected a further decrease of radiosensitivity by STX18 overexpression. Hence, apoptosis assays at early time points were not conducted. We instead focused on studying clonogenic survival following irradiation. Interestingly, no differences were observed between A549 STX18 CRISPR SAM cells and controls, indicating that moderate increases in STX18 levels had no impact on radiosensitivity in this model (Figure 18B).

To study the effects of overexpression of STX18 from a heterologous promotor we cloned the *STX18* cDNA into a retroviral MSCV vector that promotes high transgene expression. Using two vectors, MSCV.STX18-1 and MSCV.STX18-2, A549 cells were transduced to stably express *STX18* cDNA. qRT-PCR revealed a ~12-fold increase of *STX18* RNA copies in STX18-1 cells and a ~7-fold increase in STX18-2 cells (Figure 18C). Again this overexpression of STX18 did not translate into increased radioresistance of A549 cells as determined by colony formation assays after irradiation (Figure 18D).

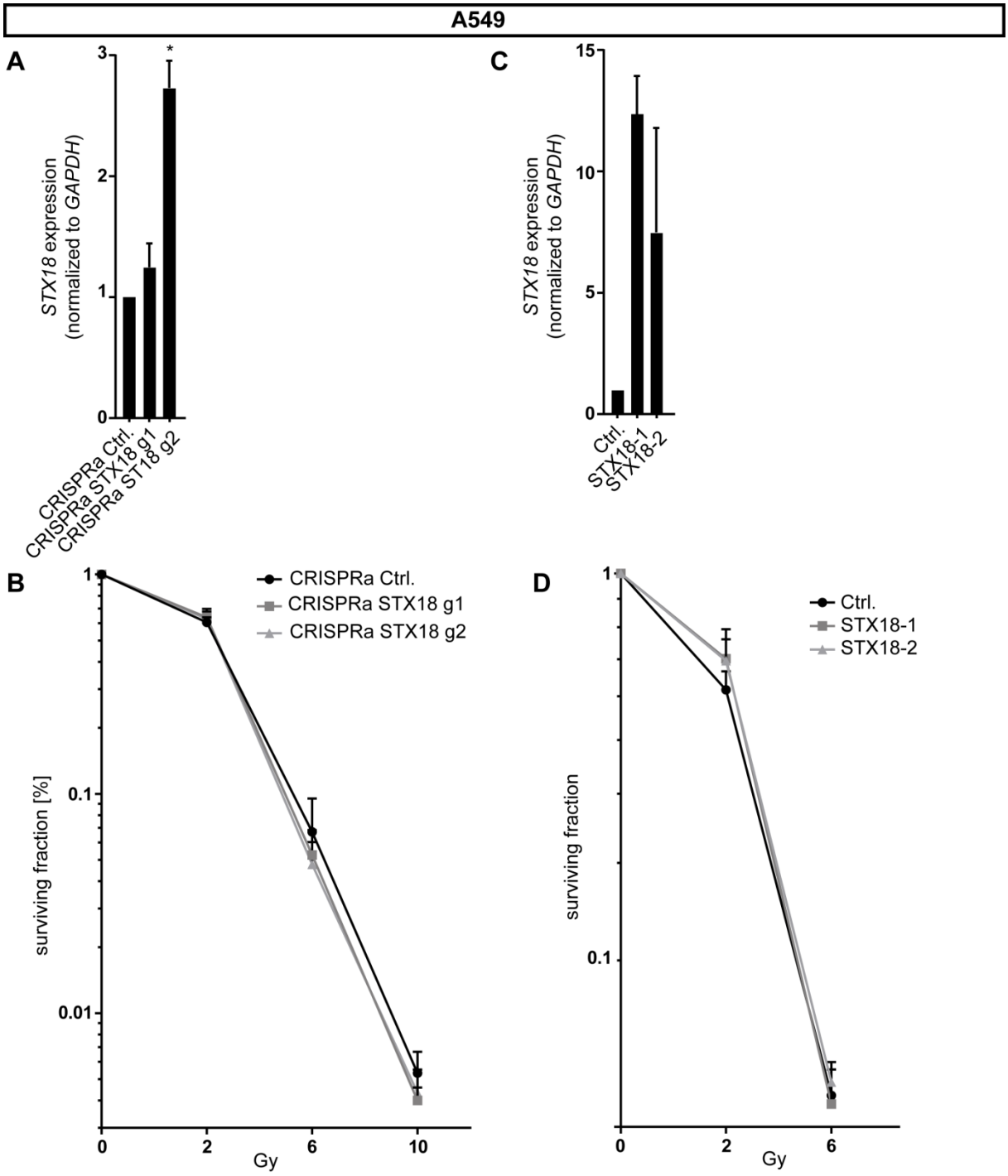

Figure 18: Overexpression of STX18 does not influence radioresistance in A549 cells.
A: RNA was isolated from CRISPRa STX18 g1, CRISPRa STX18 g2 as well as CRISPRa control cells. Expression of *STX18* mRNA was assessed using qRT-PCR. Expression is normalized to *GAPDH* and relative to expression of control. (mean ± SEM; n=3). **B:** Long-term survival upon irradiation was assessed using a Colony formation assay. Colonies were stained and counted 8-12 days after irradiation. (mean ± SEM; n=3) **C:** RNA was isolated from cells stably expressing an *STX18* cNDA vector or an empty vector control. Expression of *STX18* mRNA was assessed using qRT-PCR. Expression is normalized to *GAPDH* and relative to expression of control. (mean ± SEM; n=2) **D:** Colony formation assay was used to determine long-term survival after irradiation. (mean ± SEM; n=2)

5.2.3.4 Reintroduction of STX18 into *STX18* knockdown A549 cells partially restores the radioresistant phenotype

To verify that the observed radiosensitive phenotype of A549 shSTX18 clonal cell lines is indeed based on the knockdown of *STX18*, *STX18* cDNA was reintroduced in these cells. Towards this end, the previously generated *STX18* cDNA vectors (MSCV.STX18-1, MSCV.STX18-2, and Ctrl) were retrovirally transduced into the three A549 shSTX18 clonal cell lines. qRT-PCR confirmed the persisting decrease in *STX18* mRNA in the clonal A549 shSTX18 cells transduced with the control vector in comparison to A549 shCtrl cells transduced with the control vector. Cells stably expressing the *STX18* cDNA vectors showed a massive increase (about 12-22 fold) of *STX18* RNA when compared to the control cells (Figure 19A). Next, colony assays were performed to assess radioresistance of the STX18-restored A549 clones. A549 shCtrl cell lines reconstituted with these vectors showed no difference in survival when transduced with either of the cDNA vectors, showing again that *STX18* overexpression did not influence radioresistance in A549 cells (Figure 19B). A549 shSTX18 K1, K2 and K3 cells transduced with the control cDNA vector retained enhanced radiosensitivity as compared to control cells, further confirming that the retroviral vector itself did not impact on the radiation response (Figure 19C-D). Reconstituting these *STX18* knockdown clones with MSCV.STX18-1 and -2 vectors had variable but consistent outcomes: In A549 shSTX18 K1 cells, none of the *STX18* cDNA vectors conferred radioresistance (Figure 19C). In A549 shSTX18 K2 cells, the STX18-1 cDNA vector restored survival after 2 Gy irradiation up to the level of A549 control cells (Figure 19D). These functional outcome correlated well with the strong increase in *STX18* mRNA expression (Figure 18A). A549 shSTX18 K3 cells reconstituted with MSCV.STX18-1 also showed a slight increase in survival after irradiation (Figure 19D). In all, reexpression of STX18 in A549 shSTX18 cells resulted in full reconstitution of radioresistance in the one of 3 clones which exhibited the highest *STX18* RNA levels. Effects were less pronounced in the two other clones, which may be explained by challenges of this complex experimental setup.

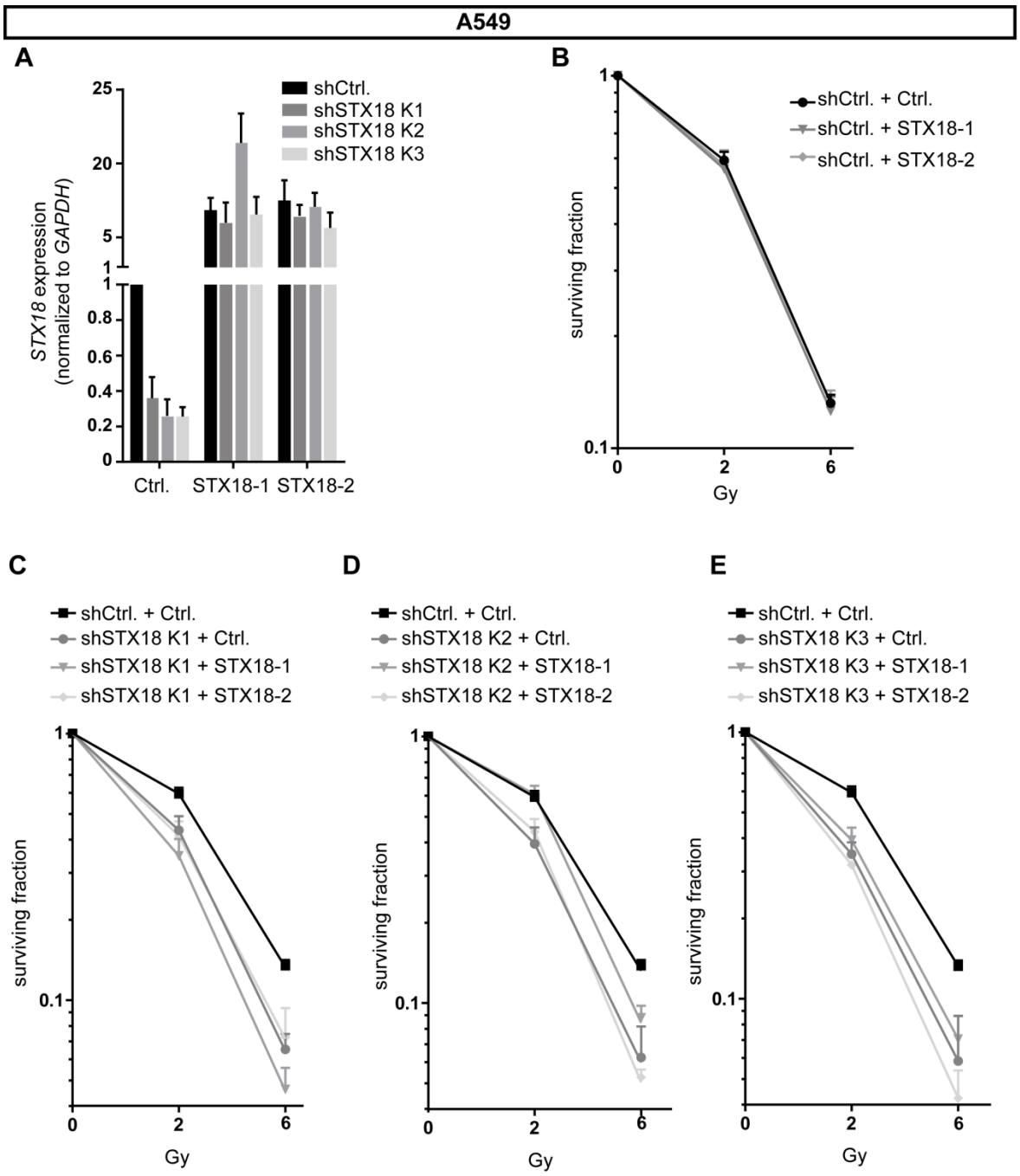

Figure 19: Rescue of the *STX18* knockdown cells.
A: A549 shSTX18 clonal cell lines and A549 shSTX18-Ctrl cell lines stably expressing either one of the two *STX18* cDNA Vectors or an empty cDNA Vector Ctrl were seeded at equal numbers and RNA was isolated the next day. Expression of *STX18* mRNA was assessed using qRT-PCR. Expression is normalized to *GAPDH* and relative to expression of control. (mean ± SEM; n=3-6) **B-E:** Colony formation assay in the "rescued" cell lines. Briefly, cells were seeded in appropriate densities, irradiated 4 hours to 6 hours later and colonies stained 8 to 10 days later. Subsequently colonies were counted and the surviving fractions were calculated (mean ± SEM; n=3-6).

5.2.3.5 Knockdown of *STX18* correlates with a decrease in MMP9 expression levels and activity

One of the hallmarks of cancer as proposed by Hanahan and Weinberg (Hanahan and Weinberg 2000) is the propensity of cancer cells to invade and metastasize. This process involves extracellular matrix (ECM) degradation, which can be mediated by cellular structures known as invadopodia. These contain integrins, that facilitate ECM adhesion and MMPs (matrix metalloproteases), which execute ECM degradation. Interestingly, the SNARE proteins Syntaxin13 and SNAP23 are necessary for invadopodia formation and cell invasion in an integrin-dependent manner (Williams and Coppolino 2014). Metastasis formation is augmented by transport of MMP14 to the invadopodia. In breast cancer models this process is mediated by VAMP7 (vesicle-associated membrane protein 7) (Steffen et al. 2008; Jacob and Prekeris 2015). This illustrates that the secretory pathway plays a vital role in the release of matrix metalloproteinases (MMPs). MMP9 has been described to drive tumor progression in e.g. breast cancer (Mehner et al. 2014). Therefore, potential changes in MMP9 expression and activity were investigated in A548 shSTX18 cells. qRT-PCR revealed a suppression of *MMP9* mRNA by approximately 50% to 70% in clonal A549 shSTX18 cells (Figure 20A). To validate the biological relevance of this observation it was decided to study the MMP9 enzymatic activity in A549 shSTX18 cells and controls. Activity of MMPs can be detected by zymography, which is based on their propensity to proteolyze gelatin. Studying MMP activity of the supernatants of cultured A549 shSTX18 cells and controls for MMP activity indeed a reduced MMP9 activity in all three clones with shRNA-mediated suppression of STX18 was found (Figure 20D). Interestingly, the activity of MMP2 was increased, possibly indicating compensatory mechanisms.

To evaluate whether irradiation affects *MMP9* levels, A549 shCtrl cells and A549 shSTX18 K1 cells were irradiated with 10 Gy and mRNA was subsequently isolated. Interestingly, basal *MMP9* RNA expression was lower in STX18-suppressed A549 cells. While radiation suppressed *MMP9* RNA in control cells, RNA level rather increased in A549 shSTX18 (Figure 20B).

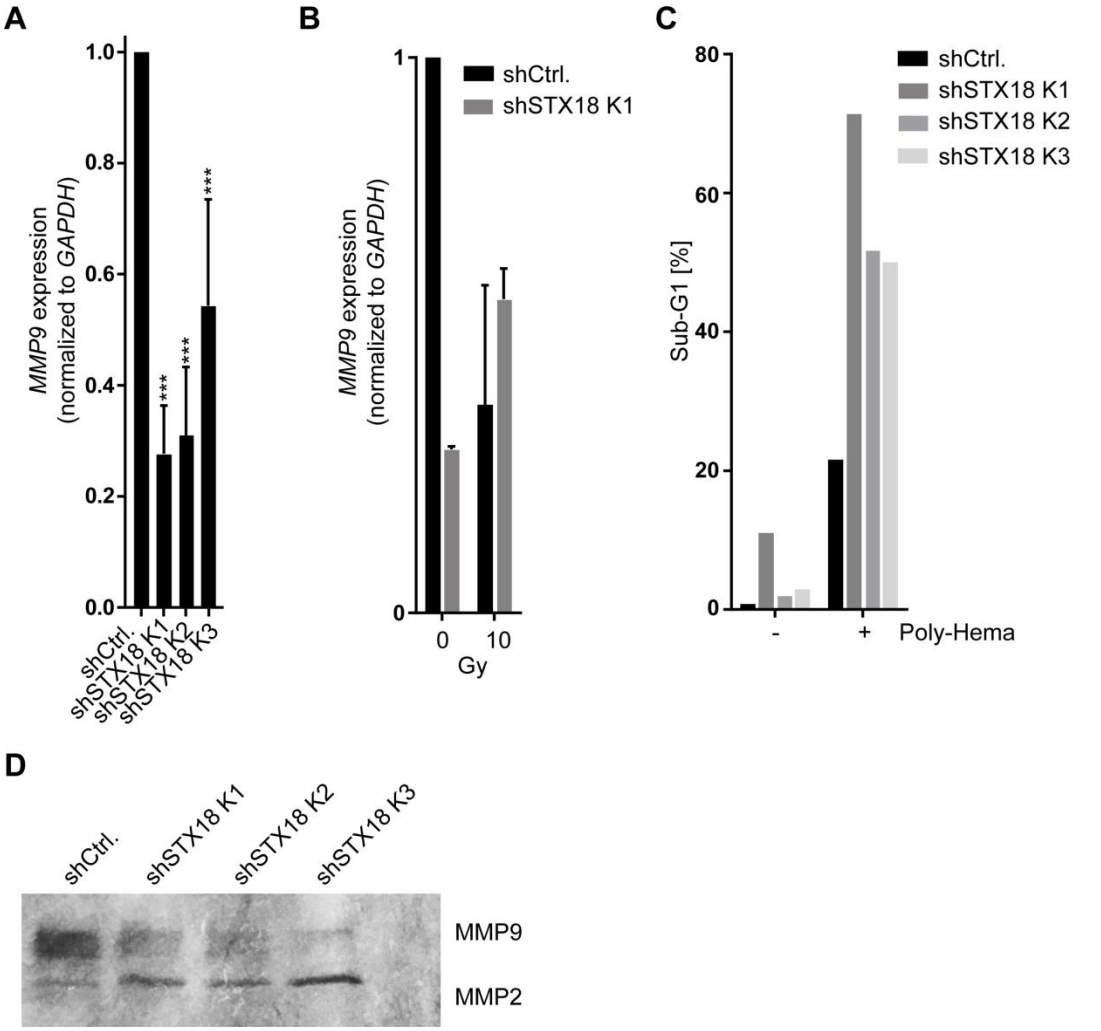

Figure 20: Knockdown of *STX18* correlates with reduced *MMP9* expression and activity and enhancment of anoikis.
A: RNA was isolated from clonal A549 *STX18* knockdown cell lines as well as the control cell line. *MMP9* RNA expression was assessed by qRT-PCR, results were normalized to RNA expression of the housekeeping gene *GAPDH* (mean ± SEM; n=3) **B:** RNA was isolated from clonal A549 *STX18* knockdown cell lines as well as the control cell line 18 hours after irradiation with 10 Gy. *MMP9* RNA expression was assessed by qRT-PCR, results were normalized to RNA expression of the housekeeping gene *GAPDH* (mean ± SEM; n=3) (mean ± SEM; n=2) **C:** Anoikis assay was performed to assess the capability of cells to survive in suspension. Briefly, cells were seeded in control dishes or poly-hema coated dishes, incubated for 72 hours, and the amount of Sub-G1 fraction cells in the supernatant was measured using flow cytometry (PI-staining). (n=1) **D:** Activity of MMPs was assessed using zymography. Cells were seeded and medium changed to 0.5% FCS 4 hours later. Subsequently MMP9 activity was measured using a gelatin gel.

MMP9 is functionally involved in the metastastic process (Mehner et al. 2014). This involves escape from anoikis, a form of cell death that occurs when cells detach from the ECM. *In vitro*, this process can be mimicked by coating cell culture dishes with poly-hema, thus keeping the cells in suspension. The A549 shSTX18 clonal cell lines and controls were seeded on regular culture dishes as well as on poly-hema coated dishes, and cell death was quantified after 72 hours. Indeed, clonal A549 shSTX18 cell were more sensitive to anoikis (50% to 70% cell death in clones K2, K3 and K1)

than A549 shCtrl cells (20% cell death; Figure 20C). In summary, knockdown of *STX18* results in decreased activity of MMP9 and increased sensitivity to anoikis. Collectively, these findings support an essential role of STX18 in the metastatic process.

5.2.3.6 Impact of *STX18* knockdown on the expression of mediators of the unfolded protein response

Tumors face various sources of stress, including increased need for oxygen and nutrients. Cancer treatments such as chemotherapy and radiation also impose stresses. The induction of ER stress can alter normal ER function and result in accumulation of un- and misfolded proteins in its lumen, activating the unfolded protein response (UPR) that aims to restore cellular homeostasis. UPR has been implicated as a mechanism in chemoresistance and general tumor progression. Overexpression of several UPR-associated proteins including XBP1, PERK, BiP, and ATF6 was described in a variety of solid tumors, and high expression of BiP was correlated with inverse outcome in prostate cancer patients (Mintz et al. 2003; Lee 2007; Dong et al. 2008; Li et al. 2008).

Against this background RNA expression of a set of UPR-associated genes was analyzed by qRT-PCR in A549 shCtrl and A549 shSTX18 cells. No significant differences were observed in expression of *BiP, ATF4, CHOP* and *EDEM.* Interestingly, RNA expression of the spliced form of *XBP1* (s*XBP1,* X-Box Binding Protein 1) was significantly increased in clonal *STX18* knockdown cell lines (Figure 21A). Spliced *XBP1* can promote expression of genes alleviating ER-stress. To verify this result, a Dual-Luciferase Assay was conducted to visualize *XBP1* splicing. This assay showed only minor changes between *STX18* knockdown and control cell lines. DTT treatment was used as positive control for ER – stress, which resulted in an increase in *XBP1* splicing thus confirming the validity of the assay (Figure 21B). Taken together these results do not support an impact of STX18 on the constitutive expression of mediators of the UPR.

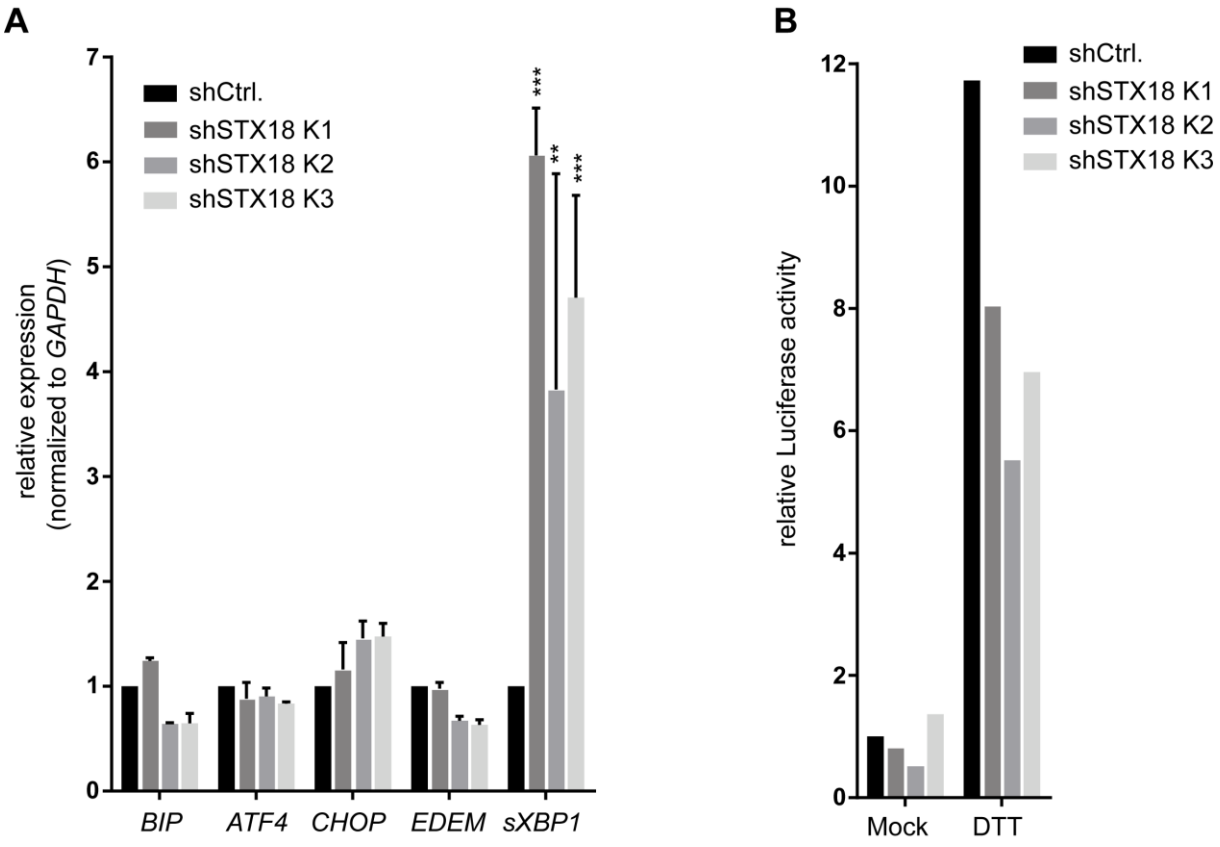

Figure 21: Analysis of the influence of *STX18* knockdown on basal expression of mediators of the UPR. **A:** qRT-PCR revealed elevated expression levels of spliced *XBP1*, while other ER-stress sensors were not altered. Data was normalized to *GADPH* and is given relative to control (mean ± SEM; n=3) **B:** Luciferase Assay revealed no changes in the amount of spliced *XBP1* between *STX18* knockdown cell lines and control cells, while splicing was increased by DTT treatment (n=1).

5.2.3.7 Knockdown of *STX18* does not alter radiation induced senescence in NSCLC cells

Senescence is a permanent resting state that can be induced by radiotherapy. Activity of β-galactosidase that can be detected at pH 6 is a canonical marker of senescence (Dimri et al. 1995; Debacq-Chainiaux et al. 2009; Burton and Krizhanovsky 2014). To explore whether suppression of STX18 impacts on radiation-induced senescence senescence-associated (SA) β-galactosidase activity was assessed by a fluorometric protein assay. A549 shSTX18 clonal populations exhibited a higher background activity of SA-β-galactosidase. However, the relative induction by irradiation was not altered in comparison to control cells (Fig. 22A). Also, induction of the cyclin-dependent kinase inhibitor p21/CIP1, a canonical p53 target gene and mediator of senescence, was not significantly altered in cells with suppressed STX18 (Fig. 22B). In summary, we found no evidence for functional importance of STX18 in radiation-induced senescence which could explain its modulation of the radiation response of A549 lung cancer cells.

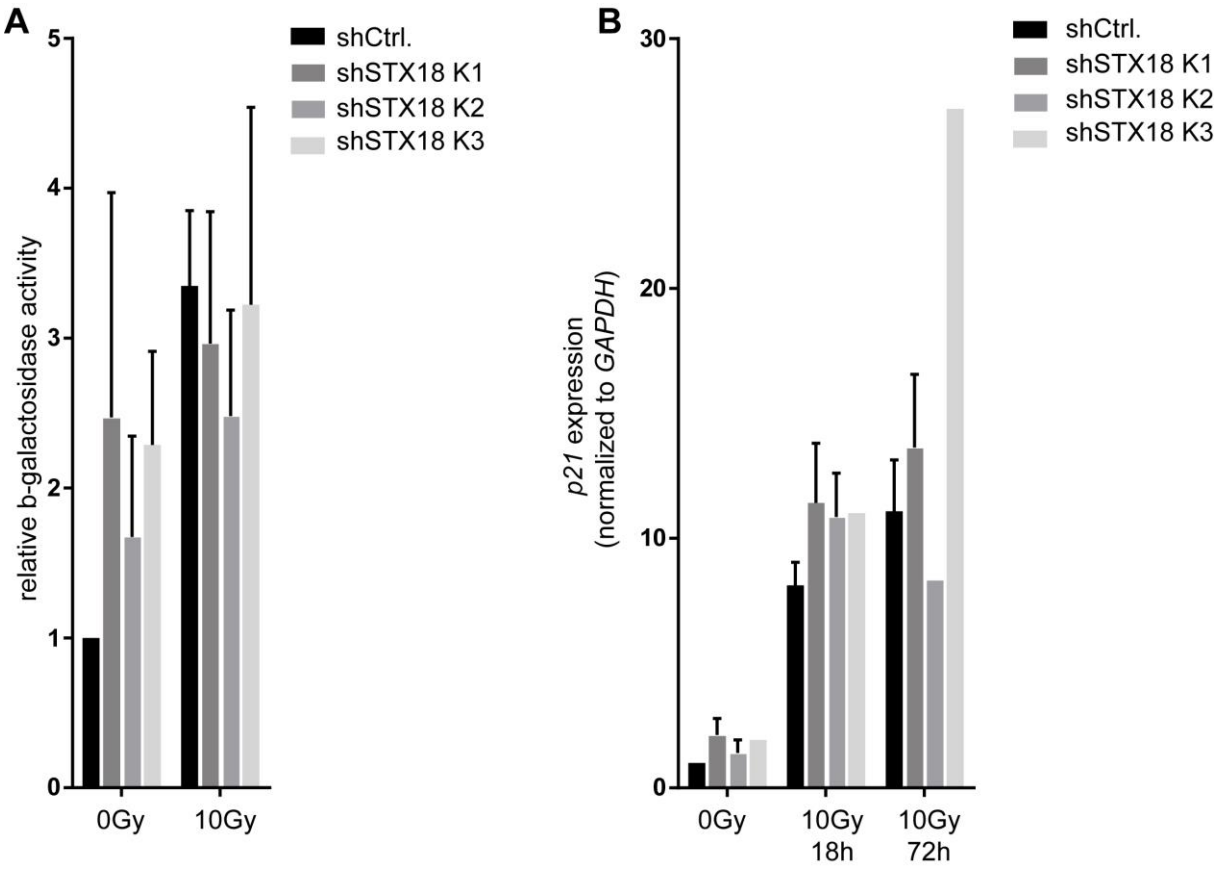

Figure 22: Effect of *STX18* knockdown on cellular senescence
A: *STX18* knockdown slightly increases cellular senescence, as does radiation in A549 shCtrl and shSTX18 knockdown cells in general (mean ± SEM; n=2-3). Data was normalized to *GADPH* and is given relative to control. **B:** qRT-PCR showed increase in *p21* mRNA expression levels following irradiation. Data normalized to *GAPDH*, relative to control. (mean ± SEM; n=1-3).

5.2.3.8 Effect of *STX18* knockdown on tumor growth *in vivo*

Next we examined the effect of *STX18* knockdown on the growth and radiosensitivity of A549 tumors that were orthotopically grafted in the lungs of immune deficient NOD/SCID mice. For visualization of tumor growth and metastasis *in vivo* we transduced A549 shSTX18 K3 and A549 shCtrl cells with a vector expressing the reporter gene luciferase. The resulting cell lines were named A549 shCtrl + Luc and A549 shSTX18 K3 + Luc. Tumor cells (suspended in growth factor reduced Matrigel®/PBS) were injected into the left lung of 10 animals per cell line. 9 days after injection, tumor progression was monitored by *in vivo* imaging. Animals were narcotized using isoflurane, injected with luciferin and imaged using the Caliper Lumina II system. This first image determined the starting “size” of the tumor. Established lung tumors were irradiated 4 days later with a setup that allows irradiation of the left lung while the rest of the body is shielded (Figure 23). Five mice from the A549 shCtrl + Luc group and 4 mice from the A549 *shSTX18* K3 + Luc

group were irradiated with doses of 10 Gy. The remaining tumor-bearing mice served as controls. *In vivo* images of the tumors were taken 10, 16, 21, and 38 days after irradiation. The radiance of luciferase-expressing tumors was measured at the site of the primary tumor and used as marker of tumor burden. Changes in radiance were monitored by normalizing each individual tumor to the starting value determined by imaging before irradiation.

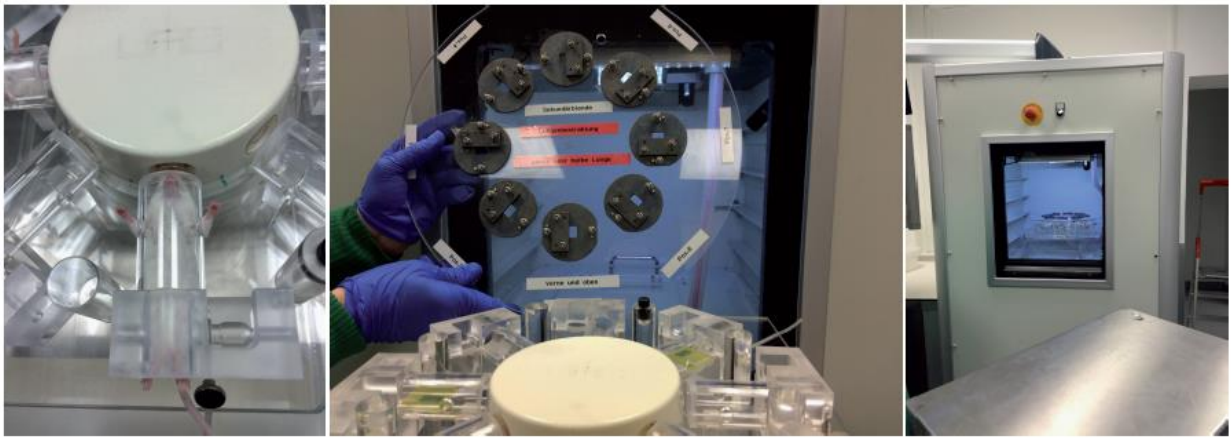

Figure 23: *In vivo* irradiation setup.
From left to right: Tubes for fixing mice while they are narcotized with isoflurane, lead cover for shielding the body, RS320-X-ray irradiator.

Overall, no strong differences in the tumor growth could be observed between the non-irradiated shSTX18 K3 + Luc and the non-irradiated shCtrl + Luc injected mice. Also, A549 shCtrl + Luc tumors showed only a moderate response to irradiation. A mild decrease in tumor burden became detectable 16 days after irradiation and was slightly more pronounced until termination of the experiment (Figure 24A). Interestingly, A549 shSTX18 K3 + Luc tumors did not show a therapeutic response to irradiation (Figure 24A). Furthermore, nearly all mice showed tumor metastasis into the right lung very early. However, 3 out of 10 A549 shCtrl-transplanted mice showed excessive distant metastases while none of the mice injected with the *STX18* knockdown cell line showed distant metastases (Figure 24B). This might be due to the lower MMP9 expression in A549 shSTX18 K3 cells.

At termination of the experiment tumors were isolated and preserved for further analyses. RNA was isolated from one tumor per treatment group for qRT-PCR analysis of *STX18* RNA expression. Suppression of *STX18* RNA was maintained in A549 shSTX18 K3 + Luc tumors (Figure 24B).

Overall, independent of STX18-status no convincing therapeutic effects of the radiation could be observed, leading to the conclusion that the experimental conditions need to be optimized.

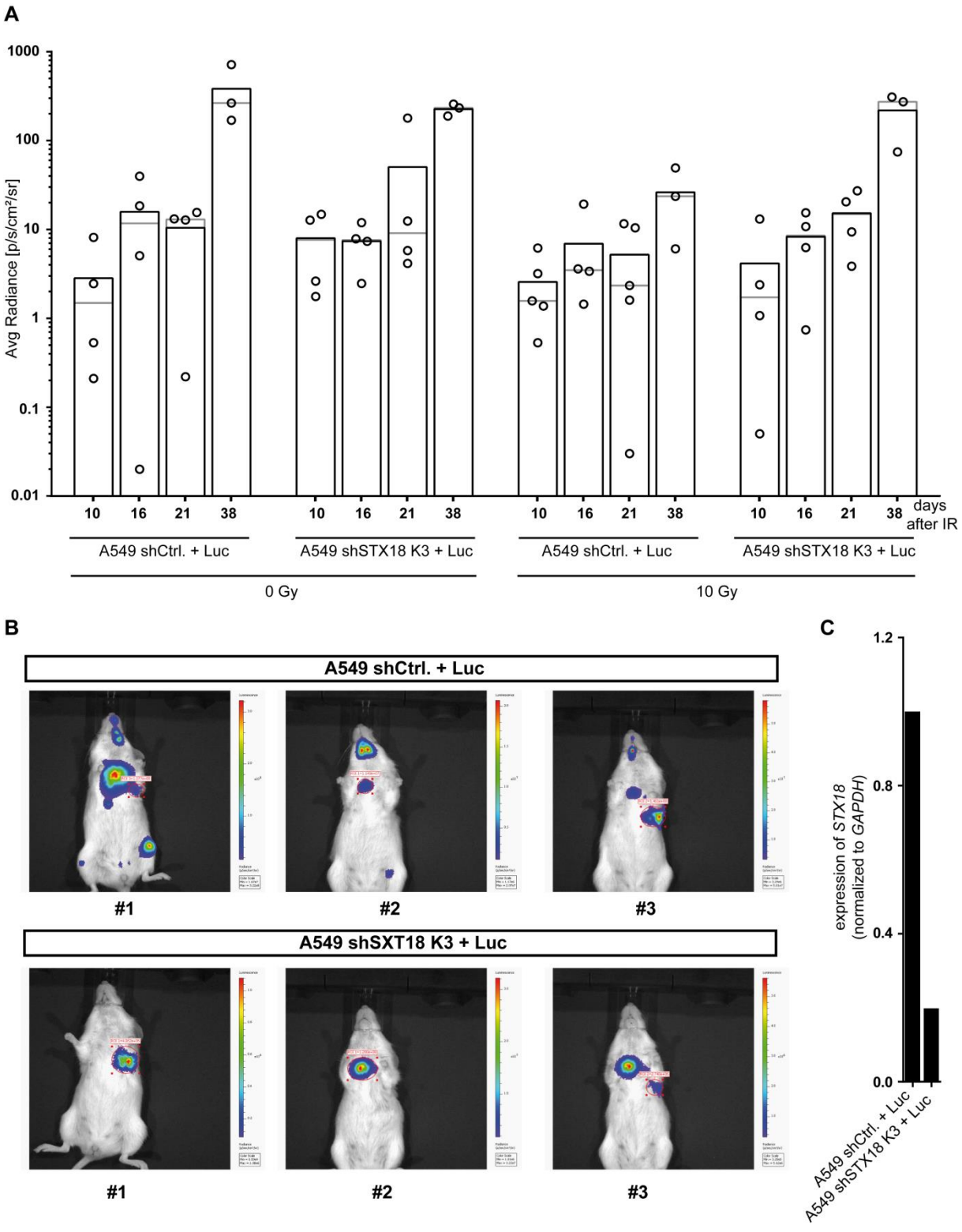

Figure 24: Effect of *STX18* knockdown on the irradiation response *in vivo*.
A: Measured tumor radiance of individual (dots) mice at day 10, 16, 21 and 38 after irradiation. Mean values are displayed as bars. Median displayed as grey line. Data is normalized to average radiance measured before irradiation (set to 1). **B:** *In vivo* images taken of mice injected with the indicated cell lines. **C:** RNA was isolated from one tumor of mice injected with either A549 shCtrl + Luc or A549 shSTX18 K3 + Luc cells. qRT-PCR was done to assess expression of *STX18* RNA.

5.3 Characterization of GADD45B as putative modulator of the Radiation Response

The second aim of this thesis was to characterize the impact of GADD45B (Growth Arrest and DNA Damage-inducible 45b) on the radiation response of lung cancer models. This protein is a member of the evolutionary highly conserved GADD45B protein family. GADD45 proteins are upregulated upon DNA damage and additional conditions inducing growth arrest (Fornace et al. 1988; Liebermann and Hoffman 2008; Salvador et al. 2013). In a functional cDNA screen conducted previously in our laboratory by F. Breitenbücher, GADD45B was identified as putative resistance factor to the TKI afatinib, which is approved first-line treatment for patients with *EGFR*-mutated NSCLC (Sequist et al., JCO 2013). Afatinib was also shown to have radiosensitizing activity in NSCLC models (Zhang et al. 2015), and GADD45B mediated radioresistance in preliminary experiment from our laboratory. Against this background we set out to dissect at a molecular level how GADD45B confers radioresistance.

5.3.1 Establishment of lung cancer models with inducible GADD45B expression

Inducible transgene expression is one mean to reduce the risk of bias that can arise from compensatory mechanisms selected in cells with permanent transgene expression. To provide models for molecular dissection of GADD45B-mediated radioresistance we generated H1975 and HCC827 NSCLC cell lines that express the *GADD45B* cDNA under the control of a tetracycline-inducible promotor (H1975 rtTA-GADD45B and HCC827 rtTA-GADD45B). This system enables transgene expression *in vitro* and *in vivo* upon treatment with doxycycline. To increase reproducibility and robustness of the models single cell clones were generated by serial dilution and clonal populations were expanded under antibiotic selection in the absence of doxycycline. Conditional transgene expression upon doxycycline (1µg/ml) treatment for 24 hours before proteins was confirmed by Western blotting. Figure 25A shows six clonal H1975 rtTA-GADD45B cell lines with varying levels of GADD45B induction upon doxycycline treatment as well as one clonal HCC827 cell line. Detection of *GADD45B* RNA by qRT-PCR was used as a second assay to monitor conditional transgene expression following doxycycline treatment for 24 hours in H1975 rtTA-GADD45B K9 (Figure 25B).

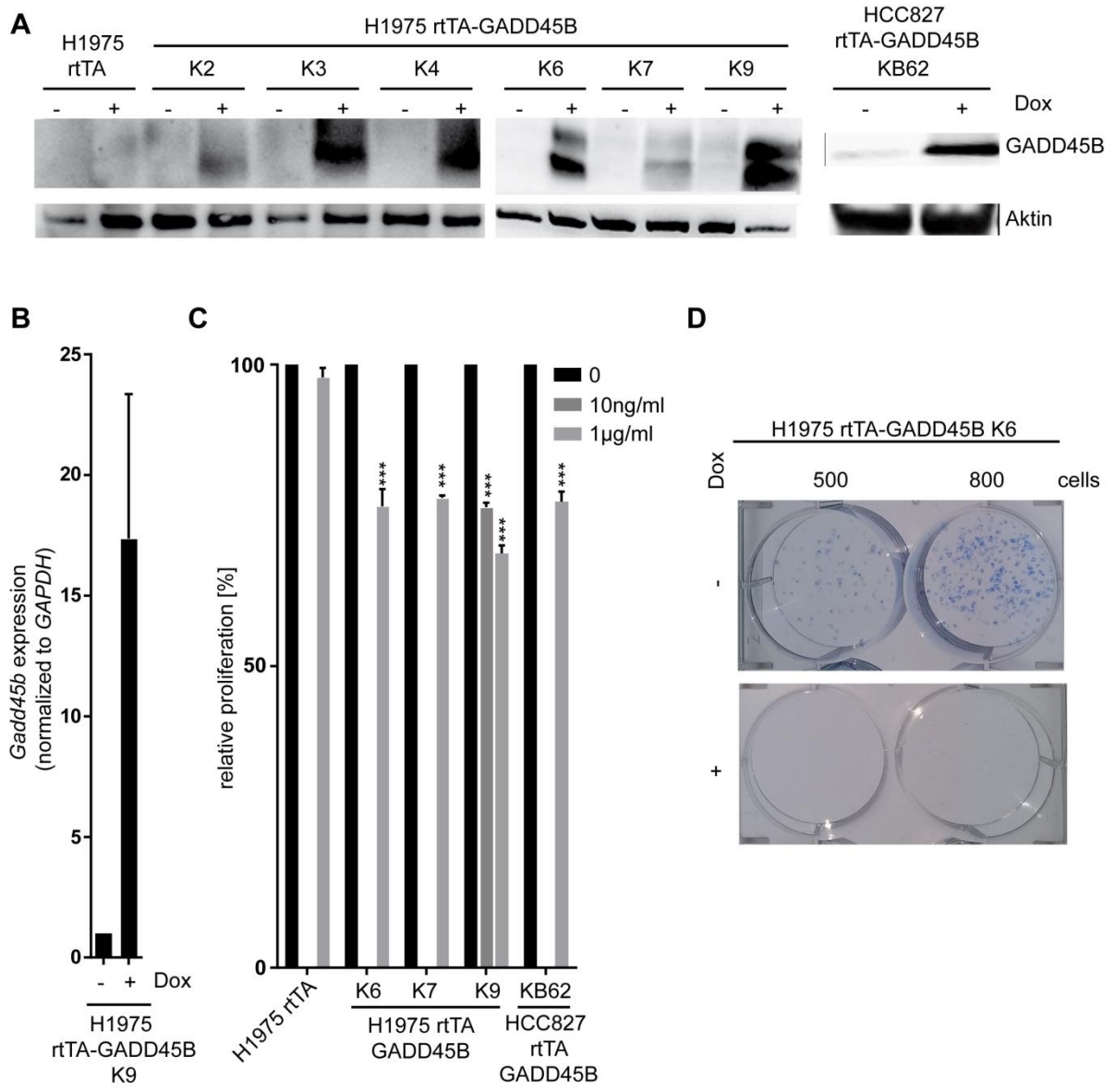

Figure 25: Generation and initial characterization of lung cancer cells with inducible expression of GADD45B.
A: Clones derived from transgenic H1975 and HCC827 lung cancer cells were treated with Doxycycline (Dox, 1µg/ml) for 24 hours, then proteins were extracted and analyzed via western blot using a GADD45B-specific primary antibody. Actin served as loading control. **B:** RNA was isolated from H1975 cells with conditional *GADD45B* expression grown in the absence of presence of doxycycline (1 µg/ml). *GADD45B* RNA expression was assessed by qRT-PCR, and results were normalized to RNA expression of the housekeeping gene *GAPDH* (mean ± SEM; n=3). **C:** Clones derived from transgenic H1975 and HCC827 lung cancer cells were grown in the absence of presence of two concentrations of doxycycline. Proliferation and metabolic viability was studied using the MTT assay (mean ± SEM; n=3). **D:** Representative colony assays of clonal H1975 rtTA GADD45B cells grown for 9 days in the presence or absence of doxycycline.

The impact of conditional GADD45B expression on cell proliferation and metabolically active survival was studied using the MTT assay and after treatment with doxycycline at different concentrations. Doxycycline treatment of H1975 rtTA control cells had no effect on relative cell proliferation (Figure 25C). In contrast, doxycycline treatment of H1975 rtTA-GADD45B clones K6, K7 and K9 led to a

significant decrease in cell proliferation (Figure 25C). To explore the effect of conditional GADD45B expression on long-term clonogenic survival, H1975 rtTA-GADD45B K6 cells were seeded at low densities in either control medium or medium containing doxycycline. Colonies were allowed to form before they were fixed and stained. Doxycycline completely abrogated clonogenic survival of H1975 rtTA-GADD45B cells K6 (Figure 25D).

Next, the effect of conditional GADD45B expression on cell cycle distribution and the reversibility of its antiproliferative effects upon withdrawal of doxycycline were studied. To determine the half-life of transgenic GADD45B protein, H1975 rtTA-GADD45B K9 cells were treated with different concentrations of doxycycline for 24 hours which was then withdrawn. Protein extracts were generated at several time points following doxycycline withdrawal, and GADD45B expression was detected by Western blot. These experiments suggested that the half-life of transgenic GADD45B protein ranges from 48 to 72 hours (Figure 26A).

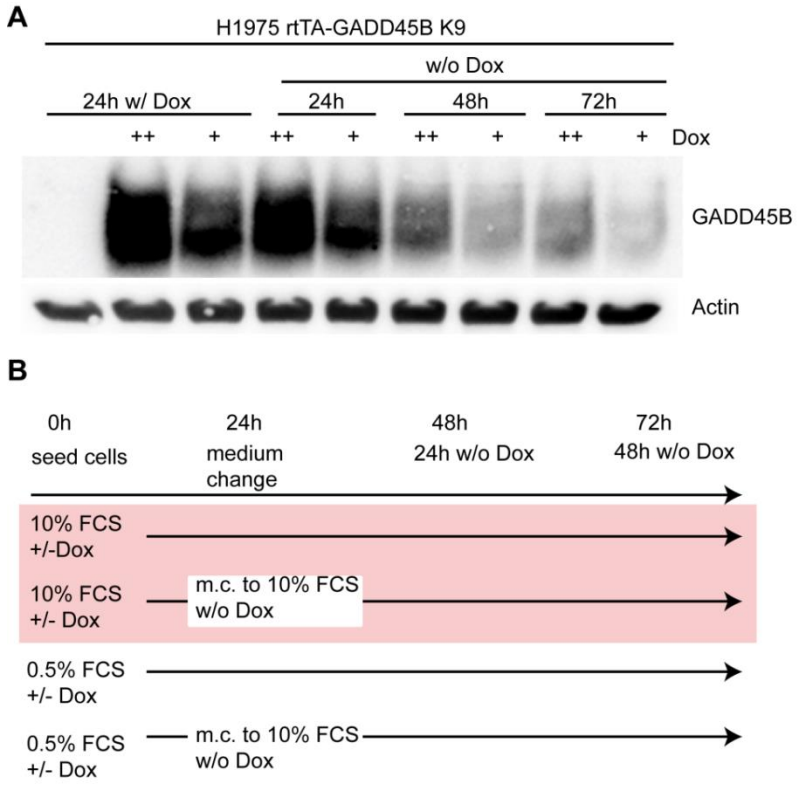

Figure 26: Determination of stability of doxycycline-inducible transgenic GADD45B protein.
A: Western blot was done at the indicated time points after doxycycline treatment/ doxycycline washout. Cells were either treated with 10ng/ml doxycycline (+) or 1µg/ml doxycycline (++). GADD45B protein levels were highly increased when compared to control cell lines until 48 hours after doxycycline washout. **B:** Schematic overview of the experimental setup to analyze the effect of GADD45B expression on cell cycle. m.c. = medium change. Red box = cells cultured in 10% FCS.

Cell-cycle distribution was determined in H1975 rtTA-GADD45B K6 and K9 as well as HCC827 rtTA-GADD45B KB62 cells treated with doxycycline at different concentrations of doxycycline and grown in medium with low and high serum (0.5% vs. 10% FCS, Figure 26B). After 24 hours of doxycycline treatment, doxycline was withdrawn in some cells. At three consecutive days starting from the day of seeding, cells were labeled with EdU to allow a precise definition of cell cycle phases.

Upon doxycycline treatment at low serum conditions (0.5% FCS) H1975 rtTA-GADD45B cells showed a marked G0/G1 arrest and concomitant S phase reduction (Figure 27 left panel). Cells reentered cell cycle within 24 hours when doxycycline was withdrawn or put under high serum conditions (10% FCS) (Figure 27 middle panel). In contrast, cell cycle distribution of HCC827 rtTA-GADD45B KB62 cells remained largely unchanged upon treatment with doxycycline. Serum starvation (0.5% FCS) conferred only a modest G0/G1 arrest and S phase reduction (Figure 27).

Overall, these results suggest that GADD45B expression mediates a reversible arrest in the G1 phase of the cell cycle, which in its intensity depends on the respective lung cancer model.

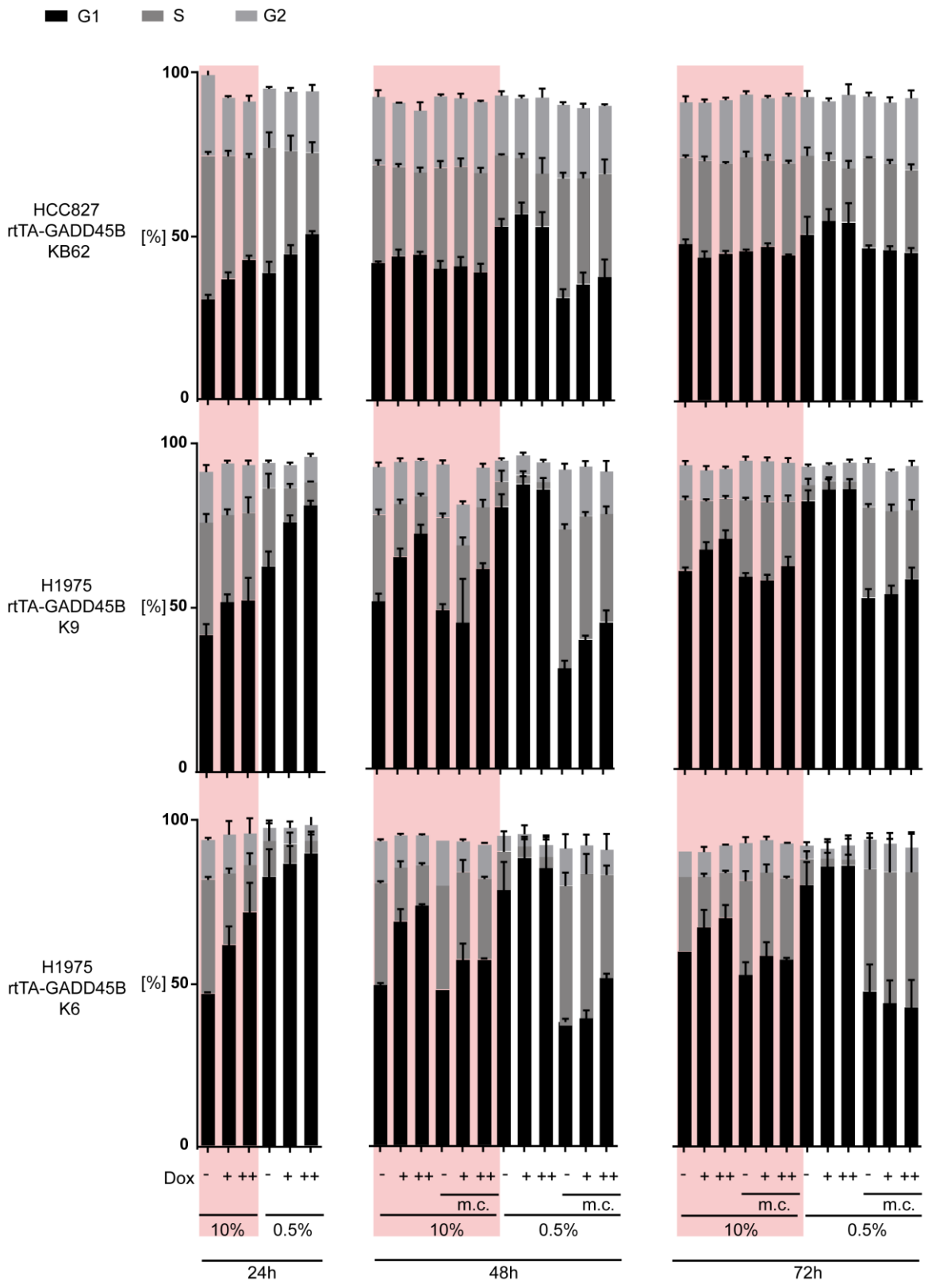

Figure 27: Cell cycle distribution of lung cancer cell in relation to transgenic GADD45B expression and growth conditions.
Relative distribution of cell cycles phases as determined by EdU staining and flow cytometry at indicated time points. Serum concentrations and doxycycline treatment as indicated in the lower panel (mean ± SEM; K6: n=2; K9: n=3; KB62: n=3).

5.3.2 Impact of conditional GADD45B expression on the radiation response of lung cancer models

Next it was queried whether conditionally expressed GADD45B impacted on the radiation response of H1975 and HCC827 lung cancer cells *in vitro*. H1975 and HCC827 rtTA-GADD45B clones were treated with doxycycline for 24 hours before they were irradiated with doses from 0 Gy to 10 Gy. Overall there were moderate effects of conditional GADD45B expression on irradiation-induced apoptosis. However, in H1975 clones K6 and K9 and in HCC827 clone KB62 a statistically significant reduction of apoptosis by GADD45B was seen at high radiation doses (Figure 28A).

Long-term clonogenic survival is seen as the most relevant assay for antitumoral effects of radiotherapy *in vitro*. Because of the constitutive anti-proliferative effect of continuous GADD45B induction (Figure 25C and D), GADD45B expression was only induced for 24 hours before irradiation and then withdrawn either 4 to 6 hours before or immediately after irradiation (Figure 28B). In this experimental setting no differences in clonogenic survival was detected between GADD45B-expressing and control cells following irradiation (Figure 28B). Hence, it was required to confirm the short-term radioprotective activity of GADD45B under these experimental conditions. To this end, cells were treated with doxycycline to induce GADD45B expression and irradiated 24 later. Cells were either i) continuously kept in doxycycline-containing medium, ii) changed to doxycycline-free medium before irradiation, or iii) changed to doxycycline-free medium after irradiation. Apoptotic cell death was assessed 72 hours after irradiation and confirmed radioprotection of cells with conditionally expressed GADD45B (Figure 29A). This indicates that either GADD45B only mediates protection against fast radiation-induced apoptotic cell, or that GADD45B's intrinsic antiproliferative activity masks radioprotection in long-term clonogenic survival assays *in vitro*. To resolve this issue, *in vivo* experiments with GADD45B-inducible tumor grafted in immune compromised mice are planned.

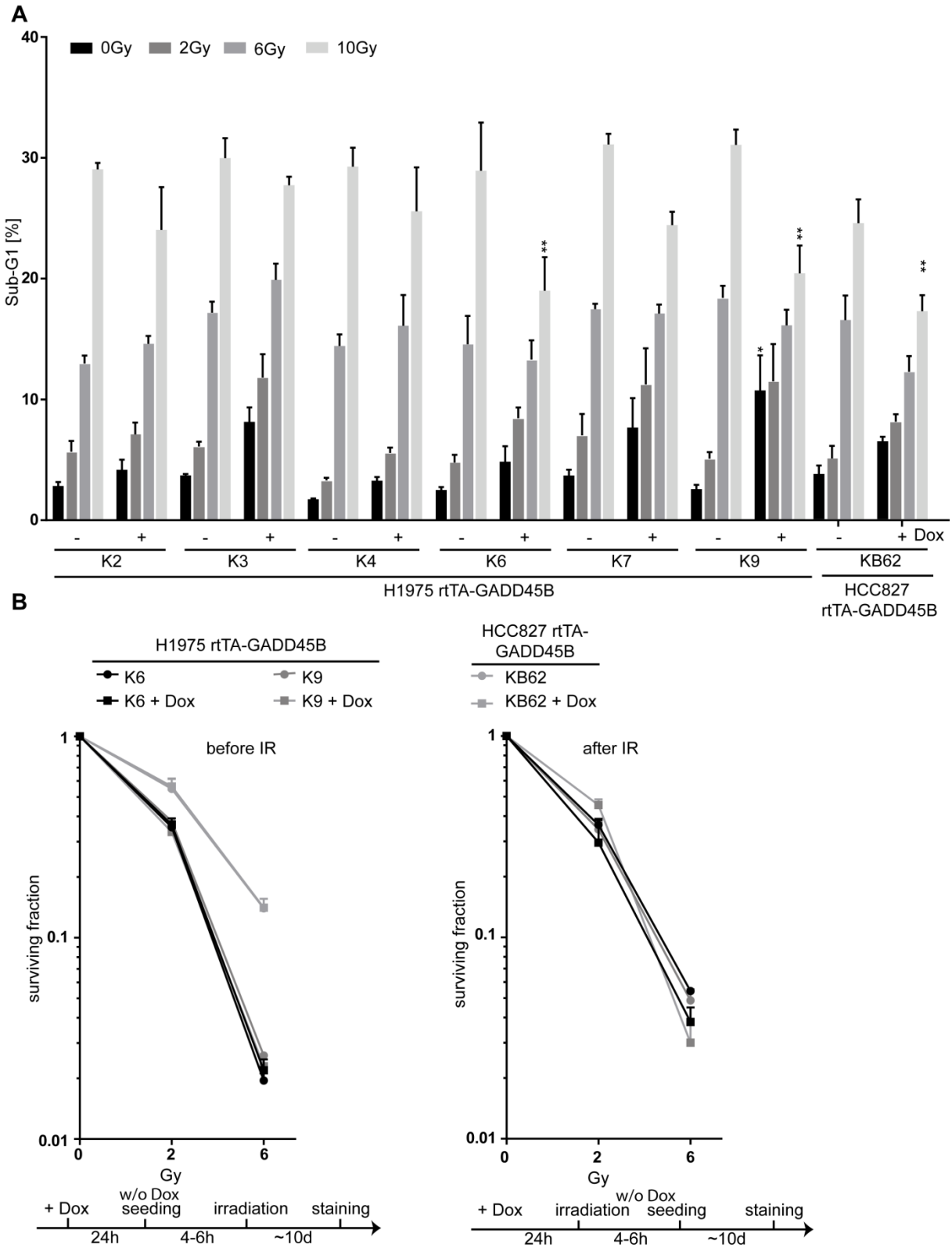

Figure 28: Radioprotection by conditionally expressed GADD45B in short-term and long-term assays *in vitro*.
A: Radiation-induced apoptosis in relation to GADD45B expression. Cells were treated with doxycycline (1µg/ml) or regular medium for 24 hours before irradiation, and the fraction of cells with subgenomic DNA content was quantified 72 hours after irradiation by flow cytometry. (mean ± SEM; n=3). **B:** Long-term clonogenic survival following radiation. Experiments were conducted by two different protocols graphically represented in the lower panels. Colonies were counted x days after irradiation (mean ± SEM; before irradiation: K6: n=3; K9: n=1; KB62: n=4; after irradiation: K6: n=2; K9: n=3)

Next it was queried whether conditionally expressed GADD45B itself induces senescence and/or modulates radiation-induced senescence. Irradiating H1975 rtTA-GADD45B K9 cells with 10 Gy lead to increased SA-b-galactosidase activity after 72 hours. This was not further enhanced by conditional expression of GADD45B (Figure 29B). To rule out bias from radiation-induced changes of GADD45B it was confirmed that irradiation itself had no significant impact on constitutive and conditionally induced GADD45B RNA expression as detected by qRT-PCR (Figure 29C).

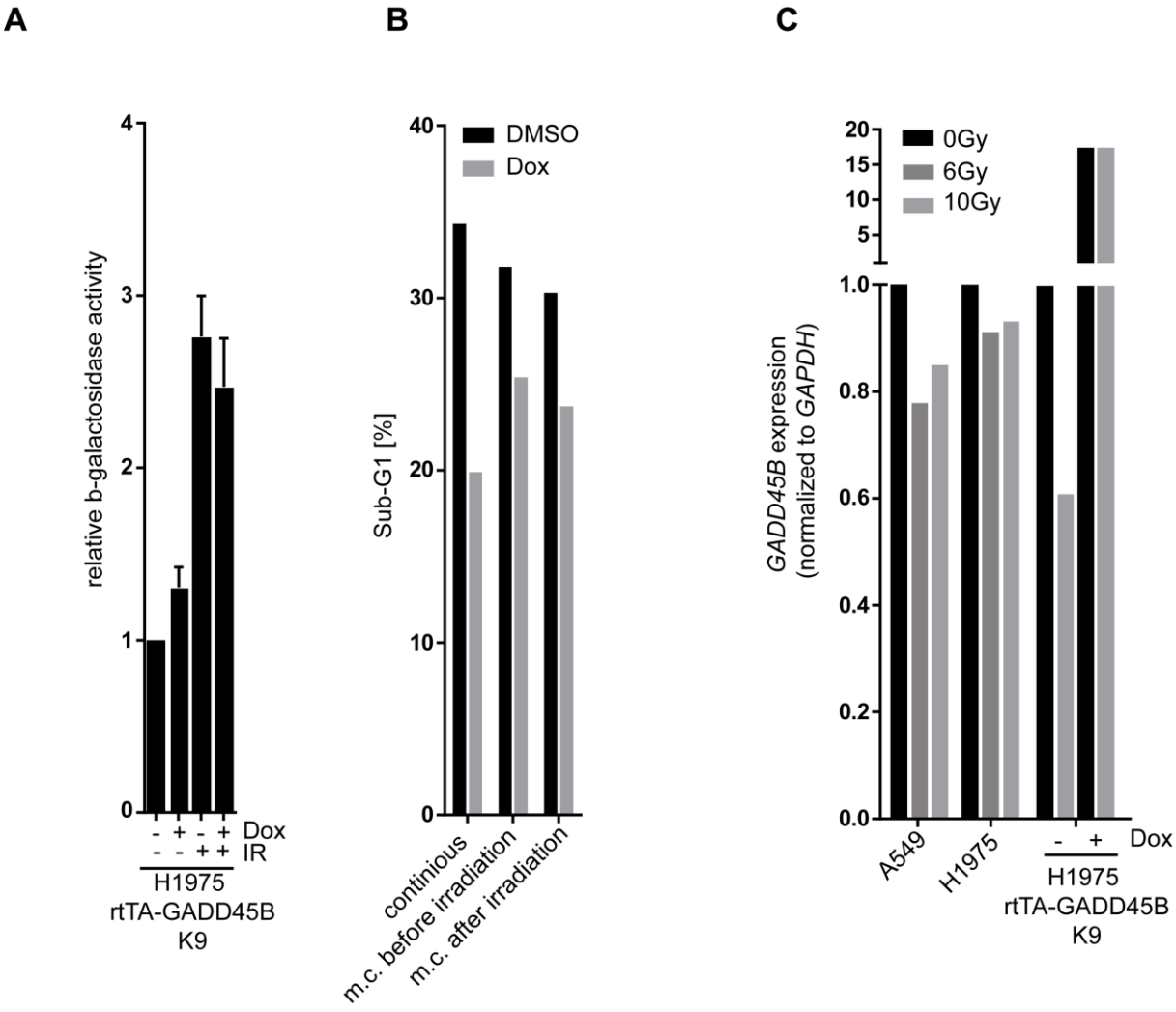

Figure 29: Impact of GADD45B induced by various experimental conditions on radiation-induced apoptosis and senescence.
A: H1975 rtTA-GADD45B K9 cells either were maintained in doxycycline-containing media (continuous) or doxycycline was withdrawn 5 hours or immediately before radiation (m.c.). Apoptotic cell death was quantified by flow cytomentry (n=1) 72h later **B:** GADD45B was induced 24 hours followed by irradiation. After 72 hours SA-b-galactosidase activity was measured fluorometrically (mean relative activity ± SEM; n=3). **C:** Cells were cultured for 24 hours with or without doxycycline followed by irradiation. RNA was isolated after 4 hours to assess *GADD45B* RNA expression by. qRT-PCR; measurement were normalized to expression of the housekeeping gene *GADPH* (n=1).

6. Discussion

The ultimate goal of any cancer therapy is to resect or kill as many cancer cells as possible in a given patient so that the cancer is either eradicated or permanently controlled by host factors. While in some cancer entities cures are possible, in particular at early stages of disease, primary treatment resistance or disease recurrence ultimately lead to death of approximately 40% of patients diagnosed with cancer in Germany (Landeskrebsregister NRW 2016; Robert Koch-Institut 2016). Patients with lung cancer still have one of the poorest long-term prognosis of all cancer entities, which does not exceed 20% overall survival at 5 years if all tumor stages are combined. Recently, major advances have been achieved in medical treatment of patients with metastatic or recurrent NSCLC, which address specific molecular mechanisms that are essential for cancer cell survival or immune tolerance in a given cancer. In contrast, locally ablative treatments including surgery and radiotherapy still do not take into account individual biologies of NSCLC. Radiotherapy is a major treatment modality in patients with advanced lung cancer as well as in inoperably early stage patients (Shtivelman et al. 2014; Chan and Hughes 2015; Yap et al. 2017). Still, tumor escape by development of resistant cells leading to progression is a frequent problem and the majority of patients succumb to localized or systemic relapse (Pignon et al. 2008).

Current radiotherapy attempts to reduce the risk of tumor escape by dose escalation studies including novel planning and fractionation technology and particle therapy (Christodoulou et al. 2014; Morgan et al. 2014). Still, normal tissue toxicity and radioresistant in-field relapse remains a clinically relevant problem (Barnett et al. 2009; Morgan et al. 2014). The underlying hypothesis of this thesis is that altered signal transduction pathways impacting the response to ionizing radiation may serve as rational targets for the biological individualization of chemo-radiotherapy strategies. This hypothesis was approached by two strategies, (i) make use of unbiased functional genomics to identify functionally relevant modulators of the radiation response, and (ii) to functionally validate and molecularly characterize candidate modulators of radioresistance in lung cancer models.

6.1 Functional genomic screens using complex barcoded shRNA libraries are suited for unbiased identification of molecules and pathways modulating the radiation response in lung cancer models

High throughput screens have been successfully applied for drug testing and target identification. Recently, annotated shRNA libraries covering the entire genome or selected gene sets of interest have become a useful tool in functional biology. The introduction of barcoding technology which enables high throughput quantitative analysis of the representation of individual shRNA in complex populations by massively parallel sequencing has provided a major technological step forward (Sims et al. 2011; Perwitasari et al. 2013).

To the best of our knowledge, in the work for this thesis the application of this technology for unbiased, functional identification of putative modulators of the radiation response in lung cancer models was achieved for the first time. Several putative candidates were identified, some of which clustered in specific pathways or cellular functions thus providing additional support of their validity. A system level approach was used to prioritize targets for validation and further characterization. The example of STX18 emerging as one of several hits involved in the same pathway stresses the strength of our experimental approach, which identified factors that were previously not implicated as modulators of the radiation response in NSCLC.

Next, three hits that were prioritized for further validation are briefly discussed:

The candidate FZD5 (Frizzled Class Receptor 5) belongs to the Frizzled receptor family. Frizzled receptors are G protein-coupled receptors that mediate WNT signal transduction and thus play key roles in many essential cellular processes. FZD5 is one of the human frizzled receptors and is activated by the Wnt5A ligand. Its activity is believed to be mainly involved in the non-canonical Wnt-Ca^{2+} pathway (Weeraratna et al. 2002; Sugimura and Li 2010; Peterson et al. 2017). Recently, inhibition of FZD5 was shown to inhibit proliferation in RNF43-mutant PDAC cell lines (Steinhart et al. 2017). Also, blocking FZD5 antibodies inhibited melanoma cell invasion (Weeraratna et al. 2002). Because of the central role of WNT pathway deregulation in several cancers drugs targeting specific components are currently under preclinical and clinical investigation as anticancer agents (Blagodatski et al. 2014; Sheikh et al. 2014; Tai et al. 2015).

Interestingly, *FZD5* knockdown showed opposing effects in a short-term survival assay in two NSCLC cell lines. While knockdown of *FZD5* in A549 cells tended to increase apoptotic cell death in response to irradiation, knockdown in H1975 cells seemed protective. Those differences might be explained by the different knockdown levels as well as the different genetic backgrounds of these cell lines. While A549 possess a wildtype p53, H1975 harbor the p53 mutation R273H (Lu et al. 2017). Also, no consistent modulation of the radiation response by *FZD5* knockdown was observed in long-term assays which are standard in radiobiology research. Therefore, FZD5 was not considered as a *bona fide* modulator in radiation response and was deprioritized in our study. Nevertheless, the shRNA screen did only consider short-term, not long-term survival of A549 cells, and confirmed the results published by others.

The second candidate, PLA2G4B that was selected for validation, is a phospholipase that mediates the conversion of PtdCho (phosphatidylcholine) to acyl-GPC (glycerophosphocholine) (Burke and Dennis 2009; Moestue et al. 2010). A transcriptional readthrough was reported between *PLA2G4B* and the neighboring *JMJD7*, known as *JMJD7-PLA2G4B*. Proteome analysis revealed elevated JMJD7-PLA2G4B levels in several cancer entities (Cheng et al. 2017). However not much is known about its function so far.

In our screen, the *PLA2G4B* shRNA barcode was found to be decreased following irradiation, implicating a role in radiosensitivity. A clonal *PLA2G4B* knockdown cell line showed increased sensitivity to radiation-induced apoptosis as well as radiation-induced reduction in clonogenic survival.

The third candidate, Syntaxin 18 (STX18), is a SNARE protein localized at the ER membrane. STX18 is involved in vesicular trafficking between ER and Golgi (Hatsuzawa et al. 2000). STX18 forms a complex with the SNARE proteins Sec22b, p31, and BNIP (Iinuma et al. 2009; Tagaya et al. 2014). The latter is a pro-apoptotic protein shown to interact with RINT-1, which itself has been implicated in cell cycle regulation because of its interaction with RAD50 (Xiao et al. 2001; Grigaravicius et al. 2016a; b). STX18 has also been implicated in global ER organization as its downregulation leads to major changes in ER structure (Iinuma et al. 2009; Varadarajan et al. 2012). Interestingly, STX18 overexpression was described in breast cancer, although *in vitro* data suggested it to be a negative growth regulator of cell growth (Bassett et al. 2008). Altogether, to our knowledge few studies have aimed to elucidate a functional role for STX18 in cancer biology. The involvement of

other SNARE proteins in tumor onset and progression, however, is widely accepted (Meng and Wang 2015), although their potential role in the response to ionizing radiation remains virtually unknown. The importance of vesicular transport was shown in studies deciphering UVA-induced communication between melanocytes and keratinocytes, where UVA lead to generation and secretion of extracellular vesicles by melanocytes that are endocytosed by keratinocytes thus protecting the latter from UV induced damage (Ando et al. 2012; Wäster et al. 2016). This suggests a negative effect of impaired vesicular transport on cell survival. While the direct DNA damage caused by UV irradiation clearly differs from the indirect DNA damage caused by ionizing radiation, those studies provide evidence for the responsiveness of the vesicular transport machinery to extracellular stressors.

While smoking is the leading risk factor for the development of lung cancer, approximately 10% to 20% of lung cancer patients are non-smokers (Pallis and Syrigos 2013). This suggests the contribution of additional, possibly also endogenous susceptibility factors for lung cancer development. Identifying genetic risk factors for lung cancer proves to be a major challenge. Genome-wide association studies were unable to provide strong evidence for genetic variants accounting for a majority of cases (Pallis and Syrigos 2013). However, one of the foci associated with an inherited susceptibility for lung cancer independent of smoking was *VTI1A* (vesicle transport through interaction with t-SNARE homolog 1A) (Oxnard et al. 2014; Su et al. 2015). This gene locus has also been associated with an increased susceptibility for development of colorectal cancer (Wang et al. 2014; Zeng et al. 2016).

Vesicular trafficking genes have also been identified to be involved in maintenance and protection against genotoxic stress caused by the radiomimetic zeocin in yeast, further implicating the involvement of the vesicular trafficking system in DNA damage response (Krol et al. 2015).

There is only limited data regarding therapeutic targeting of SNARE proteins for cancer treatment. Several studies have investigated the influence of botulinum neurotoxin (BoNT) on cancer cells (Ansiaux et al. 2006; Bandala et al. 2013). BoNT is produced by *Clostridium botulinum* in form of seven different serotypes (A-G) that target different intracellular proteins by varying mechanisms. Collectively these toxins inhibit release of acetylcholine by neuronal cells. This inhibition is mediated by cleavage of SNARE proteins, which blocks vesicle fusion that is needed for acetylcholine uptake (Dressler et al. 2005). In the context of cancer, BoNT-A is of particular interest because of its ability to enhance tumor oxygenation and perfusion

which in turn improved efficacy of radiotherapy and chemotherapy in fibrosarcoma and hepatocarcinoma models (Ansiaux et al. 2006). Also, BoNT-A treatment directly induced apoptosis in a breast cancer cell line (Bandala et al. 2013). In summary, these studies implicate the susceptibility of tumor cells to toxins acting on SNARE proteins (Ansiaux et al. 2006; Bandala et al. 2013; Zhao et al. 2014). However, tumor cells generally do not express BoNT entry receptors at high densities. Thus, for therapeutic use recombinant BoNTs capable of targeting tumor cells are requried (Meng and Wang 2015).

In this thesis we could demonstrate that interference with vesicular transport by knockdown of the SNARE protein *STX18* increases radiosensitivity of the radioresistant NSCLC cell line A549 *in vitro*, thus supporting a global role of the cellular transport machinery in the cellular stress response. However, this radiosensitization effect seems to depend on a specific biological context: Suppression of *STX18* in the relatively radiosensitive NSCLC cell line H1975 was not observed. This dependency could be based on the different genetic background of A549 and H1975 NSCLC, which vary in their mutational status e.g. of EGFR, TP53 and KRAS (Li et al. 2015; Lu et al. 2017). As the knockdown efficacy of *STX18* was much lower in H1975 cells, an alternative explanation could be that these cells are constitutively sensitive to suppression of STX18 itself. Thus compensatory mechanisms including an ineffective suppression of endogenous STX18 above the threshold for radiosensitization may be in place.

In our system, knockdown of *STX18* was correlated with a decrease in mRNA level and enzymatic activity of MMP9. While the SNARE proteins STX13, SNAP23 and VAMP3 have already been associated with the secretion of MMP9 in a fibrosarcoma cell line (Kean et al. 2009) to our knowledge there are no reports of a role of STX18 in this process. The decrease of MMP9 by STX18 suppression was associated with increased susceptibility to anoikis *in vitro* and reduced metastasis formation in an orthotopic *in vivo* model. Collectively, these findings support that the extent of STX18 suppression achieved in A549 cells by shRNA technology is sufficient to modulate specific biological processes *in vitro* and *in vivo*.

In an initial *in vivo* experiment using an orthotopic mouse model, only small therapeutic effects of radiation on tumor growth could be detected overall, independent from STX18-status in the injected cells. Also, metastasis to the right lung was observed very early in all groups. Therefore, the initial finding that *STX18* knockdown might not have an impact on radiation response is to be considered

critically. To draw meaningful conclusions experimental conditions need to be optimized by e.g. changing the injection setup, radiating the tumors at an earlier time point or establishing a protocol for fractionized radiation. Further *in vivo* experiments will be needed to ultimately uncover which impact STX18 has on radiation response *in vivo*.

6.2 Modulation of the radiation response of lung cancers by GADD45B

The second part of this thesis focused on GADD45B. GADD45B belongs to the GADD45 protein family that is activated following growth arrest conditions or DNA damage (Liebermann and Hoffman 2008; Salvador et al. 2013). Proteins of this family mediate a wide variety of cellular responses including DNA repair, senescence, apoptosis, and activation of stress response pathways. It was shown that GADD45 proteins can act through the p38/JNK pathway by inhibiting MKK7, thus promoting cell survival (De Smaele et al. 2001; Papa 2004). In multiple myeloma models, inhibition of the interaction between GADD45B and MKK7 using a selective inhibitor induced rapid cell death (Tornatore et al. 2014).

Activation of GADD45B has been reported in pro-apoptotic pathways in several tumor entities. However, it has also been described to impinge on pro-survival pathways in other models, especially in hematopoietic cell lines. Thus, the functions of GADD45 proteins seem complex and probably cell type dependent (Zhan et al. 1999; Gupta et al. 2006; Engelmann et al. 2008; Liebermann and Hoffman 2008; Tornatore et al. 2008).

In our laboratory, GADD45B was identified as a protein that mediates resistance against Afatinib, a tyrosine kinase inhibitor used for treatment of NSCLC. In this thesis, two doxycycline inducible GADD45B NSCLC cell lines were generated in H1975 and HCC827 cells for functional studies. In line with previous reports (Huang et al. 2018) , overexpression of GADD45B significantly decreased cell proliferation as seen by MTT and colony assays, the latter showing a completely hindered ability of cells to form colonies when kept under permanent transgene expression. In the H1975 model this might be due to a G1 arrest following continuous GADD45B expression that can be reversed by doxycycline withdrawal. Interestingly, HCC827 cells show only a slight increase in the G1 fraction upon enforced GADD45B expression. This might be explained by the differently preserved cell cycle checkpoints in these cell lines. For example, H1975 express a mutant p53 protein

(R273H), HCC827 are p53 null mutants (Tung et al. 2015). It is widely accepted that the tumor suppressor p53 is an essential regulator of the G1/S cell cycle checkpoint, which is triggered by DNA damage (Agarwal et al. 1995; Senturk and Manfredi 2013). While both cell lines harbor inactivated p53, the expression of a functionally defective p53 was shown to have different biological outcomes than complete loss of the tumor suppressor (Brož and Attardi 2010; Rivlin et al. 2011; Miller et al. 2016).

Interestingly, GADD45B protected both, H1975 and HCC827 cells, against rapid apoptotic cell death induced by radiation. However, this did not translate into increased long-term clonogenic survival. The latter result may however suffer from methodological differences, as the colony assay relies on the proliferative capacity of cells *in vitro*, which itself is suppressed by transgenic GADD45B. Translating the models into an *in vivo* system may be one way to find a more relevant model for studying GADD45B modulation of the radiation response of lung cancers.

6.3 Conclusion and outlook

With this thesis a framework for global functional studies of modulators of the radiation response of lung cancers was established. Several putative modulators of the irradiation response were identified, which provide leads and hypotheses for further in-depth examination of the respective pathways and molecules. Within the scope of this thesis it was only possible to validate selected targets, and to initiate molecular characterization of their mechanism of action. Three candidates, FZD5, PLA2G4B and STX18, were validated and partially characterized. In particular, *STX18* knockdown which impairs vesicular transport between Golgi and ER resulted in increased radiosensitivity *in vitro*, as confirmed by short-term and long-term experiments. The underlying mechanism remains to be further elucidated. In addition, the observed decrease in MMP9 activity provides an interesting, additional avenue how STX18 may impact on tumor progression and escape from treatment.

Another candidate radiomodulator, GADD45B, was confirmed as inhibitor of rapid cell death induced by radiotherapy of lung cancer models. While an impact on long-term clonogenic survival was not confirmed *in vitro* – most likely for methodological issues – the results obtained in this thesis merit further investigation *in vivo*.

Altogether, this thesis provides novel technologies and mechanistic insights into impact of specific cellular processes and signaling pathways on the radiotherapy response in NSCLC.

7. References

Abazeed ME, Adams DJ, Hurov KE, et al (2013) Integrative radiogenomic profiling of squamous cell lung Cancer. Cancer Res 73:6289–6298. doi: 10.1158/0008-5472.CAN-13-1616

Abbas-Terki T, Blanco-Bose W, Déglon N, et al (2002) Lentiviral-mediated RNA interference. Hum Gene Ther 13:2197–201. doi: 10.1089/104303402320987888

Abreu CECV, Ferreira PPR, de Moraes FY, et al (2015) Stereotactic body radiotherapy in lung cancer: an update. J Bras Pneumol publicação Of da Soc Bras Pneumol e Tisilogia 41:376–87. doi: 10.1590/S1806-37132015000000034

Advani SJ, Camargo MF, Seguin L, et al (2015) Kinase-independent role for CRAF-driving tumour radioresistance via CHK2. Nat Commun 6:8154. doi: 10.1038/ncomms9154

Agarwal ML, Agarwal A, Taylor WR, Stark GR (1995) p53 controls both the G2/M and the G1 cell cycle checkpoints and mediates reversible growth arrest in human fibroblasts. Proc Natl Acad Sci U S A 92:8493–8497. doi: 10.1073/pnas.92.18.8493

Alvarez C, Sztul ES (1999) Brefeldin A (BFA) disrupts the organization of the microtubule and the actin cytoskeletons. Eur J Cell Biol 78:1–14. doi: 10.1016/S0171-9335(99)80002-8

Ando H, Niki Y, Ito M, et al (2012) Melanosomes are transferred from melanocytes to keratinocytes through the processes of packaging, release, uptake, and dispersion. J Invest Dermatol 132:1222–1229. doi: 10.1038/jid.2011.413

Ansiaux R, Baudelet C, Cron GO, et al (2006) Botulinum toxin potentiates cancer radiotherapy and chemotherapy. Clin Cancer Res 12:1276–1283. doi: 10.1158/1078-0432.CCR-05-1222

Antonia SJ, Villegas A, Daniel D, et al (2017) Durvalumab after Chemoradiotherapy in Stage III Non–Small-Cell Lung Cancer. N Engl J Med NEJMoa1709937. doi: 10.1056/NEJMoa1709937

Ashburner M, Ball CA, Blake JA, et al (2000) Gene ontology: Tool for the unification of biology. Nat. Genet. 25:25–29.

Awwad HM, Geisel J, Obeid R (2012) The role of choline in prostate cancer. Clin. Biochem. 45:1548–1553.

Bandala C, Perez-Santos JLM, Lara-Padilla E, et al (2013) Effect of botulinum toxin A on proliferation and apoptosis in the T47D breast cancer cell line. Asian Pac J Cancer Prev 14:891–4. doi: 10.7314/APJCP.2013.14.2.891

Barnett GC, West CML, Dunning AM, et al (2009) Normal tissue reactions to radiotherapy: Towards tailoring treatment dose by genotype. Nat. Rev. Cancer 9:134–142.

Baskar R, Lee KA, Yeo R, Yeoh K-W (2012) Cancer and Radiation Therapy: Current Advances and Future Directions. Int J Med Sci 9:193–199. doi: 10.7150/ijms.3635

Bassett T, Harpur B, Poon HY, et al (2008) Effective stimulation of growth in MCF-7 human breast cancer cells by inhibition of syntaxin18 by external guide sequence and ribonuclease P. Cancer Lett 272:167–175. doi: 10.1016/j.canlet.2008.07.014

Bayraktar S, Rocha-Lima CM (2013) Molecularly targeted therapies for advanced or metastatic non-small-cell lung carcinoma. World J Clin Oncol 4:29–42. doi: 10.5306/wjco.v4.i2.29

Blagodatski A, Poteryaev D, Katanaev VL (2014) Targeting the Wnt pathways for therapies. Mol Cell Ther 2:28. doi: 10.1186/2052-8426-2-28

Bolus NE (2001) Basic Review of Radiation Biology and Terminology. J Nucl Med Technol 29:67–73. doi: 10.2967/jnmt.117.195230

Brož DK, Attardi LD (2010) In vivo analysis of p53 tumor suppressor function using genetically engineered mouse models. Carcinogenesis 31:1311–1318. doi: 10.1093/carcin/bgp331

Burke JE, Dennis E a. (2009) Phospholipase A 2 structure/function, mechanism, and signaling. J Lipid Res 50:S237–S242. doi: 10.1194/jlr.R800033-JLR200

Burton DG a., Krizhanovsky V (2014) Physiological and pathological consequences of cellular senescence. Cell Mol Life Sci 71:4373–4386. doi: 10.1007/s00018-014-1691-3

Carbon S, Dietze H, Lewis SE, et al (2017) Expansion of the gene ontology knowledgebase and resources: The gene ontology consortium. Nucleic Acids Res 45:D331–D338. doi: 10.1093/nar/gkw1108

Carbon S, Ireland A, Mungall CJ, et al (2009) AmiGO: Online access to ontology and annotation data. Bioinformatics 25:288–289. doi: 10.1093/bioinformatics/btn615

Carson J, Finley DJ (2011) Lung Cancer Staging: An Overview of the New Staging System and Implications for Radiographic Clinical Staging. Semin Roentgenol 46:187–193. doi: 10.1053/j.ro.2011.02.004

Cengel K a., McKenna WG (2005) Molecular targets for altering radiosensitivity: Lessons from Ras as a pre-clinical and clinical model. Crit. Rev. Oncol. Hematol. 55:103–116.

Chan B a, Hughes BGM (2015) Targeted therapy for non-small cell lung cancer: current standards and the promise of the future. Transl lung cancer Res 4:36–54. doi: 10.3978/j.issn.2218-6751.2014.05.01

Chen YM (2017) Immune checkpoint inhibitors for nonsmall cell lung cancer treatment. J. Chinese Med. Assoc. 80:7–14.

Cheng Y, Wang Y, Li J, et al (2017) A novel read-through transcript JMJD7-PLA2G4B regulates head and neck squamous cell carcinoma cell proliferation and survival. Oncotarget 8:1972–1982. doi: 10.18632/oncotarget.14081

Cho JH (2017) Immunotherapy for Non-small-cell Lung Cancer : Current Status and Future Obstacles. 17:378–391. doi: 10.4110/in.2017.17.6.378

Christodoulou M, Bayman N, McCloskey P, et al (2014) New radiotherapy approaches in locally advanced non-small cell lung cancer. Eur. J. Cancer 50:525–534.

Cohen GM (1997) Caspases: the executioners of apoptosis. Biochem J 326:1–16. doi: 10.1042/bj3260001

D'Addario G, Pintilie M, Leighl NB, et al (2005) Platinum-based versus non-platinum-based chemotherapy in advanced non-small-cell lung cancer: A meta-analysis of the published literature. J Clin Oncol 23:2926–2936. doi: 10.1200/JCO.2005.03.045

De Smaele E, Zazzeroni F, Papa S, et al (2001) Induction of gadd45b by NF-kB downregulates pro-apoptotic JNK signalling. Nature 414:308–313. doi: 10.1038/35104560

Debacq-Chainiaux F, Erusalimsky JD, Campisi J, Toussaint O (2009) Protocols to detect senescence-associated beta-galactosidase (SA-βgal) activity, a biomarker of senescent cells in culture and in vivo. Nat Protoc 4:1798–1806. doi: 10.1038/nprot.2009.191

Deriano L, Stracker TH, Baker A, et al (2009) Roles for NBS1 in Alternative Nonhomologous End-Joining of V(D)J Recombination Intermediates. Mol Cell 34:13–25. doi: 10.1016/j.molcel.2009.03.009

Diehl P, Tedesco D, Chenchik A (2014) Use of RNAi screens to uncover resistance mechanisms in cancer cells and identify synthetic lethal interactions. Drug Discov Today Technol 11:11–18. doi: 10.1016/j.ddtec.2013.12.002

Dimri GP, Lee X, Basile G, et al (1995) A biomarker that identifies senescent human cells in culture and in aging skin in vivo. Proc Natl Acad Sci 92:9363–9367. doi: 10.1073/pnas.92.20.9363

Donaldson KL, Goolsby GL, Wahl AF (1994) Cytotoxicity of the anticancer agents cisplatin and taxol during cell proliferation and the cell cycle. Int J Cancer 57:847–855. doi: 10.1002/ijc.2910570614

Dong D, Ni M, Li J, et al (2008) Critical role of the stress chaperone GRP78/BiP in tumor proliferation, survival, and tumor angiogenesis in transgene-induced mammary tumor development. Cancer Res 68:498–505. doi: 10.1158/0008-5472.CAN-07-2950

Dressler D, Saberi FA, Barbosa ER (2005) Botulinum toxin: mechanisms of action. Arq Neuropsiquiatr 63:180–5. doi: /S0004-282X2005000100035

Duman JG, Forte JG (2003) What is the role of SNARE proteins in membrane fusion? Am J Physiol Cell Physiol 285:C237–C249. doi: 10.1152/ajpcell.00091.2003

Elbashir SM, Harborth J, Lendeckel W, et al (2001) Duplexes of 21 ± nucleotide RNAs mediate RNA interference in cultured mammalian cells. Nature 411:494–498. doi: 10.1038/35078107

Elmore S (2007) Apoptosis: A Review of Programmed Cell Death. Toxicol. Pathol. 35:495–516.

Engelmann a, Speidel D, Bornkamm GW, et al (2008) Gadd45 beta is a pro-survival factor associated with stress-resistant tumors. Oncogene 27:1429–1438. doi: 10.1038/sj.onc.1210772

Finney RE, Nudelman E, White T, et al (2000) Pharmacological inhibition of phosphatidylcholine biosynthesis is associated with induction of phosphatidylinositol accumulation and cytolysis of neoplastic cell lines. Cancer Res 60:5204–5213.

Fong PC, Boss DS, Yap TA, et al (2009) Inhibition of Poly(ADP-Ribose) Polymerase in Tumors from BRCA Mutation Carriers. N Engl J Med 361:123–134. doi: 10.1056/NEJMoa0900212

Fornace AJ, Alamo I, Hollander MC (1988) DNA damage-inducible transcripts in mammalian cells. Proc Natl Acad Sci U S A 85:8800–8804. doi: 10.1073/pnas.85.23.8800

Fujiwara T, Oda K, Yokota S, et al (1988) Brefeldin A causes disassembly of the Golgi complex and accumulation of secretory proteins in the endoplasmic reticulum. J Biol Chem 263:18545–18552.

Glunde K, Bhujwalla ZM, Ronen SM (2011) Choline metabolism in malignant transformation. Nat. Rev. Cancer 11:835–848.

Goeckenjan G, Sitter H, Thomas M, et al (2011) Prevention, diagnosis, therapy, and follow-up of lung cancer: Interdisciplinary guideline of the German respiratory society and the German cancer society. Pneumologie 65:39–59. doi: 10.1055/s-0030-1255961

Golden EB, Pellicciotta I, Demaria S, et al (2012) The convergence of radiation and immunogenic cell death signaling pathways. Front Oncol 2:1–13. doi: 10.3389/fonc.2012.00088

Gong F, Fahy D, Liu H, et al (2008) Role of the mammalian SWI/SNF chromatin remodeling complex in the cellular response to UV damage. Cell Cycle 7:1067–1074. doi: 10.4161/cc.7.8.5647

Grigaravicius P, Kaminska E, Hubner CA, et al (2016a) Rint1 inactivation triggers genomic instability, ER stress and autophagy inhibition in the brain. Cell Death Differ 23:454–468. doi: 10.1038/cdd.2015.113

Grigaravicius P, von Deimling A, Frappart PO (2016b) RINT1 functions as a multitasking protein at the crossroads between genomic stability, ER homeostasis, and autophagy. Autophagy 12:1413–1415.

Gupta M, Gupta SK, Hoffman B, Liebermann D a (2006) Gadd45a and Gadd45b protect hematopoietic cells from UV-induced apoptosis via distinct signaling pathways, including p38 activation and JNK inhibition. J Biol Chem 281:17552–8. doi: 10.1074/jbc.M600950200

Gurney a., Axelrod F, Bond CJ, et al (2012) Wnt pathway inhibition via the targeting of Frizzled receptors results in decreased growth and tumorigenicity of human tumors. Proc Natl Acad Sci 109:11717–11722. doi: 10.1073/pnas.1120068109

Hall EJ, Higgins Professor F, Giaccia AJ, et al (2012) Radiobiolgy for the Radiobiologist. 3–9, 2–23,30–60.

Hammerschmidt S, Wirtz H (2009) Lung cancer: current diagnosis and treatment. Dtsch Ärzteblatt Int 106:809–18; quiz 819–20. doi: 10.3238/arztebl.2009.0809

Hanahan D, Weinberg R a (2000) The hallmarks of cancer. Cell 100:57–70. doi: 10.1007/s00262-010-0968-0

Hatsuzawa K, Hirose H, Tani K, et al (2000) Syntaxin 18, a SNAP receptor that functions in the endoplasmic reticulum, intermediate compartment, and cis-Golgi vesicle trafficking. J Biol Chem 275:13713–13720. doi: 10.1074/jbc.275.18.13713

Helissey C, Champiat S, Soria J-C (2015) Immune checkpoint inhibitors in advanced nonsmall cell lung cancer. Curr Opin Oncol 27:108–117. doi: 10.1097/CCO.0000000000000167

Hellmann MD, Rizvi N a., Goldman JW, et al (2017) Nivolumab plus ipilimumab as first-line treatment for advanced non-small-cell lung cancer (CheckMate 012): results of an open-label, phase 1, multicohort study. Lancet Oncol 18:31–41. doi: 10.1016/S1470-2045(16)30624-6

Hsu VW, Yang JS (2009) Mechanisms of COPI vesicle formation. FEBS Lett. 583:3758–3763.

Huang H, Wang Q, Du T, et al (2018) Matrine inhibits the progression of prostate cancer by promoting expression of GADD45B. Prostate 78:327–335. doi: 10.1002/pros.23469

Iinuma T, Aoki T, Arasaki K, et al (2009) Role of syntaxin 18 in the organization of endoplasmic reticulum subdomains. J Cell Sci 122:1680–1690. doi: 10.1242/jcs.036103

Jacob A, Prekeris R (2015) The regulation of MMP targeting to invadopodia during cancer metastasis. Front Cell Dev Biol 3:1–9. doi: 10.3389/fcell.2015.00004

Kean MJ, Williams KC, Skalski M, et al (2009) VAMP3, syntaxin-13 and SNAP23 are involved in secretion of matrix metalloproteinases, degradation of the extracellular matrix and cell invasion. J Cell Sci 122:4089–4098. doi: 10.1242/jcs.052761

Kelley MR, Logsdon D, Fishel ML (2014) Targeting DNA repair pathways for cancer treatment: what's new? Futur Oncol 10:1215–1237. doi: 10.2217/fon.14.60

Kelly R, Gulley J, Giaccone G (2010) Targeting the immune system in non-small-cell lung cancer: Bridging the gap between promising concept and therapeutic reality. Clin. Lung Cancer 11:228–237.

Kim IA, Fernandes AT, Gupta AK, et al (2004) The influence of Ras pathway signaling on tumor radiosensitivity. Cancer Metastasis Rev. 23:227–236.

Klinkenbijl JH, Jeekel J, Sahmoud T, et al (1999) Adjuvant radiotherapy and 5-fluorouracil after curative resection of cancer of the pancreas and periampullary region: phase III trial of the EORTC gastrointestinal tract cancer cooperative group. Ann Surg 230:776–82; discussion 782–4. doi: 10.1097/00000658-199912000-00006

Komiya Y, Habas R (2008) Wnt signal transduction pathways. Organogenesis 4:68–75.

Konermann S, Brigham MD, Trevino AE, et al (2015) Genome-scale transcriptional activation by an engineered CRISPR-Cas9 complex. Nature 517:583–588. doi: 10.1038/nature14136

Krol K, Brozda I, Skoneczny M, et al (2015) A genomic screen revealing the importance of vesicular trafficking pathways in genome maintenance and protection against genotoxic stress in diploid saccharomyces cerevisiae cells. PLoS One 10:1–32. doi: 10.1371/journal.pone.0120702

Kvols LK (2005) Radiation sensitizers: a selective review of molecules targeting DNA and non-DNA targets. J Nucl Med 46 Suppl 1:187S–90S. doi: 46/1_suppl/187S [pii]

Landeskrebsregister NRW (2016) Jahresbericht 2016: Krebsgeschen in Nordrhein-Westfalen 2014.

Lawrence TS, Blackstock a. W, McGinn C (2003) The mechanism of action of radiosensitization of conventional chemotherapeutic agents. Semin. Radiat. Oncol. 13:13–21.

Lawrence TS, Tepper JE, Blackstock a. W (1997) Fluoropyrimidine-radiation interactions in cells and tumors. Semin. Radiat. Oncol. 7:260–266.

Lee AS (2007) GRP78 induction in cancer: Therapeutic and prognostic implications. Cancer Res. 67:3496–3499.

Lennartz K, Lu M, Flasshove M, et al (2005) Improving the biosafety of cell sorting by adaptation of a cell sorting system to a biosafety cabinet. Cytom Part A 66:119–127. doi: 10.1002/cyto.a.20157

Li J, Deng H, Hu M, et al (2015) Inhibition of non-small cell lung cancer (NSCLC) growth by a novel small molecular inhibitor of EGFR. Oncotarget 6:6749–6761. doi: 10.18632/oncotarget.3155

Li J, Ni M, Lee B, et al (2008) The unfolded protein response regulator GRP78/BiP is required for endoplasmic reticulum integrity and stress-induced autophagy in mammalian cells. Cell Death Differ 15:1460–1471. doi: 10.1038/cdd.2008.81

Lieber MR (2010) The Mechanism of Double-Strand DNA Break Repair by the Nonhomologous DNA End-Joining Pathway. Annu Rev Biochem 79:181–211. doi: 10.1146/annurev.biochem.052308.093131

Liebermann D a, Hoffman B (2008) Gadd45 in stress signaling. J. Mol. Signal. 3:15.

Lin Y, Wang X, Jin H (2014) EGFR-TKI resistance in NSCLC patients: mechanisms and strategies. Am J Cancer Res 4:411–435.

Lu W, Cheng F, Yan W, et al (2017) Selective targeting p53WTlung cancer cells harboring homozygous p53 Arg72 by an inhibitor of CypA. Oncogene

Luo SY, Lam DC (2013) Oncogenic driver mutations in lung cancer. Transl Respir Med 1:6. doi: 10.1186/2213-0802-1-6

MacDonald BT, Tamai K, He X (2009) Wnt/β-Catenin Signaling: Components, Mechanisms, and Diseases. Dev. Cell 17:9–26.

Maciejczyk A, Skrzypczyńska I, Janiszewska M (2014) Lung cancer. Radiotherapy in lung cancer: Actual methods and future trends. Reports Pract Oncol Radiother 19:353–360. doi: 10.1016/j.rpor.2014.04.012

Maemondo M, Inoue A, Kobayashi K, et al (2010) Gefitinib or Chemotherapy for Non–Small-Cell Lung Cancer with Mutated EGFR. N Engl J Med 362:2380–2388. doi: 10.1056/NEJMoa0909530

Maher J, Davies ET (2004) Targeting cytotoxic T lymphocytes for cancer immunotherapy. Br. J. Cancer 91:817–821.

Mao Z, Bozzella M, Seluanov A, Gorbunova V (2008) Comparison of nonhomologous end joining and homologous recombination in human cells. DNA Repair (Amst) 7:1765–1771. doi: 10.1016/j.dnarep.2008.06.018

Massarelli E, Papadimitrakopoulou V, Welsh J, et al (2014) Immunotherapy in Lung Cancer. Transl. Lung Cancer Res. 3:53–63.

McGinn CJ, Lawrence TS (2001) Recent advances in the use of radiosensitizing nucleosides. Semin Radiat Oncol 11:270–280. doi: 10.1053/srao.2001.26002

McGuire S (2016) World Cancer Report 2014. Geneva, Switzerland: World Health Organization, International Agency for Research on Cancer, WHO Press, 2015. Adv Nutr An Int Rev J 7:418–419. doi: 10.3945/an.116.012211

McKenna WG, Muschel RJ, Gupta AK, et al (2003) The RAS signal transduction pathway and its role in radiation sensitivity. Oncogene 22:5866–5875.

Mehner C, Hockla A, Miller E, et al (2014) Tumor cell-produced matrix metalloproteinase 9 (MMP-9) drives malignant progression and metastasis of

basal-like triple negative breast cancer. Oncotarget 5:2736–2749. doi: 10.18632/oncotarget.1932

Meng J, Wang J (2015) Role of SNARE proteins in tumourigenesis and their potential as targets for novel anti-cancer therapeutics. Biochim. Biophys. Acta - Rev. Cancer 1856:1–12.

Mi H, Dong Q, Muruganujan A, et al (2009) PANTHER version 7: Improved phylogenetic trees, orthologs and collaboration with the Gene Ontology Consortium. Nucleic Acids Res 38:204–210. doi: 10.1093/nar/gkp1019

Michel V, Yuan Z, Ramsubir S, Bakovic M (2006) Choline transport for phospholipid synthesis. Exp Biol Med (Maywood) 231:490–504. doi: 231/5/490 [pii]

Miki Y, Swensen J, Shattuck-Eidens D, et al (1994) A strong candidate for the breast and ovarian cancer susceptibility gene BRCA1. Science (80-) 266:66–71. doi: 10.1126/science.7545954

Miller M, Shirole N, Tian R, et al (2016) The evolution of TP53. J Cancer Biol Res 1848:3047–3054. doi: 10.1016/j.bbamem.2015.02.010.Cationic

Mintz PJ, Kim J, Do KA, et al (2003) Fingerprinting the circulating repertoire of antibodies from cancer patients. Nat Biotechnol 21:57–63. doi: 10.1038/nbt774

Mladenov E, Iliakis G (2011a) Induction and repair of DNA double strand breaks: The increasing spectrum of non-homologous end joining pathways. Mutat Res - Fundam Mol Mech Mutagen 711:61–72. doi: 10.1016/j.mrfmmm.2011.02.005

Mladenov E, Iliakis G (2011b) The Pathways of Double-Strand Break Repair. DNA Repair - Pathways to Fixing DNA Damage Errors 380. doi: 10.5772/24574

Mladenov E, Magin S, Soni A, Iliakis G (2013) DNA Double-Strand Break Repair as Determinant of Cellular Radiosensitivity to Killing and Target in Radiation Therapy. Front Oncol 3:1–18. doi: 10.3389/fonc.2013.00113

Moestue SA, Borgan E, Huuse EM, et al (2010) Distinct choline metabolic profiles are associated with differences in gene expression for basal-like and luminal-like breast cancer xenograft models. BMC Cancer 10:1–12. doi: 10.1186/1471-2407-10-433

Mok TS, Wu Y, Thongprasert S, et al (2009) Gefitinib or Carboplatin–Paclitaxel in Pulmonary Adenocarcinoma. N Engl J Med 361:947–957. doi: 10.1056/NEJMoa0810699

Morgan M a., Parsels L a., Maybaum J, Lawrence TS (2014) Improving the efficacy of chemoradiation with targeted agents. Cancer Discov. 4:280–291.

Morgillo F, Della Corte CM, Fasano M, Ciardiello F (2016) Mechanisms of resistance to EGFR-targeted drugs: lung cancer. ESMO Open 1:e000060. doi: 10.1136/esmoopen-2016-000060

Normanno N, De Luca A, Bianco C, et al (2006) Epidermal growth factor receptor (EGFR) signaling in cancer. Gene 366:2–16.

Oslowski CM, Urano F (2011) Measuring ER stress and the unfolded protein response using mammalian tissue culture system. Methods Enzymol 490:71–92. doi: 10.1016/B978-0-12-385114-7.00004-0

Oxnard GR, Nguyen KSH, Costa DB (2014) Germline mutations in driver oncogenes and inherited lung cancer risk independent of smoking history. J Natl Cancer Inst 106:2013–2015. doi: 10.1093/jnci/djt361

Paez JG, Jänne PA, Lee JC, et al (2004) EGFR mutations in lung, cancer: Correlation with clinical response to gefitinib therapy. Science (80-) 304:1497–1500. doi: 10.1126/science.1099314

Pallis AG, Syrigos KN (2013) Lung cancer in never smokers: Disease characteristics and risk factors. Crit. Rev. Oncol. Hematol. 88:494–503.

Papa S (2004) Linking JNK signaling to NF- B: a key to survival. J Cell Sci 117:5197–5208. doi: 10.1242/jcs.01483

Park K, Tan EH, O'Byrne K, et al (2016) Afatinib versus gefitinib as first-line treatment of patients with EGFR mutation-positive non-small-cell lung cancer (LUX-Lung 7): A phase 2B, open-label, randomised controlled trial. Lancet Oncol 17:577–589. doi: 10.1016/S1470-2045(16)30033-X

Perwitasari O, Bakre A, Mark Tompkins S, Tripp R a. (2013) siRNA genome screening approaches to therapeutic drug repositioning. Pharmaceuticals 6:124–160. doi: 10.3390/ph6020124

Peterson YK, Nasarre P, Bonilla I V., et al (2017) Frizzled-5: a high affinity receptor for secreted frizzled-related protein-2 activation of nuclear factor of activated T-cells c3 signaling to promote angiogenesis. Angiogenesis 20:615–628. doi: 10.1007/s10456-017-9574-5

Pierce AJ, Jasin M (2001) NHEJ deficiency and disease. Mol Cell 8:1160–1161. doi: 10.1016/S1097-2765(01)00424-5

Pignon JP, Tribodet H, Scagliotti G V., et al (2008) Lung adjuvant cisplatin evaluation: A pooled analysis by the LACE collaborative group. J Clin Oncol 26:3552–3559. doi: 10.1200/JCO.2007.13.9030

Pirollo KF, Hao Z, Rait A, et al (1997) Evidence supporting a signal transduction pathway leading to the radiation-resistant phenotype in human tumor cells. Biochem Biophys Res Commun 230:196–201. doi: 10.1006/bbrc.1996.5922

Prahallad A, Sun C, Huang S, et al (2012) Unresponsiveness of colon cancer to BRAF(V600E) inhibition through feedback activation of EGFR. Nature 483:100–104. doi: 10.1038/nature10868

Prasanna PGS, Stone HB, Wong RS, et al (2012) Normal tissue protection for improving radiotherapy: Where are the Gaps? Transl Cancer Res 1:35–48. doi: 10.3978/j.issn.2218-676X.2012.05.05

Ran FA, Hsu PD, Wright J, et al (2013) Genome engineering using the CRISPR-Cas9 system. Nat Protoc 8:2281–2308. doi: 10.1038/nprot.2013.143

Rivlin N, Brosh R, Oren M, Rotter V (2011) Mutations in the p53 tumor suppressor gene: Important milestones at the various steps of tumorigenesis. Genes and Cancer 2:466–474. doi: 10.1177/1947601911408889

Robert Koch-Institut (2016) Bericht zum Krebsgeschehen in Deutschland 2016. Bericht zum Krebsgeschehen Deutschl 16–77. doi: 10.17886/rkipubl-2016-014

Roizin-Towle L, Hall EJ, Pirro JP (1986) Oxygen dependence for chemosensitization by misonidazole. Br J Cancer 54:919–924. doi: 10.1038/bjc.1986.262

Rose PG, Bundy BN, Watkins EB, et al (1999) Concurrent Cisplatin-Based Radiotherapy and Chemotherapy for Locally Advanced Cervical Cancer. N Engl J Med 340:1144–1153. doi: 10.1056/NEJM199904153401502

Rosell R, Carcereny E, Gervais R, et al (2012) Erlotinib versus standard chemotherapy as first-line treatment for European patients with advanced EGFR mutation-positive non-small-cell lung cancer (EURTAC): A multicentre, open-label, randomised phase 3 trial. Lancet Oncol 13:239–246. doi: 10.1016/S1470-2045(11)70393-X

Safranek J, Pesta M, Holubec L, et al (2009) Expression of MMP-7, MMP-9, TIMP-1 and TIMP-2 mRNA in lung tissue of patients with non-small cell lung cancer (NSCLC) and benign pulmonary disease. Anticancer Res 29:2513–2517. doi: 29/7/2513 [pii]

Salvador JM, Brown-Clay JD, Fornace Jr AJ (2013) Stress Sensor Genes.

Sambrook J, Russell DW (2006) The Condensed Protocols: From Molecular Cloning: A Laboratory Manual.

Sanders LM, Zeisel SH (2007) Choline: Dietary requirements and role in brain development. Nutr. Today 42:181–186.

Saunders M, Dische S, Barrett A, et al (1999) Continuous, hyperfractionated, accelerated radiotherapy (CHART) versus conventional radiotherapy in non-small cell lung cancer: Mature data from the randomised multicentre trial. Radiother Oncol 52:137–148. doi: 10.1016/S0167-8140(99)00087-0

Schaake-Koning C, van den Bogaert W, Dalesio O, et al (1992) Effects of Concomitant Cisplatin and Radiotherapy on Inoperable Non-Small-Cell Lung Cancer. N Engl J Med 326:524–530. doi: 10.1056/NEJM199202203260805

Schipler A, Iliakis G (2013) DNA double-strand-break complexity levels and their possible contributions to the probability for error-prone processing and repair pathway choice. Nucleic Acids Res 41:7589–7605. doi: 10.1093/nar/gkt556

Schlabach MR, Luo J, Solimini NL, et al (2008) Cancer proliferation gene discovery through functional genomics. Science (80-) 319:620–624. doi: 10.1126/science.1149200

Senturk E, Manfredi JJ (2013) p53 and Cell Cycle Effects After DNA Damage. Methods Mol Biol 962:49–61. doi: 10.1007/978-1-62703-236-0_4

Sheikh A, Niazi AK, Ahmed MZ, et al (2014) The role of Wnt signaling pathway in carcinogenesis and implications for anticancer therapeutics. Hered. Cancer Clin. Pract. 12:2–5.

Shtivelman E, Hensing T, Simon GR, et al (2014) Molecular pathways and therapeutic targets in lung cancer. Oncotarget 5:1392–1433. doi: 10.18632/oncotarget.1891

Sims D, Mendes-Pereira AM, Frankum J, et al (2011) High-throughput RNA interference screening using pooled shRNA libraries and next generation sequencing. Genome Biol 12:R104. doi: 10.1186/gb-2011-12-10-r104

Steffen A, Le Dez G, Poincloux R, et al (2008) MT1-MMP-Dependent Invasion Is Regulated by TI-VAMP/VAMP7. Curr Biol 18:926–931. doi: 10.1016/j.cub.2008.05.044

Steinhart Z, Pavlovic Z, Chandrashekhar M, et al (2017) Genome-wide CRISPR screens reveal a Wnt-FZD5 signaling circuit as a druggable vulnerability of RNF43-mutant pancreatic tumors. Nat Med 23:60–68. doi: 10.1038/nm.4219

Su WM, Chen ZH, Zhang XC, et al (2015) Single nucleotide polymorphisms in VTI1A gene contribute to the susceptibility of Chinese population to non-small cell lung cancer. Int J Biol Markers 30:e286–e293. doi: 10.5301/jbm.5000140

Sugimura R, Li L (2010) Noncanonical Wnt signaling in vertebrate development, stem cells, and diseases. Birth Defects Res. Part C - Embryo Today Rev. 90:243–256.

Tagaya M, Arasaki K, Inoue H, Kimura H (2014) Moonlighting functions of the NRZ (mammalian Dsl1) complex. Front Cell Dev Biol 2:25. doi: 10.3389/fcell.2014.00025

Tai D, Wells K, Arcaroli J, et al (2015) Targeting the WNT Signaling Pathway in Cancer Therapeutics. Oncologist 20:1189–1198. doi: 10.1634/theoncologist.2015-0057

Teng FY, Wang Y, Tang BL (2001) The syntaxins. Genome Biol 2:REVIEWS3012.

Thomas PD, Campbell MJ, Kejariwal A, et al (2003) PANTHER: A library of protein families and subfamilies indexed by function. Genome Res 13:2129–2141. doi: 10.1101/gr.772403

Thomas PD, Kejariwal A, Guo N, et al (2006) Applications for protein sequence-function evolution data: mRNA/protein expression analysis and coding SNP scoring tools. Nucleic Acids Res 34:645–650. doi: 10.1093/nar/gkl229

Tornatore L, Marasco D, Dathan N, et al (2008) Gadd45?? forms a Homodimeric Complex that Binds Tightly to MKK7. J Mol Biol 378:97–111. doi: 10.1016/j.jmb.2008.01.074

Tornatore L, Sandomenico A, Raimondo D, et al (2014) Cancer-Selective Targeting of the Nf-KB Survival Pathway With Gadd45B/Mkk7 Inhibitors. Cancer Cell 26:495–508. doi: 10.1016/j.ccr.2014.07.027

Torre L a., Bray F, Siegel RL, et al (2015) Global cancer statistics, 2012. CA Cancer J Clin 65:87–108. doi: 10.3322/caac.21262

Tung M-C, Lin P-L, Wang Y-C, et al (2015) Mutant p53 confers chemoresistance in non-small cell lung cancer by upregulating Nrf2. Oncotarget 6:41692–705. doi: 10.18632/oncotarget.6150

Varadarajan S, Bampton ETW, Smalley JL, et al (2012) A novel cellular stress response characterised by a rapid reorganisation of membranes of the endoplasmic reticulum. Cell Death Differ 19:1896–1907. doi: 10.1038/cdd.2012.108

Vijayalakshmi R, Krishnamurthy A (2011) Targetable “Driver” Mutations in Non Small Cell Lung Cancer. Indian J. Surg. Oncol. 2:178–188.

Wagner JM, Karnitz LM (2009) Cisplatin-Induced DNA Damage Activates Replication Checkpoint Signaling Components that Differentially Affect Tumor Cell Survival. Mol Pharmacol 76:208–214. doi: 10.1124/mol.109.055178

Walsh CS (2015) Two decades beyond BRCA1/2: Homologous recombination, hereditary cancer risk and a target for ovarian cancer therapy? Gynecol. Oncol. 137:343–350.

Wang F, Kumar P (2011) The role of radiotherapy in management of pancreatic cancer. J Gastrointest Oncol 2:157–67. doi: 10.3978/j.issn.2078-6891.2011.032

Wang H, Burnett T, Kono S, et al (2014) Trans-ethnic genome-wide association study of colorectal cancer identifies a new susceptibility locus in VTI1A. Nat Commun 5:4613. doi: 10.1038/ncomms5613

Wang L, Xiao X, Li D, et al (2012) Abnormal expression of GADD45B in human colorectal carcinoma. J Transl Med 10:215. doi: 10.1186/1479-5876-10-215

Wang Q, Ma J, Lu Y, et al (2017) CDK20 interacts with KEAP1 to activate NRF2 and promotes radiochemoresistance in lung cancer cells. Oncogene 36:5321–5330. doi: 10.1038/onc.2017.161

Wang R, Zhang Y, Pan Y, et al (2015) Comprehensive investigation of oncogenic driver mutations in Chinese non-small cell lung cancer patients. Oncotarget 6:1–9. doi: 10.18632/oncotarget.5549

Wardman P (2007) Chemical Radiosensitizers for Use in Radiotherapy. Clin Oncol 19:397–417. doi: 10.1016/j.clon.2007.03.010

Wäster P, Eriksson I, Vainikka L, et al (2016) Extracellular vesicles are transferred from melanocytes to keratinocytes after UVA irradiation. Sci Rep 6:1–13. doi: 10.1038/srep27890

Weeraratna AT, Jiang Y, Hostetter G, et al (2002) Wnt5a signaling directly affects cell motility and invasion of metastatic melanoma. Cancer Cell 1:279–288. doi: 10.1016/S1535-6108(02)00045-4

Wieczorek S a., Breitenbuecher F, Soni A, et al (2017) Deregulated BCL-2 family proteins impact on repair of DNA double-strand breaks and are targets to overcome radioresistance in lung cancer. J Cancer Res Clin Oncol 143:1733–1744. doi: 10.1007/s00432-017-2427-1

Williams KC, Coppolino MG (2014) SNARE-dependent interaction of Src, EGFR and 1 integrin regulates invadopodia formation and tumor cell invasion. J Cell Sci 127:1712–1725. doi: 10.1242/jcs.134734

Wooster R, Bignell G, Lancaster J, et al (1995) Identification of the breast cancer susceptibility gene BRCA2. Nature 378:789–792. doi: 10.1038/378789a0

Wu W, Wang M, Wu W, et al (2008) Repair of radiation induced DNA double strand breaks by backup NHEJ is enhanced in G2. DNA Repair (Amst) 7:329–338. doi: 10.1016/j.dnarep.2007.11.008

Wu YL, Cheng Y, Zhou X, et al (2017) Dacomitinib versus gefitinib as first-line treatment for patients with EGFR-mutation-positive non-small-cell lung cancer (ARCHER 1050): a randomised, open-label, phase 3 trial. Lancet Oncol 18:1454–1466. doi: 10.1016/S1470-2045(17)30608-3

Xiao J, Liu CC, Chen PL, Lee WH (2001) RINT-1, a Novel Rad50-interacting Protein, Participates in Radiation-induced G2/M Checkpoint Control. J Biol Chem 276:6105–6111. doi: 10.1074/jbc.M008893200

Yap T a., Macklin-Doherty A, Popat S (2017) Continuing EGFR inhibition beyond progression in advanced non-small cell lung cancer. Eur. J. Cancer 70:12–21.

Yazbeck VY, Villaruz L, Haley M, Socinski MA (2013) Management of normal tissue toxicity associated with chemoradiation (primary skin, esophagus, and lung). Cancer J. (United States) 19:231–237.

Zang S, Liu N, Wang H, et al (2014) Wnt signaling is involved in 6-benzylthioinosine-induced AML cell differentiation. BMC Cancer 14:1–10. doi: 10.1186/1471-2407-14-886

Zappa C, Mousa S a. (2016) Non-small cell lung cancer: current treatment and future advances. Transl Lung Cancer Res 5:288–300. doi: 10.21037/tlcr.2016.06.07

Zeng C, Matsuda K, Jia WH, et al (2016) Identification of Susceptibility Loci and Genes for Colorectal Cancer Risk. Gastroenterology 150:1633–1645. doi: 10.1053/j.gastro.2016.02.076

Zhan Q, Antinore MJ, Wang XW, et al (1999) Association with Cdc2 and inhibition of Cdc2/Cyclin B1 kinase activity by the p53-regulated protein Gadd45. Oncogene 18:2892–2900. doi: 10.1038/sj.onc.1202667

Zhan T, Rindtorff N, Boutros M (2017) Wnt signaling in cancer. Oncogene 36:1461–1473.

Zhang S, Zheng X, Huang H, et al (2015) Afatinib increases sensitivity to radiation in non-small cell lung cancer cells with acquired EGFR T790M mutation. Oncotarget 6:5832–45. doi: 10.18632/oncotarget.3332

Zhao CM, Hayakawa Y, Kodama Y, et al (2014) Denervation suppresses gastric tumorigenesis. Sci Transl Med. doi: 10.1126/scitranslmed.3009569

Zhao W, Steinfeld JB, Liang F, et al (2017) BRCA1-BARD1 promotes RAD51-mediated homologous DNA pairing. Nature. doi: 10.1038/nature24060

Zhou L, Yuan R, Serggio L (2003) Molecular mechanisms of irradiation-induced apoptosis. Front Biosci 8:d9–19.

8. Appendix

8.1 shRNA Screen: hits

Table 3: Targets identified in the shRNA screen.
Targets listed in alphabetical order.

Gene ID	Gene Name
APEX1	Apurinic-Apyrimidinic Endonuclease 1
ATP5G2	ATP Synthase Membrane Subunit C Locus 2
B3GAT3	Beta-1,3-Glucuronyltransferase 3
BPTF	Bromodomain PHD Finger Transcription Factor
BUB1B	Budding Uninhibited By Benzimidazoles 1 houromolog Beta
CAMKK1	Calcium/Calmodulin Dependent Protein Kinase Kinase 1
CDKN1C	Cyclin Dependent Kinase Inhibitor 1C
CES1	Carboxylesterase 1
CXCL13	C-X-C Motif Chemokine 13
CYLD	Ubiquitin Specific Peptidase Like 2
DCC	Deleted In Colorectal Carcinoma
DDX18	DEAD-Box Helicase 18
DUOX1	Dual Oxidase 1
FABP1	Fatty Acid Binding Protein 1
FOXC2	Forkhead Box C2
FZD5	Frizzled Class Receptor 5
GMPPB	GDP-Mannose Pyrophosphorylase B
GPR39	G Protein-Coupled Receptor 39
GSK3A	Glycogen Synthase Kinase 3 Alpha
HCLS1	Hematopoietic Cell-Specific Lyn Substrate 1
HEXB	Hexosaminidase Subunit Beta
IRF2	Interferon Regulatory Factor 2
KIF11	Kinesin Family Member 11
LPHN1	Adhesion G Protein-Coupled Receptor L1
LRP2	LDL Receptor Related Protein 2
MBTPS2	Membrane Bound Transcription Factor Peptidase, Site 2
METTL2B	Methyltransferase Like 2B
MSX1	Msh Homeobox 1-Like Protein
MTHFD1L	Methylenetetrahydrofolate Dehydrogenase (NADP+ Dependent) 1
NRG3	Pro-Neuregulin-3, Membrane-Bound Isoform
NT5C2	Cytosolic Purine 5-Nucleotidase
PCYT1B	Phosphate Cytidylyltransferase 1, Choline, Beta
PDE2A	Cyclic GMP-Stimulated Phosphodiesterase
PLA1A	Phospholipase A1 Member A
PLA2G4B	Phospholipase A2 Group IVB
PRMT5	protein arginine N-methyltransferase 5
PSMA1	Proteasome subunit alpha type-1
PSMA5	Proteasome subunit alpha type-5
ROCK1	Rho Associated Coiled-Coil Containing Protein Kinase 1
RPA1	Replication Protein A1

RPS13	Ribosomal Protein S13
RPS6	Ribosomal Protein S6
RXRB	Retinoid X Receptor Beta
SH2B2	SH2B Adaptor Protein 2
SREBF2	Sterol Regulatory Element Binding Transcription Factor 2
STX16	Syntaxin 16
STX18	Syntaxin 18
STX19	Syntaxin 19
TIMP2	Tissue Inhibitor Of Metalloproteinases 2
TPP2	Tripeptidyl-Peptidase II
WIPI1	WD Repeat Domain Phosphoinositide-Interacting Protein 1
WNT5B	Wnt Family Member 5B
XCL1	Small-Inducible Cytokine C1

8.2 Material

8.2.1 Cell lines

Table 4: Cell lines used and established in this project.

Cell line, abbreviation used in this work	**Plasmid**	**source**
82-6 hTERT	-	Iliakis lab, University Hospital Essen, Germany
A549	-	Molecular Oncology lab, University Hospital Essen, Germany
A549 CRISPRa Ctrl	Lenti dCas-VP64-Blast; Lenti-MS2-P65 HSF1-Hygro	M. Schulte
A549 CRISPRa STX18 g1	CRISPRa g1; Lenti dCas-VP64-Blast; Lenti-MS2-P65 HSF1-Hygro	M. Schulte
A549 CRISPRa STX18 g2	CRISPRa g1; Lenti dCas-VP64-Blast; Lenti-MS2-P65 HSF1-Hygro	M. Schulte
A549 Ctrl	mscv.PGK.Neo	Generated in this work
A549 FZD5	MISSION® pLKO.1-puro FZD5 shRNA plasmid	Generated in this work
A549 shCtrl	MISSION® pLKO.1-puro Non-Mammalian shRNA Control Plasmid	Generated in this work
A549 shCtrl + Ctrl	MISSION® pLKO.1-puro Non-Mammalian shRNA Control Plasmid; mscv.PGK.Neo	Generated in this work
A549 shCtrl + STX18-1	MISSION® pLKO.1-puro Non-Mammalian shRNA Control Plasmid ; Mscv.STX18 #1	Generated in this work
A549 shCtrl + STX18-2	MISSION® pLKO.1-puro Non-Mammalian shRNA Control	Generated in this work

	Plasmid ; Mscv.STX18 #2	
A549 shPLA2G4B	MISSION® pLKO.1-puro PLA2G4B shRNA plasmid	Generated in this work
A549 shSTX18	MISSION® pLKO.1-puro STX18 shRNA plasmid	Generated in this work
A549 shSTX18 K1, K2, K3	MISSION® pLKO.1-puro STX18 shRNA plasmid	Generated in this work
A549 shSTX18 K1-3 + Ctrl	MISSION® pLKO.1-puro STX18 shRNA plasmid; mscv.PGK.Neo	Generated in this work
A549 shSTX18 K1-K3 + STX18-1	MISSION® pLKO.1-puro STX18 shRNA plasmid; Mscv.STX18 #1	Generated in this work
A549 shSTX18 K1-K3 + STX18-2	MISSION® pLKO.1-puro STX18 shRNA plasmid; Mscv.STX18 #2	Generated in this work
A549 STX18-1	Mscv.STX18 #1	Generated in this work
A549 STX18-2	Mscv.STX18 #2	Generated in this work
FNX	-	Nolan lab, Stanford University, USA
H1975	-	Molecular Oncology lab, University Hospital Essen, Germany
H1975 rtTA	pQC_rtTA-M2_IP	V. Ritter
H1975 rtTA GADD45B clonal cells	pQC_rtTA-M2_IP, pRevTRE GADD45ß	E. Buchholz, J. Phasue
H1975 shCtrl	MISSION® pLKO.1-puro Non-Mammalian shRNA Control Plasmid	Generated in this work
H1975 shFZD5	MISSION® pLKO.1-puro FZD5 shRNA plasmid	Generated in this work
H1975 shSTX18	MISSION® pLKO.1-puro STX18 shRNA plasmid	Generated in this work
H1975 shTGFBI	MISSION® pLKO.1-puro_shRNA_TGFBI	S. Nothdurft
H460	-	Molecular Oncology lab, University Hospital Essen, Germany
HCC827 rtTA GADD45B clonal cells	pQC_rtTA-M2_IP, pRevTRE GADD45ß	E. Buchholz, J. Phasue
HEK293FT	-	Molecular Oncology lab, University Hospital Essen, Germany

8.2.2 Plasmids

Table 5: Plasmids used and generated in this project.

Plasmid name	Function	Int. #	Comments	origin
Hit60 (MLV gag-pol)	Retroviral polymerase	MS33		C. Benedict
pCMV.VSV-G	Retroviral envelope	MS32		W. Nishioka
pFLAG-XBP1u-FLuc	XBP1 activity			Provided by Group of Prof. Metzen; gift from Jimtong Horng (Addgene #31239
pMD2	Lentiviral envelope	MS652		Scholl/Fröhling – Ulm
pSPAX	Lentiviral polymerase	MS651		Scholl/Fröhling – Ulm
Lenti dCas-VP64-Blast	CRISPR SAM	MS774	Lentiviral plasmid	Lenti cCAS-VP64_Blast was a gift from Feng Zhang (Addgene plasmid #61425)
Lenti-MS2-P65 HSF1-Hygro	CRISPR SAM	MS773	Lentiviral plasmid	Lenti MS2-P65-HSF1_Hygro was a gift from Feng Zhang (Addgene plasmid #61426)
Lenti-sgRNA(MS2) Puro	CRISPR SAM		Lentiviral plasmid	Lenti sgRNA (MS2)_puro optimized backbone was a gift from Feng Zhang (Addgene plasmid #73797)
mscv.tdTomato.PGK.NEO	Overexpression of cDNA	MS791	Retroviral plasmid	Barbara Grüner lab, University Hospital Essen
mscv.PGK.Neo	Control vector for cDNA overexpression	MS792	Retroviral plasmid, generated from mscv.tdTomato.PGK.NEO	Generated in this work
Mscv.STX18 #1	Overexpression STX18	MS793	Retroviral plasmid, generated	Generated in this work

			from mscv.PGK.Neo	
Mscv.STX18 #2	Overexpression STX18	MS794	Retroviral plasmid, generated from mscv.PGK.Neo	Generated in this work
pHRST-ires-GFP	GFP expression	MS599	Lentiviral plasmid	J.-S. Lee
pQC_rtTA-M2_IP	rtTA-System	MS334	Retroviral plasmid	M.Schuler
pRevTRE GADD45ß	rtTA-System, GADD45B vector	MS700	Retroviral plasmid	V.Ritter
MISSION® pLKO.1-puro Non-Mammalian shRNA Control Plasmid	shRNA control plasmid	MS743	Lentiviral plasmid	Sigma-Aldrich, Inc.
MISSION® pLKO.1-puro STX18 shRNA plasmid	STX18 knockdown	MS753	Lentiviral plasmid; SHCLNG-NM_016930	Sigma-Aldrich, Inc.
MISSION® pLKO.1-puro PLA2G4B shRNA plasmid	PLA2G4B knockdown	MS755	Lentiviral plasmid; SHCLNG-NM_005090	Sigma-Aldrich, Inc.
MISSION® pLKO.1-puro FZD5 shRNA plasmid	FZD5 knockdown	MS756	Lentiviral plasmid; SHCLNG-NM_003468	Sigma-Aldrich, Inc.
pLPC_EGFP	GFP expression	MS244	Retroviral plasmid	M. Schuler
CRISPRa STX18 g1	Overexpression STX18	MS777	CRISPR plasmid; Lenti-sgRNA(MS2) Puro	M. Schulte
CRISPRa STX18 g2	Overexpression STX18	MS778	CRISPR plasmid; Lenti-sgRNA(MS2) Puro	M. Schulte
MISSION® pLKO.1-puro_shRNA_TGFBI	TGFBI knockdown	MS731	Lentiviral plasmid; (TRCN0000062174)	Sigma-Aldrich, Inc.

8.2.3 Oligonucleotides

Table 6: Oligonucleotide primers used in this project.
Oligonucleotides were ordered at Thermo Fisher or IDT, subsequently diluted in H2O and stored at -20°C

Name	Sequence (3' → 5')	comment
Human Actin forward	GGATTCCTATGTGGGCG	qRT-PCR
Human Actin reverse	GGCGTACAGGGATAGC	
Human GAPDH forward	ATTGCCCTCAACGACCACT	qRT-PCR
Human GAPDH reverse	TCTTCCTCTTGTGCTCTTGCT	
Human GADD45B forward	TGACAACGACATCAACATC	qRT-PCR; (Wang et al. 2012)
Human GADD45B reverse	GTGACCAGAGACAATGCAG	
Human STX18 forward	TTGAAGGGAAAGGAGTTCAG	qRT-PCR
Human STX18 reverse	CTGCATTCAGTCTGTCTTGC	
gRNA_STX18_TSS53t_sen	caccgCGGCCTGCGCCCTGCTACCG	M. Schulte (sam.genome-engineering.org CRISPRa guide RNAs für 73797)
gRNA_STX18_TSS53t_rev	aaacCGGTAGCAGGGCGCAGGCCGc	
gRNA_STX18_TSS25b_sen	caccgCTTCTCGCGTCGCCGTTGCC	
gRNA_STX18_TSS25b_rev	aaacGGCAACGGCGACGCGAGAAGc	
Human MMP9 forward	GCA CGA CGT CTT CCA GTA CC	qRT-PCR; (Safranek et al. 2009)
Human MMP9 reverse	CAG GAT GTC ATA GGT CAC GTA GC	
Human STX18 forward #2	CAG GAC CGC TGT TTT GGA TT	qRT-PCR
Human STX18 reverse #2	CTC GGA TGG CTC TCT GTT CT	qRT-PCR
BIP Forward	CGA GGA GGA GGA CAA GAA GG	qRT-PCR; (Oslowski and Urano 2011)
BIP Reverse	CAC CTT GAA CGG CAA GAA CT	
ATF4 Forward	GTT CTC CAG CGA CAA GGC TA	
ATF4 Reverse	ATC CTG CTT GCT GTT GTT GG	
CHOP Forward	AGA ACC AGG AAA CGG AAA CAG A	
CHOP Reverse	TCT CCT TCA TGC GCT GCT TT	
GRP94 Forward	GAA ACG GAT GCC TGG TGG	
GRP94 Reverse	GCC CCT TCT TCC TGG GTC	
EDEM Forward	CAA GTG TGG GTA CGC CAC G	
EDEM Reverse	AAA GAA GCT CTC CAT CCG GTC	
sXBP1Forward	TGAGTCCGCAGCAGGTGCA	
sXBP1 Reverse	GTCCATGGGAAGATGTTCTGG	

8.2.4 Antibodies

Table 7: Antibodies used in this project.
Primary antibodies were used in a 1:1000 – 1:2000 dilution, secondary antibodies were used in a 1:4000 dilution.

Name	Source
AlexaFluor488	Life Technologies
Anti-PLA2G4B antibody	Sigma
Anti-STX18 antibody	Sigma
Anti-STX18 antibody	Abcam
Frizzled5 (D2H2) Rabbit mAb	NEB
Anti-GADD45B antibody - C-terminal	Abcam
Anti-actin (clone C4)	MP Biomedicals
Anti-mouse-HRP	Thermo Scientific
Anti-rabbit-HRP	Thermo Scientific

8.2.5 Commercial Kits

Table 8: Commercially available Kits used in this project.

Name	Source
QIAprep Spin Miniprep Kit	QIAGEN
High Pure RNA Isolation Kit	Roche Molecular Systems, Inc.
QIAGEN Plasmid Plus Maxi Kit	QIAGEN
Trans Blot Turbo RTA Transferkit Nitrocellulose	Bio Rad
Annexin V-FITC Apoptosis Detection Kit	Abcam
Quick Ligation Kit	New England Biolabs
Transcriptor High Fidelity cDNA Synthesis Kit	Roche Molecular Systems, Inc.
LightCycler 480 SYBR Green I Master	Roche Molecular Systems, Inc.
QIAquick PCR Purification Kit (50)	QIAGEN
QIAquick Gel Extraction Kit (50)	QIAGEN
QIAGEN Genomic-tip 500/G	QIAGEN
Genomic DNA buffer set	QIAGEN
Dual-Luciferase® Reporter Assay System	Promega

8.2.6 Chemicals

Table 9: Chemicals used in this project.

Name	Source
0.05% Trypsin-EDTA (1X), Phenol Red	Gibco
2-Mercaptoethanol	Sigma-Aldrich, Inc.
Acetic acid	Roth
Acrylamide mix Rotiphorese® Gel 30 (37.5:1)	Roth
Ammonium peroxodisulfate	Roth
Aqua dest	Braun
Blasticidin S HCl 50mg	Invitrogen

Brefeldin A	NEB
Brilliant blue	Roth
Bromophenol blue	Merck
BSA fraction V	Roth
Calcium chloride (CaCl2)	Roth
Carprieve (Carprofen)	abbvie
Circlegrow (Capsules)	MP Biomedicals
Circlegrow ® medium (Capsules)	MP Biomedicals
cOmplete, Protease Inhibitor Cocktail Tablets in glass vials	Roche Molecular Systems, Inc.
Corning® Matrigel® Growth Factor Reduced (GFR) Basement Membrane Matrix, Phenol Red-Free, 10mL	Corning
DAPI	Roth
Dimethyl sulfoxide	Sigma-Aldrich, Inc.
D-Luciferin-K+ Salt	Caliper Life Science, Perkin Elmer
DMEM, je 500ml, ohne L-Glu.	Gibco
DPBS	Gibco
Ethanol absolute	Sigma-Aldrich, Inc.
Ethidiumbromidlsg.0,025% 15ml	Roth
Gelatin from cold water fish skin	Sigma-Aldrich, Inc.
Gelatin from porcine skin	Sigma-Aldrich, Inc.
Glucose	Roth
Glycerol	Roth
Glycine	Roth
Human Plasma Fibronectin, je 10 mg	Chemicon
Forane (Isofluran)	Norbrook
Kupfer(II)-sulfat	Roth
L-Glutamine, sterile	Gibco
Nonidet® P40 Substitute (NP40)	Sigma-Aldrich, Inc.
O'GeneRuler DNA Ladder Mix, ready-to-use	Thermo Scientific
One Shot® Stbl3™ Chemically Competent *E. coli*	Invitrogen
PageRuler Prestained Protein Ladder	Thermo Scientific
Pen/Strep, sterile	Gibco
Phosphatase Inhibitor Cocktail 2/3	Sigma-Aldrich, Inc.
Ponceau S	Roth
Propidium iodide	Sigma-Aldrich, Inc.
RPMI 1640, je 500ml, ohne L-Glu.	Gibco
SDS	Roth
Sodium chloride	Roth
Sodium citrate	Roth
Sulfo-Cyanin-3-azid	Lumiprobe
Super Signal West Pico ECL	Thermo
SuperSignal West Femto Maximum Sensitivity Substrate (luminol and peroxide buffer)	Thermo Scientific
TEMED	Roth
Trichloressigsäure	Roth

Tris Ultra Qualität	Roth
Triton-X100	Roth
Tween20	Roth
Ultra Pure Agarose	Invitrogen
EcoRI	Roche
BgIII	Roche

8.2.7 Buffers and Solutions

Recipes are listed in alphabetical order.

Colony Staining Solution (colony assay)

Brilliant blue	0.25%
Acetic Acid	10%
Methanol	40%

Store at RT.

Destaining-Solution (Zymography)

Methanol	30%
Acetic Acid	10%

Store at RT.

Enzyme buffer (Zymography)

1.5M Tris HCL pH 8.8	16,6ml
5M NaCl	20ml
1M CaCl2	2.5ml
Triton X-100	5ml

Adjust pH to 7.3 before adding Triton X-100. Ad 500ml H2O. Store at RT.

HFS buffer

Propidium Iodide	5mg
Sodium Citrate	100 mg
Triton-X100	100µl

Add 100ml H2O. Store at 4°C in the dark.

Lower gel buffer, 12% (SDS-PAGE)

30% Acrylamide mix	2.0 ml

1.5M Tris pH 8.8	1.3ml
10% SDS	0.05ml
H2O	1.6ml
10% APS	0.05ml
TEMED	0.002ml

Add APS and TEMED last. Mix carefully and add to chamber. Cover with isopropanol until gel polymerized. Discard isopropanol before adding upper gel. (Sambrook and Russell 2006)

Lower-gel-buffer (Zymography)

H2O	3ml
Acrylamid 30%	3.3ml
Gelatine 1%	1ml
1.5M Tris pH 8.8	2.5ml
10% SDS	0.1ml
10% APS	0.1ml
TEMED	0.004ml

Lysis buffer (b-galactosidase activity, fluorometric)

CHAPS 100mM	2.5ml
Na2HPO4 pH6, 500mM	4ml
H2O	43.5ml

Adjust pH to 6.0 with citric acid. This step is critical! Store at 4°C.

10x Net-G (western blot)

NaCl	175.5g
EDTA	32.2g
Tris-HCL pH 7.5	121.1g
Tween 20	10ml
Gelatine	8g

Dissolve NaCl, Tris, EDTA in 1.5L H2O. Adjust pH to 7.5 with HCL. Add Tween. Heat Gelatine in 200ml H2O, boil till dissolved and add to rest. Ad 2L with H2O. Store at 4°C.

1% NP40-Zymography-Lysisbuffer

Tris pH 7.5	25mM
NaCl	100mM
NP40	1%

Store at 4°C.

PBG (Edu/DAPI staining; immunofluorescence staining)

Gelatin, cold water fish	0.2%
BSA fraction V	0.5%

Dissolve Gelatin in PBS using a microwave. Let cool down before adding BSA. Store at -20°C.

Ponceau S (western blot)

Ponceau S	0.2%
Acetic Acid	5%

Store at RT.

2x Reaction buffer (b-galactosidase activity, fluorometric)

Na2HPO4, ph6, 500mM	240µl
NaCl 5M	180µl
b-Mercaptoethanol	2.1µl
MgCl2 1M	12µl
MUG 34mM	150µl
H2O	2415.9µl

Adjust pH to 6.0 with citric acid before adding b-Mercaptotheanol and MUG. Add MUG immediately prior to use. Prepare fresh before use.

RIPA Lysis-buffer (western blot)

NaCl	150mM
Tris HCL	50mM
Triton X-100	1%
Sodium Deoxycholate	0.5%
SDS	0.1%

Adjust pH to 8, store at 4°C

5x SDS-PAGE-Running buffer (SDS PAGE)

Tris-HCL	15.1g
Glycin	72g
SDS	5g

Add 1L H2O. Store at RT

6x SDS-Sample Buffer (SDS PAGE)

1M Tris-HCL pH 6,8	6ml
SDS	2.4g
Bromphenol blue	0.02g
Glycerol	2ml
ß-Mercaptoethanol	0.14ml

Add 10ml H2O. Heat to 50°C until dissolved, let cool down, add ß-Mercaptoethanol last. Aliquot and store at -20°C

Staining-Master-Mix (Edu/DAPI staining); 50µl

1M Tris ph7.4	5µl
PBS	39.875µl
10mM CuSo4	3.25µl
1mM Cy3 azide dye	0.625µl
500mM Ascorbic Acid	1.25µl

Prepare immediately prior to use, keep in the dark.

Staining-Solution (Zymography)

Coomassieblue	0.05%
Methanol	30%
Acetic Acid	10%

Filtrate before use. Store at RT.

Stripping Buffer (western blot)

1M Tris-HCL pH 6.8	62.5ml
SDS	20g

Add 1L H2O.

Store at RT. Add b-Mercaptoethanol prior to use.

Stop solution (b-galactosidase activity, fluorometric)

Na2CO3	400mM

Store at RT.

Upper gel 5% (SDS-PAGE)

30% Acrylamide mix	0.67ml
1M Tris pH 6.8	0.5ml
10% SDS	0.04ml
H2O	2.7ml
10% APS	0.04ml
TEMED	0.004ml

Add APS and TEMED last. Mix carefully. (Sambrook and Russell 2006)

Upper-gel-buffer (Zymography)

H2O	2.7ml
Acrylamid 30%	0.67ml
1M Tris pH 6.8	0.5ml
10% SDS	0.04ml
10% APS	0.04ml
TEMED	0.004ml

5x Zymography-sample buffer

Tris HCL pH 6.8	0.4M
SDS	5%
Glycerol	20%
Bromphenolblue	0.03%

Store at -20°C.

8.2.8 Consumables and laboratory equipment

Table 10: Consumables and laboratory equipment used in this work.
Standard equipment and standard consumables are not listed.

Name	Source
FACS Celesta with HTS module	BD
FC 500 Flow Cytometer	Beckman Coulter
FACS Fortessa	BD
FACSVantage SE with FACSDiVA Option	BD

Gallios Flow Cytometer	Beckman Coulter
CountessTM Automated Cell Counter	Invitrogen
RS320 x-ray irradiatior	X-Strahl
CountessTM Cell Counting Chamber Slide	Invitrogen
Gene Quant Pro spectrophotometer	GE Healthcare
LightCycler® 480 System	Roche Molecular Systems, Inc.
NanoDrop lite spectrophotometer	Thermo
Trans-Blot® Turbo™ Transfer System	BioRad
Mini-PROTEAN electrophoresis system	BioRad

8.2.9 Software

Adobe Illustrator CS3

Adobe Photoshop CS3

GraphPad Prism 6

R

8.3 List of figures

8.4 List of tables

8.5 List of abbreviations

°C	degree Celsius
AKT	Proteine Kinase B
alt-NHEJ	alternative NHEJ
Apaf-1	apoptotic protease activating factor 1
APC	Adenomatosis polyposis Coli
APEX1	DNA-(apurinic or apyrimidinic site) lyase
ATF	activating transcription factor
ATM	Ataxia telangiectasia Mutated
ATR	Ataxia Telangiectasia And Rad3-Related protein
B3GAT3	Galactosylgalactosylxylosylprotein 3-beta-glucuronosyltransferase 3
BARD1	BRCA1 associated RING domain protein 1
BCL-2	B-cell lymphoma 2
BCL-xL	B-cell lymphoma extra-large
BFA	Brefeldin A
BIP	binding immunoglobulin rpotein
BLM	Bloom’s syndrome protein
BNIP	Bcl2 Interacting protein
BPTF	Nucleosome-remodeling factor subunit BPTF
BRCA1	breast cancer 1
Ca	calcium
CAMK2	Calcium/Calmodulin Dependent Protein Kinase 2
CBCT	cone-beam computed tomography
cDNA	complementary DNA
CES1	Metallothionein-2
CHART	continuous, hyperfractionated, accelerated radiotherapy
c-NHEJ	classical NHEJ
COP	coat protein complex
CtIP	C-terminal binding interacting protein
CTLA-4	cytotoxic T-lymphocyte-associated Protein 4
Ctrl	Control
CXCL13	C-X-C motif chemokine 13
CYLD	Ubiquitin carboxyl-terminal hydrolase

DDR	DNA Damage Response
DDX18	ATP-dependent RNA helicase
DMEM	Dulbecco’s modified eagle medium
DMSO	Dimethyl sulfoxide
DNA	deoxyribonucleic acid
DNA-PK	DNA dependent protein kinase
DNA-PKcs	DNA-PK catalytic subunits
Dox	doxycycline
DSB	double-strand break
DVL	Disheveled
e.g.	for example
ECM	extracellular matrix
EGF	epidermal growth factor
EGFR	epidermal growth factor receptor
EMT	epithelial-mesenchymal transition
ER	endoplasmatic reticulum
EXO1	exonuclease 1
FDA	Food and Drug Administration
FOXC2	Forkhead box protein C2
FZD5	Frizzled Class Receptor 5
GADD45B	growth arrest and DNA damage inducible beta
GSK3A	Glycogen synthase kinase-3 alpha
GSK3b	glycogen synthase kinase 3 beta
Gy	Gy
H	hour(s)
HCLS1	Hematopoietic lineage cell-specific protein
HRR	homologous recombination repair
IMRT	intensity modulated radiation therapy
IR	ionizing radiation
IRE1a	transmembrane protein kinase inositol-requiring enzyme 1
IRF2	Interferon regulatory factor 2
JAK	janus kinase
JNK	c-Jun N-terminal kinase
LET	linear energy transfer
Lig	Ligase

MAPK	mitogen-activated protein kinase
MBTPS2	Membrane-bound transcription factor site-2 protease
Min	minute(s)
MKK7	mitogen-activated protein kinase kinase 7
MMP	matrix metalloproteases
MOMP	mitochondrial outer membrane permeabilization
MRN	Mre11-Rad50-Nbs1
mRNA	messenger RNA
MSX1	Homeobox protein MSX-1
MTT	3-(4,5-Dimethylthiazol-2-yl)-2,5-Diphenyltetrazolium Bromide
NGS	next generation sequencing
NHEJ	non-homologous end-joining
NRF2	nuclear factor (erythroid-derived 2)-like 2
NSCLC	non-small-cell lung cancer
PARP	Poly(ADP-ribose)-Polymerase 1
PBS	phosphate-buffered saline
PCP	planar cell polarity pathway
PCR	polymerase chain reaction
PD-1	programmed cell death protein 1
PDAC	pancreatic ductal adenocarcinoma
PDE2A	cGMP-dependent 3',5'-cyclic phosphodiesterase
PD-L1	programmed cell death 1 ligand 1
PERK	PKR-like ER kinase
PI	propidium iodide
PI3K	phsophpatidylinositol-4,5-bisphosphate 3-kinase
PKC	protein kinase c
PLA2G4B	Cytosolic phospholipase A2 beta
PlC	phospholipase C
POI	Plasmid of interest
PSMA	Proteasome subunit alpha type
qRT-PCR	quantitative real-time PCR
RAF	rapidly accelerated fibrosarcoma
RAS	rat sarcoma
RINT-1	Rad50-Interacting Protein 1
RIPK	Receptor Interacting Serin/Threonine Kinase 1

RISC	RNA-induced silencing complex
RNA	ribonucleic acid
ROI	region of interest
RPMI	Roswell Park Memorial Institute Medium
rtTA	reverse tetracycline controlled transactivator
RXRB	Retinoic acid receptor RXR-beta
Sec22b	SEC22 Vesicle Trafficking Protein Homolog B
SH2B2	SH2B adapter protein 2
shRNA	small hairpin RNA
SNARE	soluble N-ethylmaleimide-sensitive-factor attachment receptor
SREBF2	Sterol regulatory element-binding protein 2
SSB	single strand break
ssDNA	single-stranded DNA
STAT	Signal Transducer And Activator Of Transcription 3
STX18	syntaxin 18
SWI/SNF	Switch/Sucrose Non-Fermentable
TGFbi	Transforming Growth Factor Beta Induced
TK	tyrosine kianse
TKI	tyrosine kinase inhibitor
TRAF2	TNF receptor-associated factor 2
TSS	Transcription starting site
UPR	unfolded protein response
VAMP	vesicle-associated membrane protein
w/o	without
WIPI1	WD repeat domain phosphoinositide-interacting protein 1
Wnt	Wingless-Type MMTV Integration Site Family
WNT5B	Protein Wnt-5b
XBP1	X-box binding protein 1
XCL1	Interferon regulatory factor 2
XLF	XRCC4-linked factor
XRCC4	x-ray repair cross-complementing protein 4

9. Acknowledgements

This work is implemented in the Research Training Group RTG1739 and is supported by the Deutsche Forschungsgemeinschaft (DFG).

First of all, I want to thank my supervisor Prof. Dr. Martin Schuler for the opportunity to work on my PhD project in the Molecular Oncology Group. I am very grateful for his continuous guidance and counsel and his broad knowledge in cancer research.

I also want to thank Prof. Dr. George Iliakis for mentoring me and for giving me access to his lab whenever needed.

Special thanks also to Dr. Frank Breitenbücher for all the support throughout the past years and especially for all the help with the *in vivo* experiments. This would not have been possible without him.

In addition, I would like to thank Dr. Barbara Grüner for all her support, advice, and counsel.

A huge thank you also to PD Dr. Laura Steenpaß for critically proofreading this thesis and for her many helpful remarks.

Thank you also to Prof. Dr. Alexander Schramm for his support within the last year.

Furthermore, I would like to thank all the “old” and “new” members of the Molecular Oncology Group for the great working atmosphere, for sharing knowledge and advice, and also for the never-ending supply of sweets. Thank you to Sarah Wieczorek, Stephanie Meyer and Jeannette Phasue for all the support. I terribly missed having you around. Thank you also to Marc Schulte, for his never-ending ideas and all the work he did with CRISPR and to Katharina Batzke, for all the help with the mice. Also thank you to our intern Eric Buchholz for generating the new GADD45B cells. Especially, I want to thank Silke Nothdurft, for all the support, advice, magically wonderful blots and detailed protocols. I really would not have made it without you. Many thanks also to our “honorary” group member Madeleine Dorsch. I enjoyed working with you.

Furthermore, I want to thank Anna Broich from the Group of Prof. Dr. Iliakis for sharing her knowledge. Thank you also to Philip Kranz from the Group of Prof. Dr. Eric Metzen for sharing the Dual-Luciferase Assay protocol and for all his advice regarding ER-stress.

Additionally, I want to thank Prof. Dr. Martin Stuschke and Dr. Ali Sak for giving me access to their X-ray irradiator. Here, I also want to thank Michael Groneberg for all his support and all his help, especially during the animal irradiation. For all the help

during the *in vivo* imaging process I want to thank the members of the IMCES. Thank you to Dr. Dr. Simon Bogner for his advice during the analysis of the *in vitro* screen.
I also want to thank Prof. Dr. Karl Lang for giving me access to his flow cytometer, Prof. Dr. Jens Siveke for giving me access to the TECAN reader, Klaus Lennartz for taking time to sort my cells and Dr. Dieter Brandhorst for his help with IT problems.
Many thanks also to Prof. Dr. Verena Jendrossek for organizing the RTG1739, and to the coordinators Ivonne Schulte and Dr. Gabriele Siedenburg, for their help with all the bigger and smaller problems throughout the last 3 years. In general, I want to thank all the PhD students belonging to this program. I enjoyed meeting you and appreciate all the support.

Last, but certainly not least, I want to thank my family for their never-ending trust and support.

So, thank you:

To my wonderful husband whose encouragement carried me through all the “downs” and without whom I would surely have given up.

To my parents, who never failed to believe in me.

To my magnificent little sister, whom I love dearly and am very proud of.

To my parents in law, who provided shelter and distractions from work whenever needed.

10. CV

Der Lebenslauf ist in der Online-Version aus Gründen des Datenschutzes nicht enthalten.

Der Lebenslauf ist in der Online-Version aus Gründen des Datenschutzes nicht enthalten.

Der Lebenslauf ist in der Online-Version aus Gründen des Datenschutzes nicht enthalten.

Der Lebenslauf ist in der Online-Version aus Gründen des Datenschutzes nicht enthalten.

11. Declarations

Erklärung:

Hiermit erkläre ich, gem. § 6 Abs. (2) g) der Promotionsordnung der Fakultät für Biologie zur Erlangung der Dr. rer. nat., dass ich das Arbeitsgebiet, dem das Thema „Identification of novel targets for rational chemoradiotherapy strategies in non-small-cell lung cancer“ zuzuordnen ist, in Forschung und Lehre vertrete und den Antrag von Sophie Kalmbach befürworte und die Betreuung auch im Falle eines Weggangs, wenn nicht wichtige Gründe dem entgegenstehen, weiterführen werde.

Essen, den _____ _____

Unterschrift eines Mitglieds der Universität Duisburg-Essen

Erklärung:

Hiermit erkläre ich, gem. § 7 Abs. (2) d) + f) der Promotionsordnung der Fakultät für Biologie zur Erlangung des Dr. rer. nat., dass ich die vorliegende Dissertation selbständig verfasst und mich keiner anderen als der angegebenen Hilfsmittel bedient, bei der Abfassung der Dissertation nur die angegeben Hilfsmittel benutzt und alle wörtlich oder inhaltlich übernommenen Stellen als solche gekennzeichnet habe.

Essen, den _____ _____

Unterschrift des/r Doktoranden/in

Erklärung:

Hiermit erkläre ich, gem. § 7 Abs. (2) e) + g) der Promotionsordnung der Fakultät für Biologie zur Erlangung des Dr. rer. nat., dass ich keine anderen Promotionen bzw. Promotionsversuche in der Vergangenheit durchgeführt habe und dass diese Arbeit von keiner anderen Fakultät/Fachbereich abgelehnt worden ist.

Essen, den _____ _____

Unterschrift des Doktoranden